Processing and Characterization of High Performance Piping Materials For Geothermal Applications

By

Murat TOĞULGA

**A Dissertation Submitted to the
Graduate School in Partial Fulfillment
of the Requirements for the Degree of**

MASTER OF SCIENCE

**Department: Energy Engineering
Major: Energy Engineering
(Energy and Power Systems)**

**Izmir Institute of Technology
Izmir, Turkey**

July, 2003

We approve the thesis of **Murat Toğulga**

Signature | Date of Signature

---------- **09 / 07 /2003**

Asst. Prof. Dr. Metin Tanoğlu
Asst. Professor of Mechanical Engineering
Thesis Advisor

Signature

---------- **09 / 07 /2003**

Asst. Prof. Dr. Gülden G. Günerhan
Asst. Professor of Mechanical Engineering
Thesis Co-Advisor

Signature

---------- **09 / 07 /2003**

Prof. Dr. Zafer İlken
Professor of Mechanical Engineering

Signature

---------- **09 / 07 /2003**

Asst. Prof. Dr. Hacer Aygün
Asst. Professor of Mechanical Engineering

Signature

---------- **09 / 07 /2003**

Asst. Prof. Dr. Funda Tıhmınlıoğlu
Asst. Professor of Chemical Engineering

ACKNOWLEDGEMENTS

I wish to express my sincere gratitude to my advisors Asst. Prof. Metin Tanoğlu and Asst. Prof. Gülden Günerhan for their süpervisions, guidance, encouragement and supports during the courses of this thesis and in the experimental study.

I acknowledge the supports from IYTE Ar-Fon Project, MÜH 05,2002 and DPT project. I would like to thank to Prof. Dr. Macit Toksoy and Prof. Dr. Zafer İlken for their comments and suggestions during my thesis. Besides, I would like to add my special gratitude to my friends. I am also greatful to Balçova Geothermal A.Ş. for help on accessing to Balçova geothermal facilities.

Finally, I would like to thank my family for their understanding, encouragement and supports.

ABSTRACT

Polymer composite based pipes are being recently utilized in transportation of geothermal fluids. The utilization of composites is due to their resistance to aggressive chemicals and hot-wet environment with relatively high specific strength and design flexibility. Exposure of materials to wide range of temperatures and humidity level, while under the action of load, may degrade them and cause to severe reduction in their properties and service life. Understanding the complex degradation mechanism of the composites exposed to a variety of temperature and fluid chemistry (including geothermal fluid) is essential to improve their durability.

This research focuses on the investigation of interactions between geothermal fluid and composite piping materials made of various matrices and the mechanism of degradation in these composites. The matrix materials include polyester, epoxy and graphite particle added epoxy materials. In this study, E-glass fiber reinforced polymer composites were fabricated by employing filament winding and tube rolling techniques. Fabricated composites and neat polymers were exposed to dry environment, distilled water and geothermal fluid of Balçova geothermal field until the saturation of weight gains due to water uptakes. In addition, the specimens with neat polymers were prepared to simulate and follow the degradation of matrix materials under hot-wet environments. Once the saturation occurred, the specimens were subjected compressive mechanical testing. For both dry and wet specimens, the mechanical testing was performed to obtain stress-strain behavior, modulus of elasticity, strain at failure values and energy absorption during the loading. The results were compared to evaluate the degradation of the properties due to various exposures. Moreover, the thermal conductivity of the various composites fabricated in this research was measured to determine the heat losses and temperature distribution within the materials. The temperature distribution within the cross-section of the pipes for various materials was analyzed using a finite element-modeling tool, LUSAS for uninsulated pipes. The heat loss occurring during the transportation of hot geothermal fluid was calculated as a case study to compare composites and traditional metal piping.

It was found that polyester composite pipes have higher mechanical performance under axial and radial compression as compared to the composite with epoxy matrices. For all the composite types, some considerable degradations were

measured due to exposure to hot-wet environments. The extend of degradation was less for graphite particles added epoxy composite pipes that exhibited the lowest water uptake values. The graphite particles incorporated into the matrix affected the water uptake and thermal conductivity of the epoxy. The water uptake of polyester matrix composite pipes was the highest that might be related to the most extensive degradation of polyester based composite. Moreover, it was found that the thermal conductivity of the composites is much lower than traditional materials. The graphite particles cause reduction in thermal conductivity, simultaneously in heat loss for uninsulated pipes. However, if the isolation is used, heat loss is not sensitive to pipe material.

ÖZ

Polimer kompozit esaslı borular, günümüzde jeotermal sıvıların taşınmasında kullanılmaktadır. Kompozitlerin kullanılması, kuvvetli ve dizayn esnekliğine sahip olmasıyla birlikte onların agresif kimyasallara ve sıcak-nemli ortama direnç gösterebilmesinden kaynaklanmaktadır. Malzemelerin yük altında yüksek sıcaklık ve nemli ortamlara maruz bırakılması onların bozulması ve özelliklerinde ve servis ömürlerinde bir düşüşe neden olabilmektedir. Farklı sıcaklık ve sıvı kimyasına (jeotermal sıvılarda dahil) maruz bırakılmış kompozitlerdeki kompleks bozunum mekanizmaların anlaşılması dayanıklılıklarının geliştirilmesi için gerekmektedir.

Bu araştırma, jeotermal sıvıyla değişik matriks malzemelerden oluşan kompozit borular arasındaki etkileşiminin ve bu kompozitlerdeki bozunum mekanizmaları üzerinde odaklanmıştır. Matriks malzemeleri polyester, epoksi ve karbon parçacıkları eklenmiş epoksileri ihtiva eder. Bu çalışmada E tipi cam fiberle güçlendirilmiş polimer kompozitler, filament sarma ve tüp sarma teknikleriyle üretilmişlerdir. Üretilen kompozit boru ve katkısız matriks polimerleri kuru ortam ile saf su ve Balçova jeotermal alanındaki jeotermal sıvıya su emmeleri için doygunluğa ulaşıncaya kadar maruz bırakılmıştır. Ayrıca, sıcak-nemli ortamlar altında matriks polimerlerindeki bozunumun simulasyonun ve izlenmesi için katkısız polimer numuneler hazırlanmıştır. Numuneler su doygunluğuna ulaştığı vakit mekanik basma testine tabi tutulmuştur. Kuru ve nemli numuneler için, stress-uzama davranışları, elastik modülleri, kırılma noktasındaki uzama değerleri ve enerji emme miktarlarının bulunması için mekanik testler gerçekleştirilmiştir. Sonuçlar, farklı ortamlara maruz bırakılmış numunelerin özelliklerindeki düşüşün değerlendirilmesi için karşılaştırılmıştır. Bununla birlikte, üretilen farklı tipteki kompozitlerin ısı kayıpları ve sıcaklık dağılımlarının analizi için ısıl iletkenlik katsayıları bu çalışmada ölçülmüştür. İzolasyonsuz farklı malzemelerden oluşan boruların kesitlerindeki sıcaklık dağılımları LUSAS bilgisayar programı kullanılarak analiz edilmiştir. Sıcak jeotermal sıvıların taşınmasında oluşan ısı kayıpları da hesaplanarak, kompozit borularla geleneksel olarak kullanılan boru malzemeleri karşılaştırılmıştır.

Bu çalışmanın sonucunda, polyester kompozit boruların diğer epoksi kompozit borulara göre eksenel ve radyal baskı altında daha yüksek mekanik performansa sahip olduğu bulunmuştur. Ayrıca, her tipteki kompozit boruların sıcak-nemli ortama maruz

bırakıldıktan sonra mekanik ve termal özelliklerinde önemli derecede bir düşüş olduğu gözlenmiştir. Bu düşüşün en az su çekme değerine sahip olan karbon parçacıkları eklenmiş epoksi kompozitlerde daha az olduğu görülmüştür. Bu karbon parçaçıkları matriksin su emmesini ve epoksinin ısıl iletkenlik katsayısını etkilediği görülmüştür. Polyester kompozit boruların performansındaki düşüşün en yüksek mertebede olması diğer tip borulara oranla daha fazla su emme özelliği ile bağlantılandırabilinir. Bununla beraber karbon parçacıklarının ısıl iletkenlik katsayısında düşüşe neden olduğu ve aynı zamanda izolasyonsuz borularda oluşan ısı kayıplarını azalttığı gözlenmiştir. Ancak izolasyon kullanıldığı zaman malzemenin cinsinin ısı kayıplarında fazla bir etkisi olmadığı görülmüştür.

TABLE OF CONTENTS

NOMENCLATURE

ε	Stress (MPa)
σ	Strain
M_t	Water content percentage
m_o	Weight of dry specimen (gr)
m	Weight of wet specimen (gr)
D	Diffusivity ($m^2.s^{-1}$)
M_m	Maximum water content
h	Thickness of the composite specimen (m)
v_f	Volume fraction
V_f	Volume of fiber (cm^3)
V_m	Volume of matrix (cm^3)
m_f	Mass of fiber (gr)
m_m	Mass of matrix (gr)
ρ_f	Density of fiber (gr/cm^3)
ρ_m	Density of matrix (gr/cm^3)
E_s	Specific energy (J/kg)
A	The cross-sectional area of pipe (mm^2)
$P(\delta)$	Applied load (N)
ρ	The material density (gr/cm^3)
δ_f	The final crush displacement (m)
Q	Heat Transfer Rate (W/m)
r_1	Inner radius of Geothermal Pipe (m)
r_2	Outer radius of Geothermal Pipe (m)
r_3	Radius of Insulating Foam (m)
r_4	Radius of Coat with Insulation Foam (m)
v_f	Velocity of The Geothermal Fluid (m/s)
T_s	Geothermal Fluid Temperature (^0C)
T_1	Outer Surface Temperature of Pipe (^0C)
h_f	Heat Transfer Coefficient of Geothermal Fluid ($W/m^2.K$)
k_p	Thermal Conductivity of Pipe (W/m.K)
k_f	Thermal Conductivity of Insulating Material (W/m.K)

k_c	Thermal Conductivity of Glass Fiber Coat (Insulating Material) (W/m.K)
S	Conduction Shape Factor
z	Distance From The Ground Surface (m)
L	Length of The Pipe (m)
k_s	Thermal Conductivity of Soil (W/m.K)
T_2	Ground Temperature (^{0}C)
D	Diameter of The Buried Pipe (m)
m	Mass Flow Rate (kg/s)
c_p	Specific Heat (J/kg.^{0}C)
T_o	Outer Fluid Temperature (^{0}C)
M_t	Water Uptake Percentages at Time, t
a	Radius of Specimen (m)

LIST OF FIGURES

LIST OF TABLES

CHAPTER I
INTRODUCTION

Energy resources in the earth can be divided into two groups; i.e., fossil fuel and renewable energy resources. Geothermal energy, which is an important renewable energy resource, is the power obtained by the earth's natural heat. This heat is brought to the earth surface as steam or hot water. For our country, geothermal energy is a significant renewable resource since Turkey has the seventh richest geothermal potential in all over the world.

The source of geothermal fluid for a direct use application is often located some distance away from the user. This requires a transmission pipeline to transport the geothermal fluid. The cost of transmission lines and the distribution networks especially in direct-use application has a significant portion of the total cost for a geothermal investment. Geothermal fluid for direct use applications is usually transported in the liquid phase and requires some of the same design considerations as water distribution systems. Several factors including pipe material, dissolved chemical components, size, temperature, insulation, pipe expansion, service taps, installation method, heat loss and pumping requirements should be considered before final specification [1]. On the other hand, the composition of geothermal fluids may vary greatly. The water composition in general is characterized by the macroelements of the reservoir rock and the subsurface environment to which it is exposed. The most frequently detected elements with high concentrations are Na^+, K^+, Ca^{2+}, Mg^{2+}, Cl^-, SiO_2, HCO_3^-, CO_3^-, SO_4^{2-} and CO_2 [2]. These elements exhibit an important corrosive effect on materials. The same thermal water can be very aggressive at one time and may show a trend towards formation of scaling at another based on the change in its physico-chemical parameters. Scaling and corrosion can cause serious damages in pipes and, therefore, economical losses of the system. The traditional pipe materials for geothermal applications have been carbon steel, stainless steel, PVC and polyethylene. The experience reported in the literature so far revealed that geothermal fluid has corrosive effects, scaling potential and creep deformations on these materials [2]. Alternatively, new pipe materials, which exhibit high corrosion resistance against aggressive geothermal fluid and high mechanical and durability performance, have been sought in this area. Polymer composite materials have become one of the best candidates for this purpose and they are being installed in

various applications all over the world. As an example, these materials have been utilized in Çeşme Geothermal District Heating System in our region most recently.

Reinforced thermosetting resin pipe (RTRP) or fiberglass reinforced plastic (FRP) materials, in general, consist of two main matrix materials; epoxy and polyester resins. Both epoxy and polyester resin systems can be compounded to be serviceable to temperatures of up to 150°C [1]. At high temperatures, the RTRP systems are susceptible to damage when fluid flashes to vapor. The forces associated with the flashing may affect the fibers at the interior of the pipe surface. The leakage failure of a FRP composite pipe subjected to combined internal pressure and axial loading is commonly viewed as a result of progressive damage produced by the coalescence of microcracks, thus creating a through-thickness crack path prior to the complete loss of structural load-bearing capability. In addition, weeping in a piping system, that is fluid penetration into the tube wall, can also alter the long-term behavior of the composite. This penetration of fluid into the pipe wall may be a result of the combination of delamination and through-thickness cracks running parallel to the fibers. The most frequently observed microstructural defects in this kind of composite structure are inter- and intra-ply porosity in the matrix, non-uniform fiber distribution and fiber deviation away from $\pm \theta$ alignment [3]. It has been revealed the fiber/interface/matrix interactions and interactions between plies, which have a dominant effect on the early stages of mechanical failure, i.e., damage initiation (microcracking and delamination). There are a great number of studies that investigate the mechanical performance composite pipes and influence of water content on composite pipes [3-28]. However, to our knowledge, there is very limited study in the literature investigating the effects of geothermal fluid on the durability of composite pipe materials.

The aim of this study is to investigate the interactions between geothermal fluid and polymer composite piping materials and the mechanism of degradation in composites, to determine the durability of composite tubes and neat polymers made of various matrix materials and exposed to various environments (dry environment, distilled water and geothermal fluid). For this purpose, E-glass fiber reinforced polymer matrix composite pipes were fabricated by employing filament winding and tube rolling techniques. Fabricated composites and neat polymers were exposed to dry, distilled water and geothermal fluid in Balçova Geothermal Field. In addition, the specimens with neat polymers were prepared to simulate and follow the degradation of matrix material under hot-wet environments. Once the saturation occurred, the specimens were

subjected to compressive mechanical testing to obtain stress-strain behavior, modulus of elasticity, strain at failure values and energy absorption during the loading. A series of mechanical tests was performed under various combinations of radial and axial stresses to evaluate the mechanical behaviors of composite pipes. Moreover, the thermal conductivity of the fabricated composite pipes was measured. The temperature distribution within the cross-section of the pipes with various materials was analyzed using a finite element-modeling tool, LUSAS for uninsulated pipes. The heat loss occurring during the transportation of hot geothermal fluid was calculated as a case study to comparing composites and traditional metal piping. The results of this work presents the processing, the microstructural characteristics, the stress/strain behaviors, damage mechanisms under axial and radial loadings, the degradations after exposure to wet environments and analysis of temperature distributions and heat losses of polymer composite pipes.

In this Thesis, Chapter 2 includes some information about geothermal energy. In this chapter, geothermal fluid chemistry, corrosion and scaling problems are described. Moreover, the piping materials in geothermal application and composites are presented in Chapter 3 and Chapter 4, respectively. Next chapter, which is Chapter 5, consists of experimental section. In this chapter, which methods are used and which tests are performed are explained. Then, the results are given in Chapter 6. Finally, the conclusions and recommendations are finished with Chapter 7.

CHAPTER II
GEOTHERMAL ENERGY

2.1 What is Geothermal Energy?

"Geothermal" comes from the Greek words geo (earth) and thermal (heat). Therefore, geothermal means earth's heat. Our earth's interior like the sun provides heat energy from nature. This heat, which is geothermal energy, yields warmth and power that we can use without polluting the environment. Geothermal heat originates from Earth's fiery consolidation of dust and gas over 4 billion years ago. At earth's core, 6000 km. deep, temperatures may reach over 5000^{o}C (Figure 2.1) [29]. The heat from the earth's core continuously flows outward. It transfers or conducts to the surrounding layer of rock, the mantle. When temperatures and pressures become high enough, some mantle rock melts, becoming magma. Then, because it is lighter (less dense) than the surrounding rock, the magma rises, moving slowly up toward the earth's crust, carrying the heat from below. Sometimes the hot magma reaches all the way to the surface, where we know it as lava. But most often the magma remains below earth's crust, heating nearby rock and water (rainwater that leaks deep into the earth) sometimes as hot as 370^{o}C. Some of this hot geothermal fluid travels back up through faults and cracks and reaches the earth's surface as hot springs, but most of it stays deep underground, trapped in cracks and porous rock. This natural collection of hot water is called a geothermal reservoir (Figure 2.2).

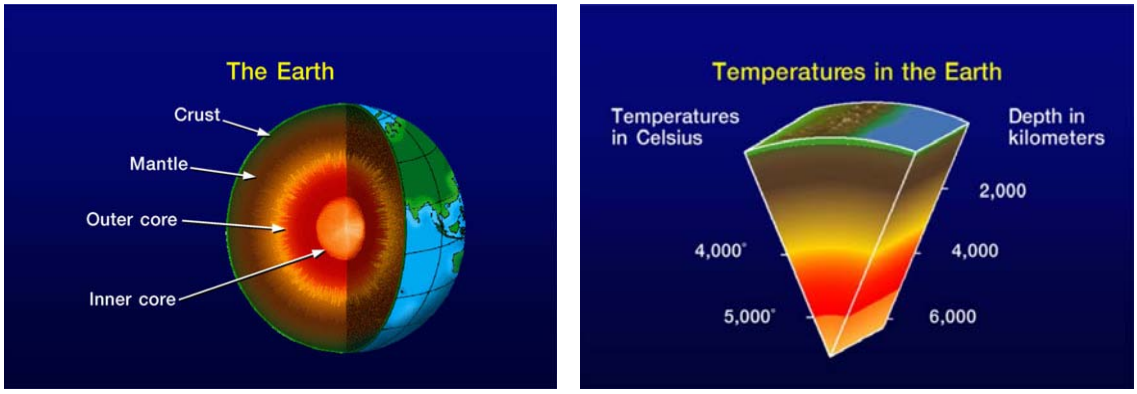

Figure 2.1 Temperatures in earth and layer of the earth [29].

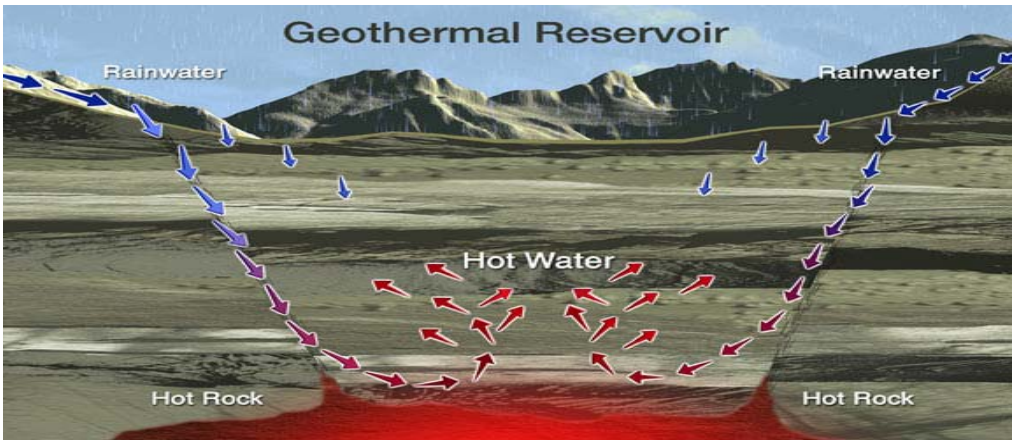

Figure 2.2 Geothermal reservoir [29].

To bring the hot water to the surface, we drill wells into the geothermal reservoirs. Geologists, geochemists, drillers and engineers do a lot of exploring and testing to locate underground areas that contain this geothermal fluid, so we can know where to drill geothermal production wells [30-38]. Then, once the hot water and/or steam travels up the wells to the surface, they can be used to generate electricity (by using turbine generator) in geothermal power plants (Figure 2.3) or for energy saving non-electrical purposes. In geothermal power plants steam, heat or hot water from geothermal reservoirs provides the force that spins the turbine generators and produces electricity. The used geothermal fluid is then returned down an injection well into the reservoir to be reheated, to maintain pressure, and to sustain the reservoir [39].

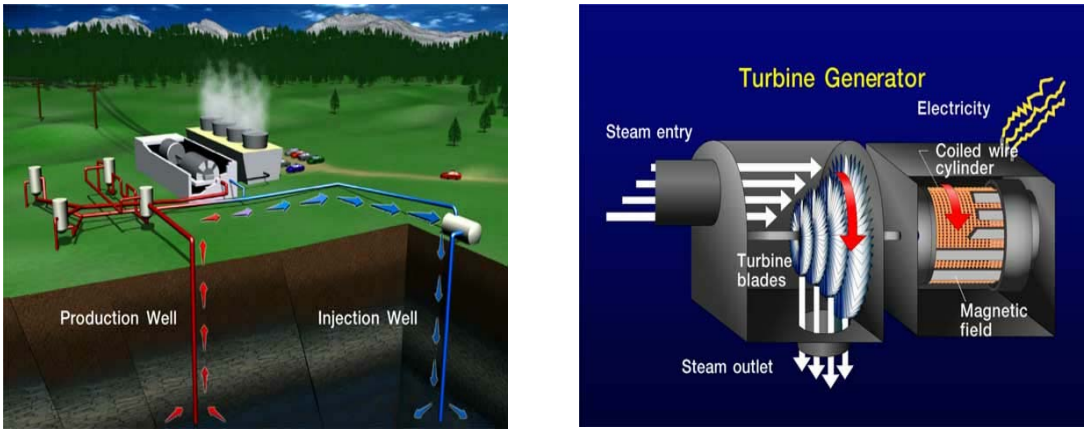

Figure 2.3 Geothermal power plant and turbine generator [29].

Using geothermal fluid directly conserves energy and replaces the use of polluting energy resources with clean ones. The main non-electric ways we use geothermal energy are direct uses and geothermal heat pumps.

Geothermal fluids are used directly from the earth to help grow flowers, vegetables and other crops in greenhouses; to shorten the time which is needed for growing fish and shrimp, to pasteurize milk, to dry onions and lumber and to wash wool (industrial uses) and also space heating of individual buildings and of entire districts, is besides hot spring bathing which is the most common and the oldest direct use of nature's hot water. Geothermal district heating systems pump geothermal fluid through a heat exchanger, where it transfers its heat to clean city water that is piped to buildings in the district. There is a second heat exchanger transfers the heat to the building's heating system [39]. The geothermal fluid is injected down a well back into the reservoir to be heated and used again (Figure 2.4).

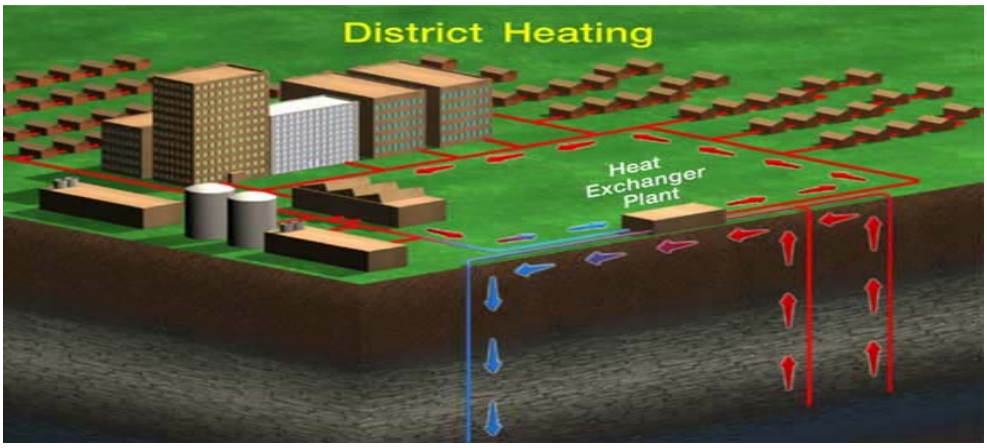

Figure 2.4 A sample of district heating system [29].

Today, with geothermal heat pumps (GHP's), we take advantage of earth temperature that is about 7-15^{o}C just a few meters below the surface to help keep our indoor temperatures comfortable. GHP's circulate water or other liquids through pipes buried in a continuous loop (either horizontally or vertically) next to a building. Depending on the weather, the system is used for heating or cooling (Figure 2.5).

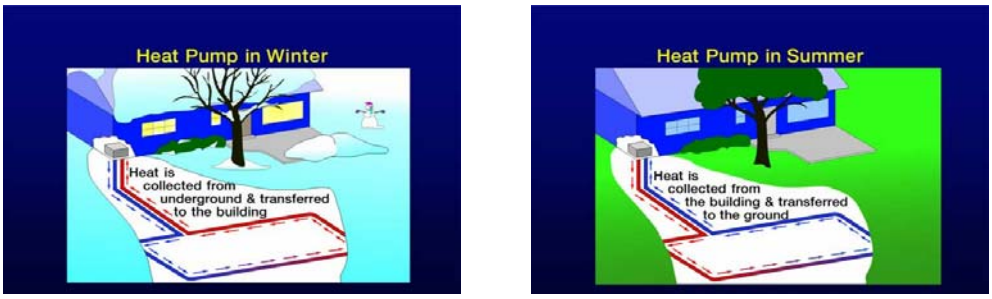

Figure 2.5 Installation of heat pump and the circulation of water in summer and winter [29].

To heat the buildings, earth's heat (the difference between the earth's temperature and the colder temperature of the air) is transferred through the buried pipes into the circulating liquid and then transferred again into the building. In addition, to cool them, during hot weather, the continually circulating fluid in the pipes picks up heat from the building so this system helps to cool it and transfers the fluid into the earth. GHP's use very little electricity and are very easy on the environment [29,39].

2.2 Geothermal Fluid

2.2.1 Geothermal Fluid Chemistry

"Geothermal fluid" means naturally occurring steam or hot water, which is at temperature of at least 35^{o}C in the natural state of free-flowing springs or pumped from wells.

Normal ground waters are usually near neutral in pH and slightly bicarbonate in character. When they are heated in a geothermal system, they tend to become more sodium chloride in character, with dissolved salt contents that can range from a few hundred mg/l to more than 300.000 mg/l. If the fluid boils at depth, gases (e.g., CO_2, H_2S) are preferentially partitioned into the steam phase and migrate independently toward the surface. The gas-rich steam phase may encounter cool groundwater produces acid-sulfate waters that react with the host rocks to produce characteristic argilicalteration assemblages of clay minerals.

Bicarbonate-rich geothermal fluids are produced where groundwater dissolves CO_2, rising with steam from the deeper geothermal system. Any of these fluid types may be diluted with low-salinity ground water or changed in other ways before being samples from a thermal spring or a well. By study of the chemistry of the various fluids

found in wells and springs in a geothermal area, the nature of the geothermal fluids at depth can sometimes be determined [1]. Geothermal fluid commonly contains seven chemical species that produce an important corrosive effect on materials. These chemicals are oxygen, hydrogen ion (pH), chloride ion, sulfide species, carbon dioxide species, ammonia species and sulfide ion. The simplest chemical parameters often quoted to characterize geothermal fluids are total dissolved solids (TDS) in parts per million (ppm) or milligrams per liter (mg/l) and pH, which of a fluid is a measure of the acidity alkalinity of the fluid. These two parameters can be measured in the field by use of conductivity meter and a pH meter. The conductivity meter measures the TDS of a fluid by measuring its electrical conductivity. The more dissolved salts, the higher the electrical conductivity. The amount and nature of chemical species in geothermal fluids are examined in such studies [34-36]. Table 2.1 shows chemical content of geothermal fluids from a various geothermal field in all over the world. Table 2.2 shows the analyses of geothermal fluid of B-10 well in Balçova Geothermal District Heating System in which the specimens were left to measure their water uptake.

Table 2.1 Representative analyses of geothermal fluids [1].

Sample	pH	SiO_2	Ca	Mg	Na	K	Li	HCO	SO	Cl	F	B	As
	(ppm)	(ppm)	(ppm)	(ppm)	(ppm)	(ppm)	(ppm)	(ppm)	(ppm)	(ppm)	(ppm)	(ppm)	(ppm)
1	-	52	257	17	570	-	0.5	-	932	625	2.8	2.6	-
2	7.9	293	5	0.8	653	71	0.7	305	-	885	1.8	4.9	2.7
3	8.4	690	17	0.03	1320	255	14.2	-	36	2.26	1.3	-	4.8
4	-	563	8	2	2320	461	25.3	232	72	3.86	6.8	-	4.3

Sample Descriptions
1. Hot Springs, Monroa, Ut.
2. Hot Springs, Steamboat, NV.
3. Well 44, Wairakei, New Zealand
4. Brine discharge from Well 54-3, Roosevelt Hot Springs, UT.

Table 2.2 Analyses of geothermal fluid in B-10 well in Balçova Geothermal District Heating System [40]

Name	T (^{0}C)	Na	K	Mg	Ca	SiO_2	HCO_3	SO_4	Cl
		mg/l	mg/l	mg/l	mg/l	mg/l	mg/l	mg/l	mg/l
B-10	99	425	39	12	38	116	783	171	193

2.2.2 Material Problems Associated with Geothermal Fluid Chemistry

2.2.2.1 Corrosion

The chemical species in the geothermal fluids have different types of corrosive effects on materials as shown in Table 2.3.

Table 2.3 Corrosive effects of the species in the geothermal fluid on various materials [1].

Corrosive Species	Corrosive Effects
Oxygen	Corrosive to carbon and low alloy steels Cause serious pitting (when con. >50 ppb*)
Hydrogen Ion (pH)	Acid attack on cements Cathodic reaction of steel corrosion
Chloride Ion	Strong promoter of corrosion of carbon, stainless steels and other alloys
Sulfide Species	Highly corrosive to alloys containing both cupronickels and monels
Carbon Dioxide Species	Increase carbon steel corrosion
Ammonia Species	Cause stress corrosion cracking of some copper based alloys
Sulfide Ion	Corrosion of cements

ppb – parts per billion

In piping systems for low temperature geothermal applications both metallic and non-metallic materials can be used. These include carbon steel, copper, PVC (polyvinyl chloride) and PE (polyethylene). When metallic structures are used, corrosion of metal surfaces and the scaling process are the major problems caused by geothermal fluids. The kinetics and mechanisms of the corrosion depend on both the physical and chemical characteristics of the environment as well as on the characteristics of the material. The chemical species in geothermal fluids mainly determine the corrosion of metals. A variety of corrosion mechanism may be observed in geothermal systems [41]. These

include general corrosion, galvanic corrosion, crevice corrosion, pitting, intergranular corrosion, selective leaching, stress corrosion cracking (SCC) and erosion corrosion.

General Corrosion: This type of corrosion occurs when the anodic and cathodic areas are distributed uniformly over the metal surface. One of the examples is the rusting of iron in seawater. General corrosion can be controlled by use of corrosion resistant alloys, surface coatings and the use of inhibitors.

Galvanic Corrosion: This is the accelerated corrosion of one metal resulting from its electrical contact with a different metal. An example of this type of corrosion is contact between copper flashing and a galvanized steel roof.

Crevice Corrosion: This form of corrosive attack concentrates in narrow fissures where oxygen access is poor. It occurs in geometrically confined spaces such as the crevices where tube and tube sheet join. Examples are crevices under washers and areas under deposits on metal surfaces.

Pitting Corrosion: This is a localized type of attack producing cavities penetrating deeply in the metal at a much faster rate than general corrosion. Pitting is particularly serious in heat exchangers because of thin walls and large area of the heat exchangers.

Intergranular Corrosion: This form of attack occurs along grain boundaries of a metal, usually due to depletion of an alloying element. This process can occur in austenitic stainless steels in low temperature geothermal environments, but only if the stainless steel is defective in heat treatment. An example is weld decay, which may occur near the hot zone of a welded seam in stainless steel.

Selective Leaching: This is a form of corrosion whereby one component of an alloy is preferentially corroded, while the more noble metal remains behind. Examples include dezincification of brasses and de-aluminification of aluminum alloys.

Stress Corrosion: SCC is the cracking of an alloy as a result of the interaction of stress, applied or residual from forming and fabrication and a specific environmental factor. For example, some stainless steels are cracked by chlorides under certain conditions and some copper alloys are attacked by traces of ammonia.

Erosion Corrosion: This is a form of corrosion found whenever a metal is subjected to flow of electrolyte or abrasion in the presence of a corroding medium [42,43].

In addition, nonmetals do not generally dissolve like metals. They are degraded or corroded because of swelling, loss in mechanical properties, softening, hardening and discoloration. A number of methods have been utilized to control corrosion and scaling

in geothermal systems. One of the common methods is the use of inhibitors and the control of carbonate-bicarbonate equilibrium by controlling the pH and CO_2 partial pressure and by periodic cleaning. Alternative protection techniques include the careful selection of appropriate materials and the application of coatings on the material surface. The effectiveness of the protective coating depends on the pretreatment of the surface and the conditions during application.

2.2.2.2 Scaling

Scaling occurs when water has high levels of minerals like calcium carbonate, which can build-up on surfaces. These chemicals are dissolved in the water under conditions of elevated temperature and pressure. Slight scaling can be considered beneficial in that the inside surfaces of pipes become coated with harmless minerals that act as a barrier to corrosion. Scaling has a number of hazardous effects such that pipes become blocked and therefore needs to be replaced in a shorter period of time, wells become blocked and they need to be drilled out so some environmental problems may arise. Scaling is also dependent on roughness of pipe surface. Except for a few isolated cases, there are only two chemical compounds that are responsible for scaling. These are silica (SiO_2) and calcium carbonate ($CaCO_3$) [31].

Pipes are the most common place for scale formation in a water system. The degree of scaling can be predicted using a Saturation Index (SI). The SI is a calculation that compares the actual pH to a theoretical pH based on physical and chemical properties of water. The values range from negative to positive. Negative numbers indicate a potential for corrosion and positive numbers predict scale formation. Values close to zero indicate that the water is balanced and there should not be problems from either corrosion or scaling [44].

CHAPTER III
PIPING MATERIALS IN GEOTHERMAL APPLICATIONS

3.1 Types of Piping Materials

A great variety of piping materials for geothermal heating systems have been utilized with great variation in cost and durability. These include carbon and stainless steel, asbestos cement (AC), ductile iron (DI), slip-joint steel (STL-S), gasketed polyvinyl chloride (PVC-G), solvent welded PVC (PVC-S), chlorinated polyvinyl chloride (CPVC), polyethylene (PE), cross-linked polyethylene (PEX), fiberglass reinforced plastic with mechanical joint (FRP-M), FRP with epoxy adhesive joint (FRP-E), FRP with gasketed joint (FRP-S), and threaded joint FRP (FRP-T) [1]. The temperature and chemical content of geothermal fluids, in addition to cost, usually determines the type of pipeline material to be used. Figure 3.1 shows the temperature limitations of some typical materials used in geothermal applications.

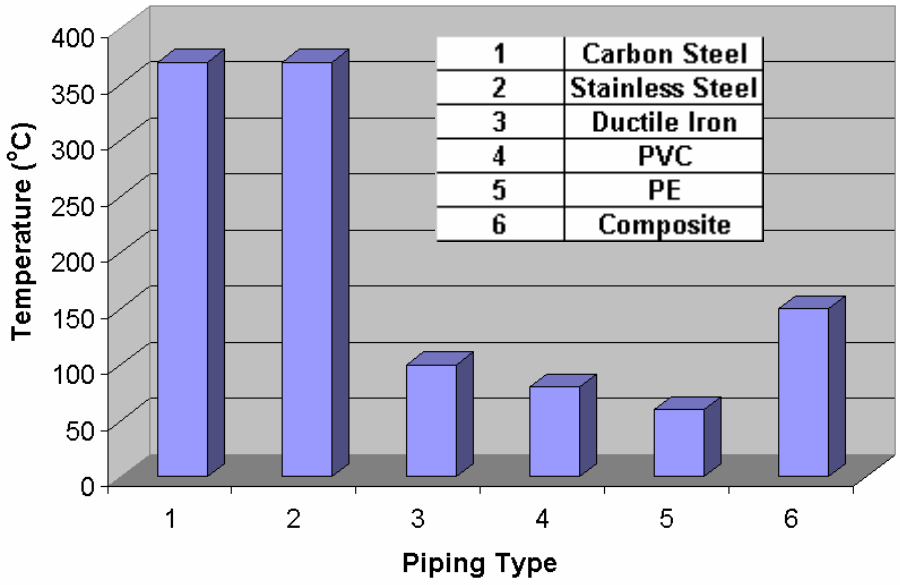

Figure 3.1 Maximum service temperatures for typical piping materials used in geothermal applications.

Both metallic and nonmetallic piping materials can be considered for geothermal applications. Carbon steel is the most widely used material and has an acceptable service life if properly applied [41-43]. Ductile iron has also found limited application. Asbestos cement (AC) was the most widely applied product; however, environmental

concerns have limited its use and availability. The attractiveness of metallic piping is primarily related to its ability to handle high temperature fluids. In addition, its properties and installation requirements are familiar to most installation crews. The advantage of non-metallic materials is that they are virtually impervious to most chemicals found in geothermal fluids. However, the installation procedures, particularly for fiberglass composites and polyethylene are, in many cases, outside the experience of typical laborers and local code officials. This is particularly true in rural areas. The following sections review some specifics of each material and cover some problems encountered in existing geothermal systems. Table 3.1 shows the cost of composite and steel pipes with various diameters. Table 3.2 shows the cost of uninsulated composite pipes. This information was taken from Technoplast Inc on May, 2003.

Table 3.1 The cost of composite and steel pipes with various diameters.

No	Diameter (Inner Pipe)	FRP+PU+FRP (coat) Unit Cost Euro/m	Steel+PU+PE (coat) Unit Cost Euro/m
1	DN - 50 / 125 mm	15.00.-	10.00.-
2	DN - 65 / 125 mm	17.50.-	11.00.-
3	DN - 80 / 150 mm	20.00.-	13.20.-
4	DN - 100 / 200 mm	26.30.-	21.00.-
5	DN - 125 / 200 mm	26.80.-	22.00.-
6	DN - 150 / 250 mm	36.40.-	26.20.-
7	DN - 200 / 300 mm	46.50.-	40.50.-
8	DN - 250 / 350 mm	65.00.-	49.00.-
9	DN - 300 / 400 mm	74.50.-	---

Table 3.2 The cost of uninsulated composite pipes.

No	Diameter (Inner Pipe)	Unit Cost Euro/m
1	DN - 50 mm	6.00.-
2	DN - 65 mm	8.80.-
3	DN - 80 mm	9.60.-
4	DN - 100 mm	10.20.-
5	DN - 125 mm	12.80.-
6	DN - 150 mm	16.00.-
7	DN - 200 mm	21.00.-
8	DN - 250 mm	31.00.-
9	DN - 300 mm	37.20.-

3.2 Performances of Piping Materials Subject To Geothermal Fluid

3.2.1 Carbon and Galvanized Steel

The maximum service temperature of carbon and stainless steel is 370^{o}C. Corrosion is a major concern with steel piping, particularly in geothermal applications. In many geothermal fluids, there are various concentrations of dissolved chemicals or gases that can result primarily in pitting or crevice corrosion on metallic surfaces [33,41]. If the potential exists for this type of attack, or if the fluid has been exposed to the air before entering the system, carbon steel should be the material of last resort. Steel piping is used primarily on the clean loop side of the isolation heat exchanger, although in a few cases it has been employed as the geothermal transmission line material.

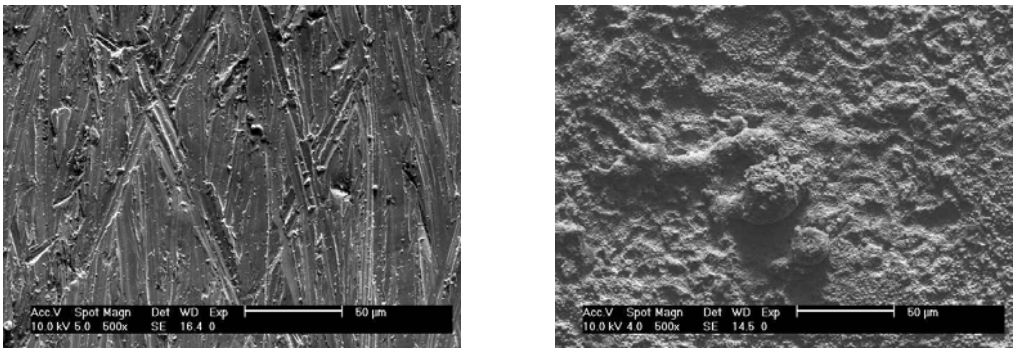

(a) **(b)**

Figure 3.2 (a) Dry steel pipe and (b) corrosion on steel pipe under geothermal fluid for 45 days (SEM analysis by M. Toğulga and M. Tanoğlu).

Corrosion of carbon steel pipe due to exposure to geothermal fluid was also investigated by Toğulga and Tanoğlu. For this purpose, samples of steel pipes were exposed to geothermal fluid of Balçova Geothermal District Heating System for 45 days and then the surface of the material was analyzed with Scanning Electron Microscopy (SEM) to compare the surface of steel pipe which is not exposed to geothermal fluid. It was observed that the surface was corroded extensively due to geothermal exposure as shown in Figure 3.2.

A distinct disadvantage of using steel pipe is that the buried pipe is also subject to external corrosion unless protected with a suitable wrapping or cathodic protection. The potential for external corrosion of metallic pipe systems should be considered for all direct buried installations. Various soil types, presence of groundwater, and induced

current fields from power lines may accelerate external pipe corrosion and early system failure.

Galvanized steel has been employed with mixed success in geothermal applications. Some geothermal fluids have demonstrated the ability to leach zinc from solder and other alloys. Selective removal of the zinc from galvanized pipe could result in severe pitting corrosion. In addition, consideration should be given to the fact that the protective nature of the zinc coating is generally not effective above 60°C [1]. As an example, Figure 3.3 shows pre-insulated carbon steel pipe system that was used in Balçova Geothermal District Heating System. Insulation material is polyurethane wrapped with E-glass reinforced composite.

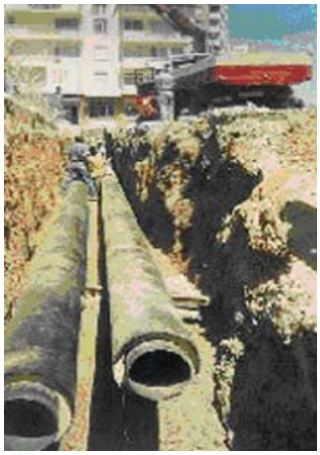

Figure 3.3 Carbon steel pipe that is used in Balçova Geothermal District Heating System in Izmir [37].

3.2.2 Ductile Iron

Ductile iron is another metal that has found piping application in geothermal systems. Ductile iron is similar to cast iron with the exception of the form of the carbon rich phases. However, in cast iron, the carbon (graphite) is in a flake-like structure. In ductile iron, the structure is more spherical or nodular. This small difference results in the greater strength, flexibility, and machinability from which the product derives its name. Ductile iron has been described as more corrosion resistant than cast iron. However, the slight difference in corrosion resistance would not be of any substantive meaning in most geothermal applications [1].

As an iron material, ductile iron is susceptible to corrosion from both external and internal sources. External protection generally involves a moisture barrier. For a pre-insulated product, special moisture protection would only be required at the joints

and other fittings. A lining usually provides internal corrosion protection. The two most common materials are cement mortar and coal tar epoxy. Coal tar epoxy is limited to a temperature of approximately 50°C. Mortar lining, according to the Ductile Iron Pipe Producers Research Association, is suitable to a service temperature of 65°C with a protective seal coat. Without the seal coat, maximum service temperature is 100°C. In some applications with very soft water, a leaching of the mortar lining has been observed when a seal coat is omitted. As a result, a special high temperature epoxy coating would be required.

Ductile iron is a much-thicker-walled product than standard carbon steel and, for uniform corrosion applications, offers the probability of longer life. In geothermal applications, corrosion occurs by both uniform and pitting modes [1]. Ductile iron piping is cost competitive with asbestos cement material. In addition, its common use in water supply systems results in wider familiarity with its installation practices. However, ductile iron pipe is the heaviest material of those covered. As a result, it would incur additional handling costs in comparison to the lighter weight materials.

3.2.3 Copper

Copper piping, one of the most common materials in standard construction, is generally not acceptable for geothermal applications. Most resources contain very small quantities of hydrogen sulfide (H_2S), the dissolved gas that results in a rotten egg odor. This constituent is very aggressive toward copper and copper alloys. In addition, the solder used to join copper has also been subject to attack in even very low total dissolved solid (TDS) within fluids. For these reasons, copper is not recommended in systems where it is exposed to the geothermal fluid [1].

3.2.4 Cross-Linked Polyethylene (PEX)

Cross-linked polyethylene is a high-density polyethylene material in which the individual molecules are "cross linked" during the production of the material. The effect of the cross-linking imparts physical qualities to the piping, which allow it to meet the requirements of much higher temperature/pressure applications than standard polyethylene material. PEX piping carries anominal rating of 6.8 atm at 82°C. Joining the piping is accomplished through the use of specially designed, conversion fittings, which are generally of brass construction. Since the piping is designed primarily for use

in hydronic radiant floor, sidewalk and street (snow melting) heating systems, a variety of specialty manifolds and control valves specific to these systems are available [1].

The tubing itself is available generally in sizes of 10 cm. and less with the 1.5 cm. and 2.5 cm. diameter most common. Piping with and without an oxygen diffusion barrier is available. The oxygen barrier prevents the diffusion of oxygen through the piping wall and into the fluid. This is necessary corrosion prevention for closed systems in which ferrous materials are included. Larger sizes of the PEX material are available as either bare or pre-insulated. The pre-insulated product is sold in rolls and includes corrugated polyethylene jacket and closed-cell polyethylene insulation. Rubber end caps are used to protect the exposed insulation at fittings. The flexible nature of the pre-insulated product offers an attractive option for small-diameter distribution and customer service lines in applications where it is necessary to route the piping around existing utility obstacles [1].

3.2.5 Polyvinyl Chloride (PVC) and Chlorinated Polyvinyl Chloride (CPVC)

PVC is a low-temperature (maximum service temperature is 80°C) rigid thermoplastic material. It is, next to steel, the most commonly available piping material. Common ratings used for plumbing applications are Schedule 40 and Schedule 80. The most common method of joining PVC is by solvent welding. The Schedule 80 material can also be threaded. Most types of fittings and some valves are available in PVC up to approximately 30 cm. in diameter. CPVC is a higher temperature rated material with a maximum temperature rating of 100°C. Pressure handling ability at this temperature is very low (as is PVC at its maximum temperature) [1].

3.2.6 Polyethylene (PE)

Polyethylene is in the same chemical family (polyolefin) as polybutylene and is similar in physical characteristics. It is a flexible material available in a wide variety of sizes from 1.3 to 106 cm. diameter. To date, this material has seen little application in direct-use geothermal systems, primarily because of its maximum service temperature of 60 to 65°C. The piping is recommended only for gravity flow applications above this temperature. Very high molecular weight/high density PE can be employed for low-pressure applications up to temperatures as high as 80°C. The SDR (standard dimension ratio--a wall thickness description) requirements under these conditions, however, greatly reduce the cost advantages normally found in polyethylene [1].

3.2.7 Fiberglass Composites (RTRP)

Fiberglass composite piping commonly referred to as RTRP (reinforced thermosetting resin pipe) or FRP (fiberglass reinforced plastic) is available in a wide variety of configurations. Two main matrix materials are epoxy and polyester resins. In addition, the piping is available in lined and unlined versions. The epoxy or polyester resin piping with a liner is generally selected for geothermal applications. Both epoxy and polyester resin systems can be compounded to be serviceable to temperatures of 150°C [1]. Regardless of the type of fiberglass material used, care must be taken to maintain operating pressure low enough to prevent flashing of hot fluids. At high temperatures (>boiling point), the RTRP systems are susceptible to damage when fluid flashes to vapor. The forces associated with the flashing may affect the fibers at the interior of the pipe surface.

As with all nonmetallic piping, the method of joining is a large consideration with respect to both installation time and expense. With FRP piping, a variety of methods are available, including mechanical (keyed, threaded and flanged) and adhesive type jointing. Of these, the bell and spigot/adhesive has seen the widest application in geothermal systems [1]. Figure 3.4 is an example showing the glass-fiber reinforced polyester composite pipes manufactured by filament winding technique and installed in Çeşme Geothermal District Heating System in 2002. The composite pipe had a polyurethane insulation and FRP cover. This figure also shows the joining operation for the mentioned composite pipes in the same system.

Figure 3.4 Fiberglass pipe (composite) that is used in Çeşme Geothermal District Heating System.

Table 3.3 summarizes the type of pipe materials used in geothermal applications, their maximum operating temperature and corrosion types observed in service. According to Table 3.3, composites, which have high performance, are promising pipe materials for future applications.

Table 3.3 Comparison of the pipe materials used in geothermal application.

Pipe Materials	Max. Temperature	Corrosion Type	Durability
Carbon Steel	370^{o}C	Uniform corrosion and pitting	Moderate
Stainless Steel	370^{o}C	Pitting and crevice corrosion	Moderate
Ductile Iron	100^{o}C	Uniform corrosion and pitting	Moderate
PVC	80^{o}C	Creep rupture	Low
PE	60^{o}C	Creep rupture	Low
Composite	150^{o}C	Corrosion resistant	High

CHAPTER IV.
PROCESSING AND PERFORMANCE OF COMPOSITE MATERIALS

4.1 Composites

4.1.1 Fundamentals of Composites

Composites are made by combining two or more materials to obtain a new material that has unique and superior properties as compared to its constituents. These materials offer some significant advantages to metals in many structural applications. These advantages are due to the ability to select various combinations of fiber reinforcement and resin material. Usually, one phase (the matrix) is continuous and completely surrounds the (the dispersed phase). The matrix acts an adhesive to bind the fibers together, keep the integrity of the composites and transfer the load onto the reinforcement constituent fibers. It also protects the fibers from environmental stress and physical damage that could initiate cracks [45].

There are a variety of materials to select from when one is faced with designing a new structure or redesigning a previous structure to meet new requirements or operational conditions. Metals are well-established materials. Although they represent a good, baseline material for many initial designs and structural applications, metals and their alloy derivatives often have disadvantages that make them unacceptable for many applications. The aerospace industry has relied heavily on aluminum and titanium alloys because they are lighter than steels and are relatively easy to work with. But aluminum and titanium have not met all of the requirements placed upon them by such a demanding industry. For instance, they often exhibit poor corrosion resistance to salt water and harsh environments; they are heavier than desired when compared to polymers, foams, and composite materials and their inadequate fatigue endurance at operational limits often causes parts to fail prematurely. Their tensile strength and stiffness are only moderate compared to those of steel, although their lighter weight makes them attractive on the same basis.

Composite materials have many advantageous over traditional material. Chief among these are high strength, lightweight, design flexibility, parts consolidation, electrical insulating properties, dimensional stability, corrosion resistance and low

tooling cost. As a result of superior performance capabilities, composites have virtually replaced traditional materials in many applications.

High Strength

Composite materials can be designed to meet the specific strength requirements of an application. A distinct advantage of composites, over other materials, is the ability to use many combinations of resins and reinforcements, and therefore custom tailor the mechanical and physical properties of a structure.

Light Weight

Composites offer materials that can be designed for both light weight and high strength. In fact, composites are used to produce the highest strength to weight ratio structures known to man.

Corrosion Resistance

Composites provide long-term resistance to severe chemical and temperature environments. Composites are the material of choice for outdoor exposure, chemical handling applications and severe environment service.

Design Flexibility

Composites have an advantage over other materials because they can be molded into complex shapes at relatively low cost. The flexibility offers designers a freedom, which is a hallmark of composites achievement.

Durability

Composite structures have an exceedingly long life span. Coupled with low maintenance requirements, the longevity of composites is a benefit in critical applications. In a half-century of composites development, well-designed composite structures have yet to wear-out [45].

There are few types of composites including metal matrix composite (MMC), ceramic matrix composite (CMC) and polymer matrix composite (PMC). Most composites in industrial use are based on polymeric matrix. These are usually reinforced with aligned ceramic fibers, such as glass or carbon. They commonly exhibit marked anisotropy, since the matrix is much weaker and less stiff than the fibers. There has been considerable interest in metal matrix composites, such as aluminum reinforced with short fibers and titanium containing long, large-diameter fibers. The property enhancements being sought by the introduction of reinforcement are often less pronounced than for polymers. Besides, ceramic materials can be classified into two major types: monolithic and composite. The major difference between these two is a

reinforcing phase. Adding a discontinuous phase such as whiskers, platelets, particulates or continuous fibers can reinforce ceramic materials [46].

4.1.2 Polymers

Polymers have conventionally been used for non-structural components in buildings, such as moldings, floor and wall coverings, pipes and windowsills [47]. In some bridges, polymeric bearings are used to allow thermal movement of the deck. In civil work, geosynthetics, which are polymeric sheets or grids, are used for soil reinforcement and drainage. Compared with other materials, the major advantages of polymers include lightweight, good corrosion resistance and flexibility of manufacturing. Since polymers can be molded, complex shapes can be formed in one piece, instead of a number of parts that need to be connected together. This can often translate into cost saving. Compared with steel and concrete, polymers have much lower stiffness. Low modulus, together with the tendency to creep, is a major disadvantage of polymer for structural applications, since there may be excessive deformation under service loading. Other disadvantages include loss of strength/stiffness at high temperature (above 100 - 200^{o}C, depending on the polymer) and degradation in the presence of ultra-violet light (from sun-light) [48].

4.1.2.1 Classes of Polymers and Properties

Polymers consist of random chains of hydrocarbons and can be classified into thermoplastics, thermosets and elastomers (or rubbers). Carbon atoms form the skeleton of the polymer chain. Along each chain, there are typically 1,000 to 100,000 carbon atoms, held together by covalent bonds. Therefore, the polymer chain is very stiff and strong. The overall properties of a polymer, however, are governed by the interaction of individual polymer chains with one another. In thermoplastics, the chains interact with one another through weak van der Waal's forces (Figure 4.1a). In other words, while there is strong bonding along the polymer chain, making it very difficult to deform, there is very weak bonding between the chains, allowing easy relative movement of one chain from the other. The stiffness values of thermoplastics are therefore very low, and range from 0.15 to 3.5 GPa at room temperature (Table 4.1). In thermosets, the individual chains interact through van der Waal's force as well as occasional cross-links. The cross-links are also hydrocarbon chains whose ends are bonded to the main polymer chains. Due to their presence, the stiffness of thermosets is higher than that of

thermoplastics. At room temperature, it ranges from 1.3 to 8 GPa. Elastomers or rubbers are thermosets with a small number of cross-links. Also, they have very low glass transition temperatures, which means that the van der Waal's force has disappeared at room temperature. Therefore, rubbers have very low stiffness values within the range of 0.002 to 0.1 GPa. In literature, a large number of papers have been published considering the mechanical behavior of neat polymers [49-53].

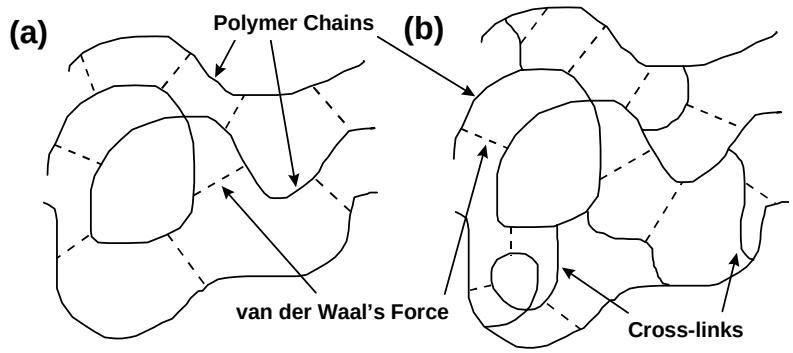

Figure 4.1 Differences between (a) thermoplastics and (b) thermosets [48].

Table 4.1 Typical values of Young's modulus (E at room temperature), tensile strength (σ_t) and glass transition temperature (T_g) for various polymers [48].

MATERIAL	E (GPa)	σ_t (MPa)	T_g(C)
Thermoplastics			
Polyethylene (PE), low density	0.15 - 0.24	7 - 17	-3
Polyethylene, high density	0.55 - 1.0	20 - 37	-125
Polypropylene (PP)	1.2 - 1.7	50 - 70	-20
Polyvinyl Chloride (PVC)	2.4 - 3.0	40 - 60	81
Thermosets			
Polyesters	1.3 - 4.5	45 - 85	110
Epoxies	2.1 - 5.5	40 - 85	130
Elastomers			
Polyisoprene	0.002 - 0.1	about 10	-73
Polybutadiene	0.004 - 0.1		-102

In some applications, the polymer matrix is a thermoset resin, which begins as liquid polymer and is converted to solid during the molding process. This conversion process, known as crosslinking, is an irreversible process. Therefore, composite materials made with thermosetting resins have increased heat and chemical resistance, higher physical properties and greater structural durability than composite materials made with thermoplastics. Selection of appropriate resin type enables the designer to vary the service temperature capabilities, chemical resistance properties, weatherability, electrical properties, fire resistance and adhesive characteristics of the finished composite.

Several important classes of thermosetting resins have been used as composite matrices in industry. These include the unsaturated polyesters, vinyl esters, epoxides, phenolics, polyimides and the modified versions of these resins such as interpenetrating networks. A thermosetting resin begins with polyfunctional monomers or oligomers, which are then cured to produce a three-dimensional network of covalent bonded chains, which are insoluble and infusible. Curing of a thermosetting resin involves chain extension, branching and cross-linking. Cross-linking imparts to the resin rigidity, high strength, solvent resistance and good thermal and oxidative stability. Thermoset matrix materials result in composites that have higher specific tensile strength and stiffness properties than metal matrix composites. Thermosetting resin composites are also more advanced in fabrication technology and lower in raw material cost and fabrication cost [45,48].

Unsaturated polyesters are very versatile polymers that impart to a fiber composite with a variety of properties at moderate cost. They are used mainly where a good balance is required between mechanical properties and chemical resistance at moderate or ambient temperatures. Their main weaknesses are:

- Relatively high shrinkage on curing
- Sensitivity to some solvents and chemicals especially under alkaline conditions
- Appreciable water absorption under certain conditions

Major areas of application for reinforced polyesters include appliances (air conditioner ducting, shower enclosures and tubs), business equipment (computer housing), consumer goods, corrosion resistant products, sporting goods (boat hulls), transportation (automotive ducting, car bodies and railroad cars) and construction (building wall and roof panels). Their poor impact resistance, inferior hot/wet

mechanical properties, limited shelf life and curing shrinkage preclude their utilization for high performance applications.

Unsaturated polyesters are made by reacting a glycol such as propylene glycol with an unsaturated acid (maleic anhydride) and cross-linking the resulting polymer with an unsaturated monomer (styrene, vinyl toluene and chlorostyrene). The first reaction is a condensation type reaction involving the formation of by-products such as water, which must be removed continuously. The cross-linking reaction occurs by addition-type polymerization reaction. The unsaturated polyesters are cured by adding free radical catalysts or indicators such as methyl ethyl ketone peroxide (MEKP), plus an accelerator such as cobalt naphthenate (CoNaP), diethyl aniline and dimethyl aniline (Figure 4.2). Anhydrides can be used to avoid the problem of by-product formation, thereby reducing the processing difficulty. Long chain reactants may be used to improve chemical resistance, thermal stability and shrinkage [45].

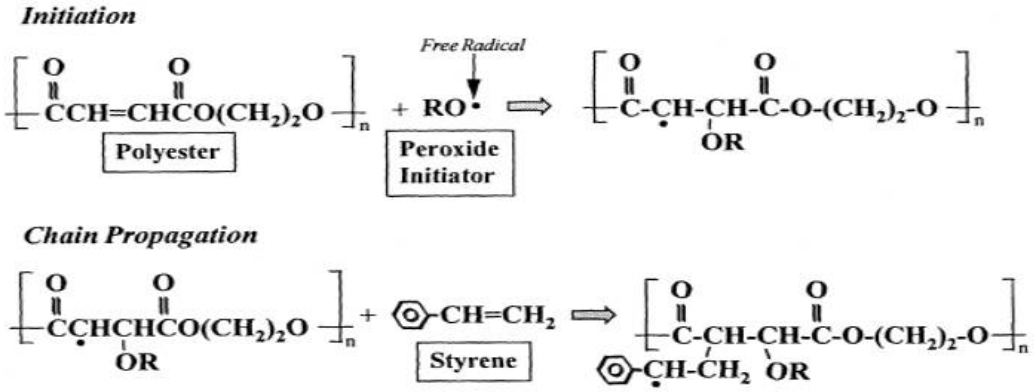

Figure 4.2 Crosslinking of unsaturated polyester.

Epoxy resins have good adhesion characteristics with glass, aramid and carbon fibers resulting in remarkable success as matrices for fiber composites. They also have good balance of physical, mechanical and electrical properties and have a lower degree of cure shrinkage than other thermosetting resins such as polyester and vinyl ester resins. Other attractive features for composite applications are relatively good hot/wet strength, chemical resistance, dimensional stability, ease of processing and low material costs. Epoxy resins are characterized by the existence of the epoxy group, which are three-membered ring with two carbons and oxygen. This epoxy group is the site of cross-linking and provides for good adhesion with solid substrate like a reinforcement surface.

Usually epoxy resins are used in conjunction with a curing agent to reduce curing time and to achieve desirable properties. Curing agents control properties such as chemical resistance, thermal stability and glass transition temperatures. Anhydrides provide good electrical insulating properties, thermal resistance and environmental stability. Aromatic amines give higher thermal resistance but require a higher cure temperature. In addition to hardeners, catalytic curing agents or accelerators may be used to aid in the curing of epoxide resins. Amine is a hardener, which reacts with epoxy groups (Figure 4.3). These agents include boron trifluoride, complexes of boron trifluoride and monoethyleneamine and stannous octoate [45].

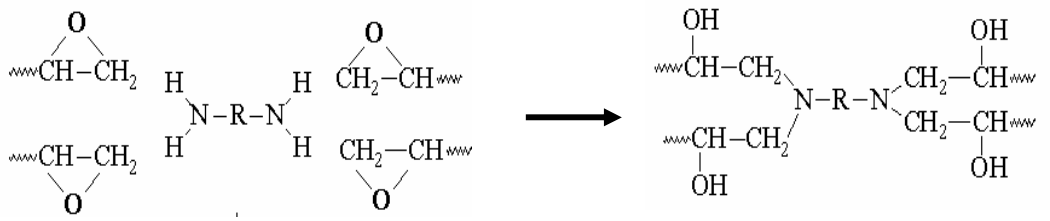

Figure 4.3 Crosslinking of epoxy groups.

4.1.2.2 Effect of Temperature on Polymer Properties

The properties of polymer can vary significantly with temperature. A typical variation of complex modulus (E) with temperature is shown in Figure 4.4. From the figure, one can observe a rapid change in E (of several orders of magnitude) within a narrow range of temperature. When heated to a certain temperature, the amorphous solid becomes softer, rubberlike and flexible, the polymer molecules now having sufficient energy to slide past one another; this temperature is called the glass transition temperature (T_g) of the polymer. What is happening physically is the gradual disappearing of van der Waal's force as the temperature goes through the transition range. When these secondary bonds between the polymer chains disappear, the chains become free to move relative to one another and the stiffness significantly decreases. Since the van der Waal's forces at different parts of the polymer structure do not disappear at the same time, the transition of behavior occurs over a range of temperature. It should be noted that the 'melting' of van der Waal's forces allows the sliding of polymer chain relative to one another. The relative sliding of chains, which takes time to happen, is the physical basis of viscoelastic behavior. Therefore, it is around the transition temperature where viscoelasticity is of greatest significance [48].

At temperature beyond the transition range, thermoplastics and thermosets behave in very different manners. In the absence of cross-links, the individual chains of a thermoplastic become free to slide relative to one another. The polymer therefore turns into a viscous liquid with reducing viscosity as temperature increases. This is a highly desirable feature as it makes possible the recycling of polymeric components. By heating up a piece of themoplastic, it will turn into a liquid that can be easily remolded into another geometric form. For thermosets, this is not possible. With cross-links, the polymer does not flow like a liquid. When the temperature is sufficiently high, the molecular bonds in the cross-links start to break. However, the bonds along the main polymer chain also break at the same time. The final result is the complete decomposition of the thermoset into gases.

Careful inspection of Figure 4.4 indicates a slight increase of E with temperature in the rubbery regime. The explanation, which is related to the entropy change of the material, is beyond the scope of this study.

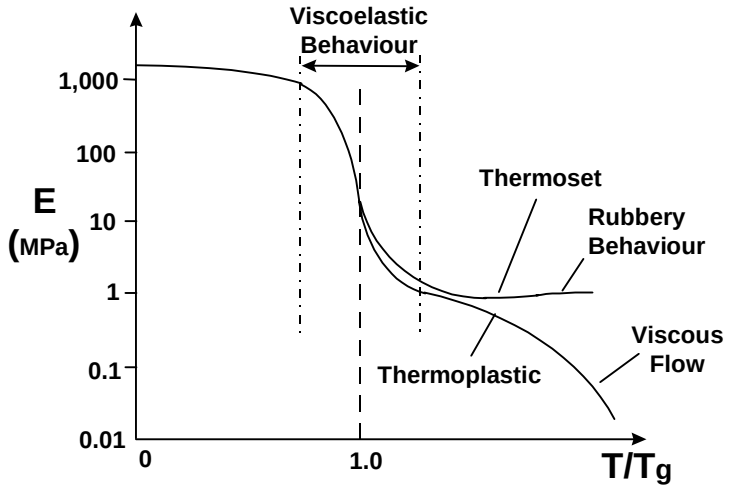

Figure 4.4 Variation of Young's modulus with temperature for thermoplastics and thermosets [48].

As temperature increases, the strength of polymer also decreases. The failure mode is also strongly dependent on temperature. Below about $0.75T_g$, polymers fail in a brittle manner by cracking. The cracking is usually initiated from small surface flaws due to machining or abrasion. At temperatures about -223^0C below T_g, a phenomenon called cold drawing is observed. Once a critical load is reached, the polymer chains start to straighten out and align themselves.

4.1.3 Fibers

Fibers are the reinforcement constituents in composites and mainly responsible to carry load and provide strength to the structure. Fibers made of glass are the most common materials, although high strength fibers such as aramid and carbon are used in advanced applications. All of the fibers, in generally have a high elastic modulus and strength other than fibers made of aramid. The diameter of a glass fiber is typically 10 μm, while it is smaller for other type of fibers such as carbon (7 μm). The glass fiber does not exhibit anisotropy along longitudinal and radial directions. The advantages of glass fibers include low cost, high tensile and impact strengths, and high chemical resistance. The disadvantages include relatively low modulus, self-abrasiveness, low fatigue resistance and poor adhesion to matrix resins. Typical compositions of three glasses used for fiber manufacture are E (electrical), C (chemical), and S (high tensile strength) type [45,46]. Table 4.2 shows compositions of glass used for fiber manufacture and their basic properties in fiber form. Glass fibers can be produced in the form of either continuous filament or staples. The glass is melted and fibers formed by passing the melted glass through small orifices.

Sizing materials are normally applied on to the surface of glass fibers immediately after forming to protect against mechanical damage, to improve adhesion between the fiber surface and matrix material and to ease handling. For glass reinforcement used in composites, the sizing usually contains a complex mixture of film, surfactant and a coupling agent to bridge the fiber surface with the resin matrix used in the composite. These coupling agents are usually organoslianes with the structure of X_3SiR, although sometimes titanate and the other chemical structures are used. The functional group, R may react with the polymer; the hydrolysable group, X can be hydrolyzed in the presence of water to form silanol groups on the surface of the glass fibers to form siloxanes.

Table 4.2 Compositions of glass used for fiber manufacture and their basic properties in fiber form [45].

Constituent	E-glass	C-glass	S-glass
SiO_2	55.2	65	65.0
Al_2O_3	14.8	4	25.0
B_2O_3	7.3	5	---
MgO	3.3	3	10.0
CaO	18.7	14	---
Na_2O	0.3	8.5	---
K_2O	0.2	---	---
Fe_2O_3	0.3	0.5	---
F_2	0.3	---	---

Specifications	E-glass	C-glass	S-glass
Liquidus temperature, ^oC	1140	---	---
Elastic modulus at 25 ^oC, kg/mm^2	7700	7400	8800
Density, g/cm^3	2.53	2.46	2.45
Coefficient of thermal expansion, 10^{-6} ^oC	5	8	5

4.2 Composite Fabrication Techniques

There are a great number of techniques to manufacture composite materials. These include pultrusion, resin transfer molding (RTM), reaction injection molding (RIM), compressing molding, sheet molding compound (SMC), injection molding, centrifugal casting, filament winding and tube rolling method. Each of these techniques produces specific part geometry, dimensions and available for special applications. Among these techniques, brief information is given in the following section about the methods to fabricate tubular shaped composites.

4.2.1 Pultrusion

Pultrusion is used for the manufacture of components having continuous lengths and a constant cross-sectional (i.e., rods, tubes, beams, etc.). The pultrusion process is one of the most cost-effective methods for the production of composite materials. It is a

continuous process that produces little waste material. In the pultrusion process for thermoset resins, fiber reinforcement is pulled through a resin impregnation area to coat the reinforcement with resin, through preform plates to begin to shape the fiber/resin bundle, and through a heated die to cure the resin. A cured part in the desired shape that requires no further processing exits from the die [54].

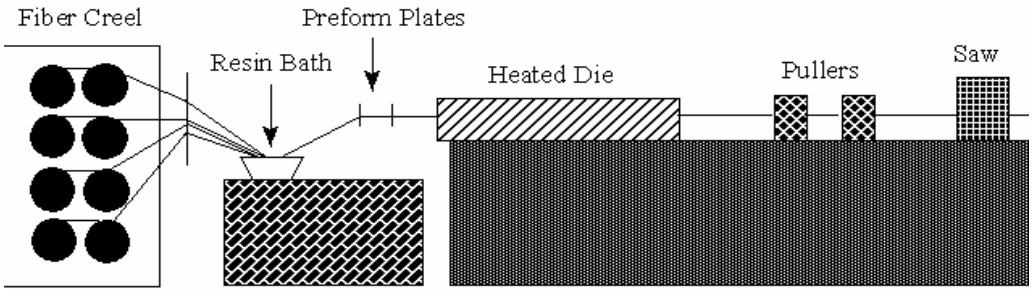

Figure 4.5 Pultrusion process [54].

Although the process appears to be simple (Figure 4.5), numerous process variables such as pull speed, die temperature, quality of fiber/resin wet-out, and fiber volume can affect the quality of pultruded composites.

4.2.2 Centrifugal Casting

Centrifugal pipe casting typically has involved depositing a reinforcing material and resin into a rotating mold. The g-forces created cause the composite material to press against the inside wall of the mold, coating it completely to form a hard pipe wall when cured. The speed of the rotation and pouring rate vary with size and shape being cast. In centrifugal casting, a permanent mold is rotated about its axis at high speeds (900 to 2400 rpm) as the reinforcing material and resin are poured. They are centrifugally thrown towards the inside mold wall, where it solidifies after cooling. Only cylindrical shapes can be produced with this process (Figure 4.6).

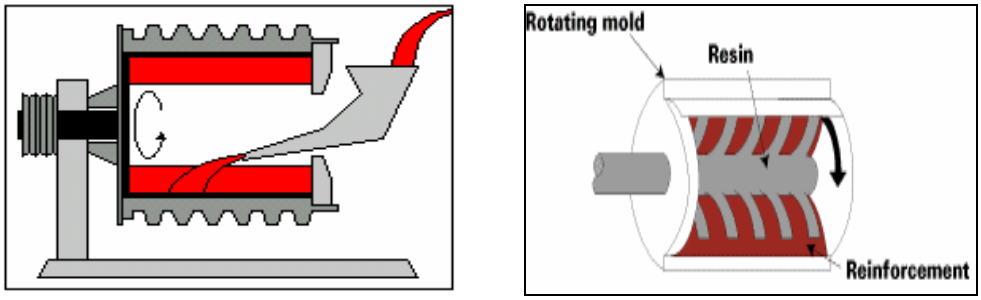

Figure 4.6 Centrifugal Casting process [55].

The 0/90 woven fiberglass fabric provides both longitudinal and hoop strength throughout the pipe wall. The cast pipe offers greater strength for the same wall thickness as filament-wound pipe wrapped in fiberglass roving at varying angles. To begin the wrapping process operators pull lengths of glass from spools of fabric, cutting each piece according to a specified ply schedule. The glass pieces are stacked on the table in a staggered fashion, parallel to the mandrel and the construction is rolled. The ply schedule is key to creating an even wall thickness throughout the pipe. Once the mandrel is wrapped, it is transported to a loading chute at the tubular casting mold, where an operator loads the mandrel into the mold. The inside diameter of the mold tube precisely controls the outside diameter of the finished pipe. As the mold spins, the fabric expands and spirals away from the mandrel to press against the inside wall of the mold, forming the exterior wall of the finished pipe. At this point, the spinning is stopped to manually extract the now bare mandrel. The pliant fiberglass fabric retains the mold shape and holds to the wall even while the mold is at a temporary standstill.

After the mandrel has been removed, the mold is reactivated to full rotational speed. A resin tube, which injects resin, is inserted. A resin counter meters the number of pump strokes required to thoroughly wet out the fiberglass, distributing the resin evenly throughout the length of the mold. The dense resin is forced through all the layers of fabric as the mold spins, creating a smooth finish on the outside of the pipe, as well as wetting out the entire structure. An excess of resin is pumped into the mold to create a neat. The resin layer affords the pipe its high corrosion and abrasion resistance and enhances flow characteristics. After about 1 hour, when the resin has cured, the spinning mold is stopped to extract pipe [56].

In addition, the other typical materials can be cast with this process such as iron, steel, stainless steels, and alloys of aluminum, copper and nickel. Two materials can be cast by introducing a second material during the process. Chopped strand mat is placed

into a hollow, cylindrical mold, or continuous roving is chopped and directed onto the inside walls of the mold. Resin is applied to the inside of the rotating mold.

4.2.3 Filament Winding

One of the main processes in producing composite structures with tubular shape and high performance is known as filament winding. Filament winding is a process for fabricating composite materials in which continuous fibers are wound onto a mandrel in a precise, predetermined pattern as illustrated in Figure 4.7. After the process, the fibers are inter-waved to form regular laminate, which can make more strength of fiber into full play than other composite technology.

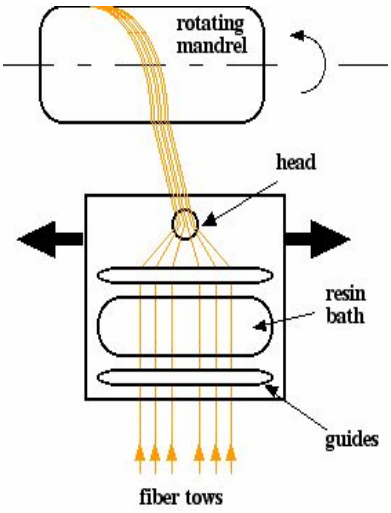

Figure 4.7 Schematic of Filament Winding process [54].

Filament winding is used for the manufacture of parts with high fiber volume fractions and controlled fiber orientation. Fiber tows are immersed in a resin bath where they are coated with low or medium molecular weight reactants. The impregnated tows are then literally wound around a mandrel (mold core) in a controlled pattern to form the shape of the part. After winding, the resin is then cured, typically using heat. The mold core may be removed or may be left as an integral component of the part.

The equipment comprises a creel stand, from which the fiber tows are fed under the required tension from a set of reels, a bath of resin, through which the fiber tows pass via a set of guides, a delivery eye, through which the fibers emerge, the position of which is controlled by a mechanical system and a rotating mandrel, onto which the fiber tows are drawn. The key parameters are the fiber tension, the resin take-up efficiency

and the winding geometry. The distribution of fiber tension in a filament wound part is very important. In addition to maintaining control of fiber position, fiber tension provides the pressure needed for compaction of the part. If the tension is too low, the compaction pressure imposed by one layer on the layers under it will be too low, resulting in resin reach areas between the layers of fiber. These areas are inherently weaker than areas of the material that have an optimal proportion of fiber and resin. This resin rich area is susceptible to delamination and matrix cracking when service loads are imposed. Just as low fiber tension can cause problems, so can extensively high tension. Differences in thermal expansion between the mandrel and composite during the cure state can produce high levels of tension in the fiber. If the resin gels while the fiber is in this state, the fiber tension is "locked in" as a residual stress. This also reduces the part's load-carrying capability, which is the burst strength for pressure vessels. The level of fiber tension during the fabrication of a filament-wound part varies with position within the part and with the stage of fabrication. When the resin viscosity is low enough, the fibers tend to move inward to a smaller radius due to the inward radial component of the fiber tension. This fiber movement displaces the resin, which must simultaneously flow outward through the fiber network [57].

In most cases, the eye motion and mandrel rotation systems are computer-controlled. Component shapes can be fairly complex, although they often exhibit a high degree of symmetry. There are also some limitations on the paths that the fibers take over the surface of the component. On any curved surface, there will be a tendency for the fibers to follow a geodesic path. This can cause problems with some shapes, since it may be difficult to ensure that fibers cover some parts of the surface, or lie in certain orientations. It is, however, possible to ensure that fibers follow certain non-geodesic paths, provided the delivery eye is moved appropriately and there is sufficient friction between the tow and the underlying surface.

Filament winding is a highly automated process by which the highest performing composite structures are manufactured. Filament winding is also therefore the most consistent and reproducible process for manufacturing composite tubular structures. It offers close control of fiber orientation, wet-out and tension while minimizing voids resulting in a superior part compared to most other composite manufacturing processes. Filament winding allows for precise machine control of varying axes of motion enabling the fabrication of complex part geometry as well as the fabrication of simple tubes and tanks.

This process makes high strength, hollow and generally cylindrical products such as pipe, storage tanks, pressure vessels and rocket motor cases. Veils are used for inner and/or outer surfaces to create a resin-rich surface for better corrosion resistance and aesthetics [46,54,57].

4.2.4 Tube Rolling

Pre-impregnated fiber is rolled on a mandrel to make a tube. Once rolled, each tube is wrapped tightly with high temperature shrink tape (Figure 4.8). However, there is an important parameter that all bubbles and wrinkles on the coat should be removed.

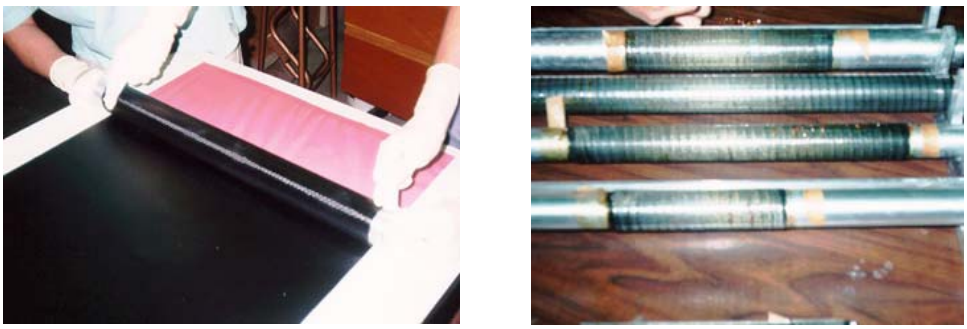

Figure 4.8 Tube rolling process [58].

The tape provides the necessary compression to reduce the number of strength-reducing voids present in the material. After curing stage, the mandrel is carried to an oven. This stage is named as post-curing. After that, the composite pipe is removed from the mandrel by using a ring.

4.3 Durability of Composites

It is widely acknowledged that the prediction of the durability of composite systems under mechanical and environmental loading is greatly complicated by the occurrence of several interacting physico-chemical and mechanical degradation mechanisms [59]. Durability analysis is the prediction of the properties of the material system for an imposed lifetime under an estimated complex mechanical loading history in interaction with changing environmental conditions [60]. The results of such a durability analysis are the necessary basis for a reliability estimation of the structural integrity of the component to be designed. In order for a polymer composite to have properties that are advantageous, the interface/interphase of the fiber and polymer matrix must have optimum adhesion. Moreover, adhesion must be maintained on

exposure to the environment, i.e. the interface/interphase must resist environmental degradation. In a microscale and using model composites, the influence of exposure to water on the interfacial strength of the fiber/matrix adhesion and on the glass fiber can be measured by a single-fiber fragmentation test [59].

4.3.1 Factors That Control The Durability of Composites

Some environmental effects have impact on the behavior of composites. Most applications involve the same environmental factors of temperature, moisture, mechanical loading and service life. Composites, which are composed of a resin, a fiber and several key interfaces (fiber-resin, layer to layer, porosity regions), present more of a challenge. Essentially more areas are open to attack. Temperature is often the most severe environmental effect. The impact of temperature on composite materials is felt over the entire service life of the part or structure from start to finish [60]. Initially, the part is subjected to cure and processing conditions which usually approach the upper limits of the resin matrix capability. Composites that cure at lower temperatures (for examples, room temperature up to 120 ^{0}C) usually have operational limits at or slightly above that condition.

Typical thermal environments often imposed on composite structures cover a wide range of conditions. These are thermal cycling, normal operational limits, extended limits, aeroheating and space environments. Thermal cycling due to solar radiation, daily temperature variations, use-temperature cycles, changes in location due to transportation and handling and other imposed cycles. Next one is the normal operational limits for static or isothermal exposure. Extended limits such as cryogenic storage tanks or operations in high temperature (engine blades), moderate temperature (aircraft leading edges) and low temperature (space structures) environments involve the full range of temperatures. Very often these exposures are of short duration (from a few seconds to a few hundred hours). If duration of exposure is very long, the exterior of the part is often protected with insulating materials. Aeroheating for nose cone and rocket motor applications requires careful analysis of the thermal stresses and a review of allowable elevated temperature mechanical properties. Finally, space environments couple several factors have such as long-term exposure, atomic oxygen attack, vacuum storage and the potential for wide temperature variations across the composite structure.

Although the fiber behaves in a rigid manner, the matrix material is often prone to creep or relax under load, particularly at elevated temperatures and long duration. Polymer matrix composites are considerably different and can exhibit pronounced creep and relaxation behavior at temperatures between (40^0C and 150^0C) where the operational loads can be susceptible to long-term deflections. They exhibit creep and relaxation phenomena as a result of their viscoelastic properties. In general, the composite materials have performed well under mechanical loading compared to metals often maintaining more than 60% of their static ultimate strength. Tension fatigue and stress rupture under tension loading have not had a substantial effect on composite strength degradation. The primary fatigue difficulty has been in compression fatigue. Fibers are normally designed to carry tension loads. Compression loading puts more dependence on the resin to transfer shear and compression loads to adjacent fibers and from layer to layer than does tensile loading. A number of studies have been reported about mechanical properties of resins [49-53].

Composites have been intensively used for many applications in humid environments. Water absorption has been recognized as the one of factors that affects the mechanical composite properties. In addition, hydrothermal aging induces matrix cracking, after a specific immersion time at temperature. There have been a number of some studies about internal interface damage during hydrothermal aging [61-71].

4.3.2 Degradation Mechanism Under Hot-Wet Environment

Composites absorb moisture through the matrix, fiber, fiber-matrix interface and porous regions or areas where microcracking (Figure 4.9) or delamination (Figure 4.10) has occurred. Absorbed water reduces strength, failure strain and Young's Modulus since water acts as a spacer between chains. Most effects of moisture and solution related degradation are on the strength of a composite, with changes in modulus, in most cases, being very small, generally of the order of 10% over a period of 10-15 years. However, it is noted that once the fiber itself is sufficiently degraded, changes in modulus of the composite can be fairly large. The loss of mechanical properties may be explained by the plasticization of the matrix and by the degradation of the fiber/matrix interface. Moreover, the progress of water molecules into the molecular structure swells the matrix, generating internal stresses and inducing loss of resilience. The fiber itself does not absorb moisture, except for the aramid fibers that can absorb up to 3 % of water (fully saturated) [61].

Delamination means the separation of ply layers due to adhesive failure. This also includes the separation of layers of fabric from the core structure. A delamination may be associated with bridging, drilling and trimming. The delamination in composites is caused by the interlaminar stresses produced by out-of-plane loading, eccentricities in load paths or discontinuities in the structure. Interlaminar stresses in a laminate may be created by variations in moisture content and temperature (the hygrothermal effect) [72-76]. Because of the differences in CTE (coefficient of thermal expansion) between neighboring plies, residual thermal stresses may be developed when the laminate is cooled down from the cure temperature to the end-use temperature. Delamination has long been recognized as one of the most life-limiting damage modes in composite laminates. The initiation and growth of delamination during the manufacturing or service life cycles of composites may result in the progressive reduction of stiffness and strength of these materials. In some cases, the degradation process is sudden and may result in catastrophic failure of the laminates.

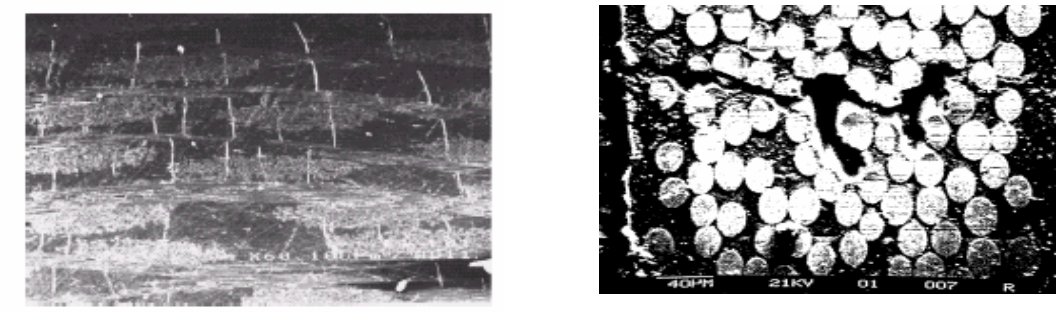

(a) **(b)**

Figure 4.9 Microcracks (a) in the matrix [61] and (b) within the intrabundle of fiber [6].

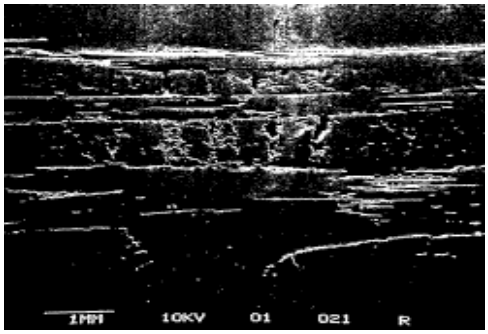

Figure 4.10 Delamination [6].

4.4 Testing Methods For Composite Tubes

4.4.1 Introduction

For years, composite pipe materials have had growing applications in different industries. Since composite pipes have been used for decades, design engineers are reluctant to specify composite for some applications unless there are reliable case history data or significant tests for predicting satisfactory performance. Fortunately, there are many standards and testing organizations whose purpose is to assure satisfactory performance of materials. One of them is the American Society for Testing and Materials (ASTM).

There are some works on the mechanical behavior of polymer-matrix composite tubular structures [4-28]. The testing of composite pipes is concentrated in four different ways in three of which a load may be applied: tension, compression and torsion and in the last one, water absorption tests were investigated [12].

4.4.2 Compressive Mechanical Testing on Composite Pipes

Compression test is conducted in a manner that the applied force is compressive and the specimen contracts along the direction of stress. The properties determined are compression strength, stress-strain response and compression modulus, generally in the fiber direction only, which means that the samples are compressed on their edge. The compressive strength values may vary with the size of the tube and with temperature and atmospheric conditions. In this test, a series of mechanical test is performed under various combination of radial and axial loading.

Ring testing, another configuration of testing tubular shapes, allows more efficient material usage as multiple tests to be performed from the same cylinder. Moreover, the failure mode in rings is the same as that in cylinders, indicating that the results are comparable with testing of pipes [8]. There have been a number of studies about compression test on composite pipes [4-11].

In one of these compression tests, Harte and Fleck studied axial compression test on the composite pipes. In this study, the specimen is circular cylindrical geometry braided from a single layer of 32 tows in the $+\theta$ direction and 32 tows in the $-\theta$ direction. The helix angle θ of the braid is controlled by expanding the braid over cylindrical mandrels of various diameters before casting with epoxy [9]. The minimum

achievable helix angle is $\theta = 21^0$ and the maximum is approximately 55^0. Table 4.3 shows that the dimensions of the specimens for compression test in this study.

Table 4.3 Dimensions of the specimens for each type of test for compression test in Harte and Fleck's test [9].

Helix Angle (θ)	Diameter 2r (mm)	Wall thickness t (mm)	Specimen gauge length l (mm)
23	25.37	1.20	25
30	31.75	1.15	35
40	42.20	0.98	42
55	53.0	0.93	53

In this study, the speed of crosshead is 0.033 mm/s, but according to ASTM standard, it should be 0.0217 mm/s and the length of specimen is 25 mm (D 348 – 89). After the test, the average inside and outside diameters of the specimen should be determined and then the average wall thickness of the specimen and the load on each specimen at the first sign of rupture should be measured.

The failure modes are dependent on the tow geometry, matrix material, tube geometry and the loading direction. After test, there may be four possible failure modes of braided tubes in compression: microbuckling, diamond shaped buckling, concertina buckling and Euler buckling as shown in Figure 4.11 [9]. In addition, collapse in transverse shearing may be the observed failure modes for filament wound composite pipes as shown in Figure 4.12 [10].

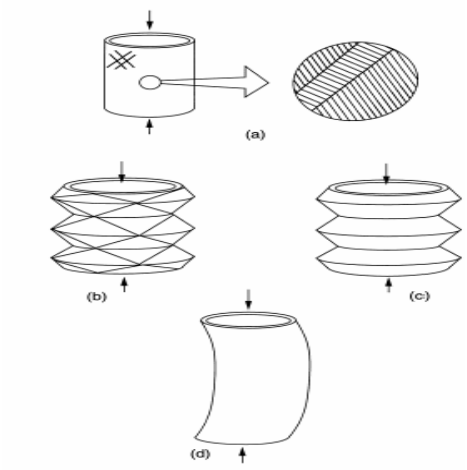

Figure 4.11 The four possible modes of buckling for braided circular tubes in axial compression **a**. Fiber microbuckling **b**. diamond shaped buckling **c**. Concertina buckling **d**. Euler macrobuckling [9].

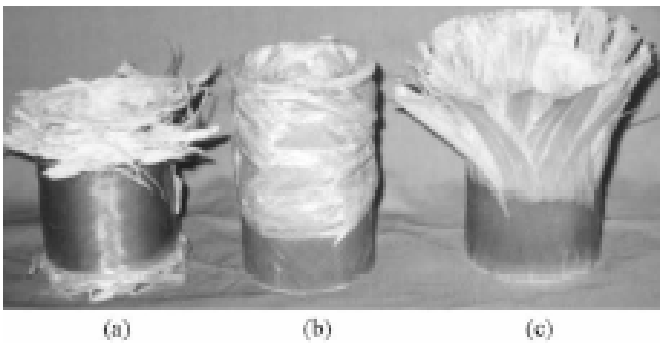

Figure 4.12 The three failure modes for filament wound composite pipes in axial compression **a.** Collapse in transverse shearing $(\pm[75]_n)$ **b**. Collapse in local buckling $(\pm[45]_n)$ **c**. Collapse in lamina bending $(\pm[15]_n)$ [10].

Microbuckling is a localised material instability involving the rotation of fibers within a narrow bandwidth about 20 fiber diameters. In Harte and Fleck's test, it occured in regular braids with $\theta < 35^0$. The result of this test revealed that for the braid of angle of $\theta = 23^0$ and 30^0 the composites failed by microbuckling and the measured nominal stress–nominal strain responses were given as in Figure 4.13. They consist of a single peak with a long tail. The residual compressive strength at the end of the test is associated with frictional sliding of the failure surfaces past each other. Out of plane microbuckles formed within individual tows near the crossover point with another tow, creating a saw tooth pattern around the specimen.

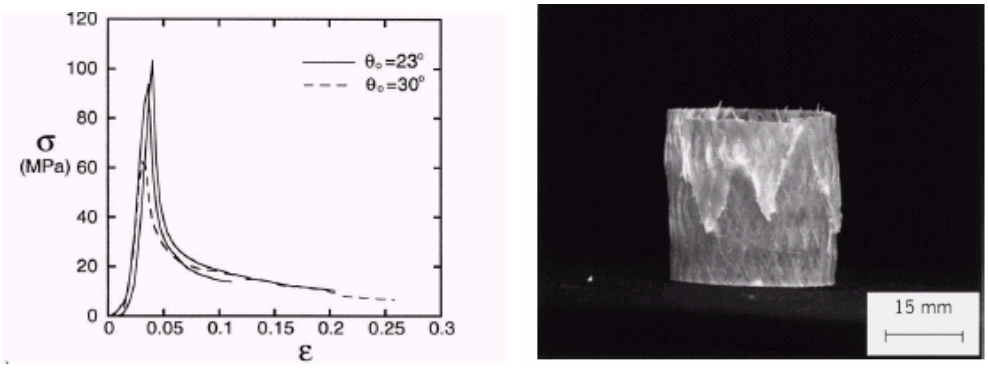

(a) **(b)**

Figure 4.13 (a) Nominal stress±nominal strain behavior for braids of initial helix angle $\theta=23^0$ and 30^0 failing by microbuckling in compression. **(b)** The sawtooth fracture path of a compressive specimen which has failed by microbuckling [9].

Diamond shaped buckling and concertina buckling are two competing shell-buckling modes. The axial collapse load and the buckle wavelength depend upon both the diameter of the tube and the wall thickness. The dominant mode depends upon the aspect ratio wall thickness to diameter and upon the ratio of circumferential to axial stiffness of the tube. Diamond shaped buckling occured in regular braids with $\theta > 35^0$. The braids of initial helix angle of $\theta = 40$ and 55 collapsed by a diamond shaped buckling mode; the associated nominal stress – nominal strain curves are shown in Figure 4.14. Collapse by diamond shaped buckling involves localized buckling along diagonal lines on the surface of the cylinders.

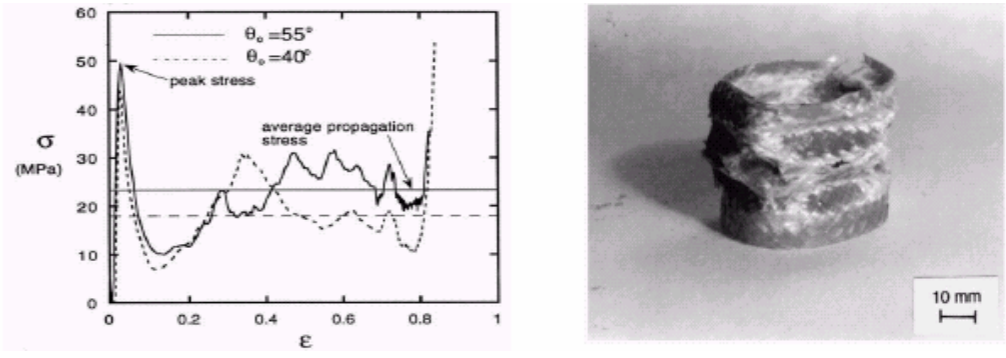

(a) **(b)**

Figure 4.14 (a) Compressive nominal stress vs nominal strain curves for braided tubes with braid angles $\theta = 40^0$ and 55^0 that have failed by diamond shaped buckling **(b)** Photograph of a $\theta = 40^0$ braid which has failed by diamond shaped buckling [9].

The nominal stress vs nominal strain curve displays an initial peak corresponding to the initiation of buckling. The folding pattern propagates along the length of the specimens until the entire cylinder has collapsed. The subsequent load maxima after the initial peak in the stress-strain curve correspond to the triggering of consecutive bands of folding in the cylinder.

There are several papers considering the axial compression of composite tubes. However, studies of lateral collapse behavior of composite tubes are scarce [11]. As an example, in this study, the composite pipes with different diameter and thickness were subjected to lateral crushing in compression test machine at a crosshead speed of 2 mm/min. The composite tubes of mean diameter to thickness ratio (D/t) varying from 7,33 to 39 are tested in lateral compression between rigid flat plates. These tubes are obtained commercially in the lengths of about 1 m from which specimens of different lengths are cut. In all experiments, load – deformation curves are obtained. The lengths of the tubes being different, load per unit length for all the tubes are plotted.

CHAPTER V
EXPERIMENTAL

5.1 Materials

Fiber reinforced polymer matrix composite pipes were produced by using filament winding and tube rolling methods. In these systems, polyester, epoxy and graphite particle added epoxy were used as a thermosetting resin. The weight fractions of the resin components used with these processes are shown in Table 5.1. The reinforcements were continuous filaments of E-glass and $0/90^0$ woven glass fabric used in filament winding and tube rolling method, respectively. The graphite particles incorporated into with matrix as filler was characterized with SEM. Figure 5.1 shows SEM micrograph of graphite particles and their chemical content.

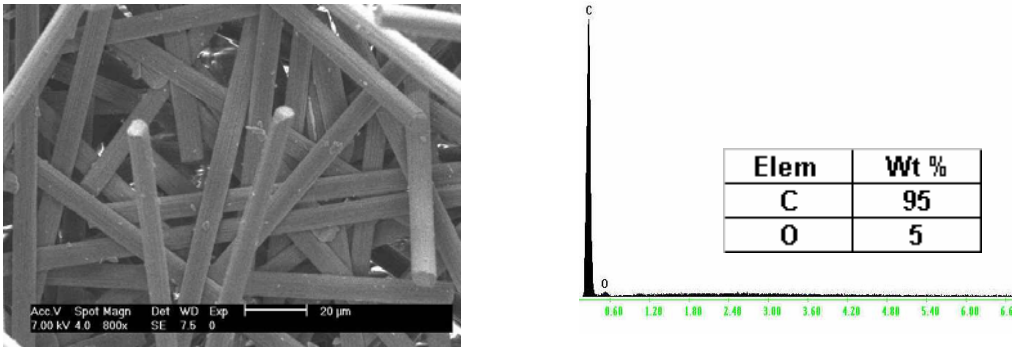

(a) **(b)**

Figure 5.1 (a) SEM micrograph of particulate graphite and (b) SEM-EDX analyses showing the chemical content of the graphite.

Table 5.1 Weight fractions of resin components used in fabrication of composite pipes.

Resin Types	Provider	Fraction on Curing Agent	Weight Fraction of Additive Graphite particles (gr)
Polyester CE 266	Camelyaf Inc., Turkey	1% Mekp 0.11% CoNap	-
Epoxy 816	Shell Inc.	55% of total resin	-
Graphite particles added Epoxy 816	Graphite Shell Inc.	55% of total resin	3%

* **CoNap** is Cobalt Naphthenate used as an *accelerator*

** **Mekp** is Methyl Ethyl Ketone Peroxide used as *initiators*

5.2 Processing of Composite Pipes

Composites in the form of cylinders were produced by filament winding and tube rolling techniques. Employing these techniques, three types of composite pipes; E-Glass/Polyester, E-Glass/Epoxy and E-Glass/Graphite particle added epoxy reinforced composite pipes were fabricated.

5.2.1 Processing by Filament Winding Technique

The angle ply tubes were manufactured by filament-winding technique. These tubes have a lamination of [± 67^{o}] configuration. The experimental setup was established on a lathe as shown in Figure 5.2. This mechanism consists of resin bath for impregnation of fibers, moving crosshead for angle and rotating mandrel for applying fibers. During the process, continuous rovings of E-glass fibers were wound around the cylindrical mandrel. During filament winding, fiber tows impregnated by the thermosetting resin were applied on a suitably shaped rotating mandrel with a diameter of 85 mm. Before the processing, the surface of mandrel was polished to remove roughness and a mold releaser agent was applied to ease the de-molding stage of part from the mold. At the end of this process, the mandrel was left for an hour for drying. After preparing the mandrel, the fiber tows were inserted into resin bath to be impregnated by the thermosetting resin as shown in Figure 5.3.

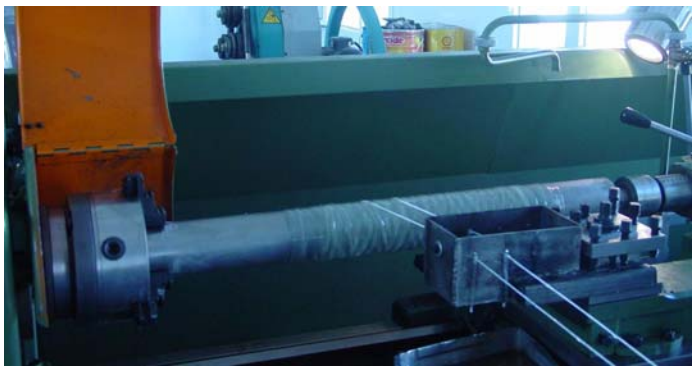

Figure 5.2 The experimental setup (filament winding machine).

Figure 5.3 The experimental setup (resin bath).

The tows were wound on the mandrel with a mandrel angular speed of 45 period/min. and winding angle of 67^{o} was obtained. The winding process was performed at room temperature (25^{0}C) and the full curing of the parts took about 2 hours (for polyester) and 8 hours (for epoxy and graphite particles added epoxy). After curing, the ends of pipes were trimmed properly using cutting implement in lathe. Afterwards, the pipe was taken from lathe and left in oven with the mandrel for post-cure. The post-curing took place at 120^{o}C for polyester and 140^{o}C for epoxy composite for about one and half-hour for each pipe. After post-curing, the pipes were left for cooling. Once the parts were cooled, the composite pipe was de-molded from mandrel using a metallic pushing ring.

5.2.2 Processing by Tube Rolling Technique

During tube rolling process, the woven glass fabric was used as reinforcement. Similar to filament winding process, the surface of the rolling mandrel was cleaned by polishing to remove roughness. After polishing, the surface of mandrel was treated with mold release agent to ease the de-molding of the part. The treated mandrel was left for an hour for drying in air. In the tube rolling process, the glass fabric was impregnated by the resins (polyester, epoxy and graphite particles added epoxy for each process) as shown in Figure 5.4. The pre-impregnated fiber was rolled on the metal mandrel to form tubes as shown in Figure 5.5. After rolling, the composite tubes were cured at room temperature (25^{o}C) for about 2 hours (for polyester) and 8 hours (for epoxy and graphite

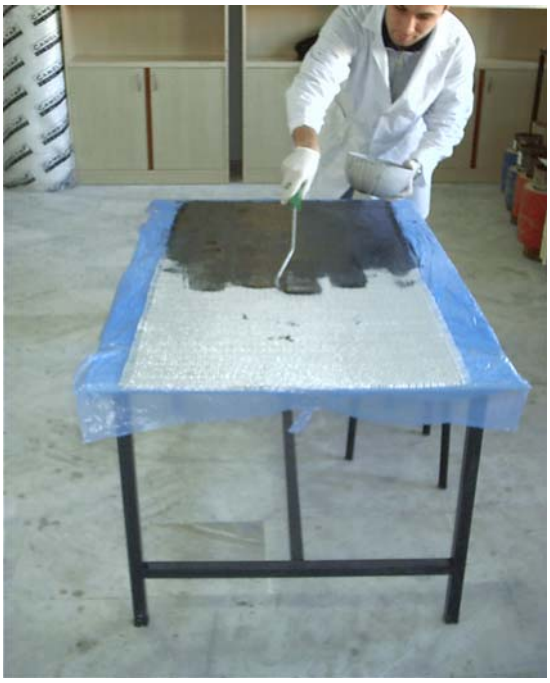

Figure 5.4 Pre-impregnation of the fiber.

particles added epoxy). After curing, the both ends of pipes were cut properly by using cutting implement in lathe. Afterwards, the pipe was left in oven with the mandrel for post-cure. The post-cure temperatures were 120^{o}C and 140^{o}C for polyester and epoxy composite pipe, respectively. It took one and half-hour for each pipe. The post-cured pipe was cooled in an open air. Finally, the pipe was de-molded from mandrel by using a separator metal ring.

Figure 5.5 Rolling of pre-impregnated fiber on the mandrel.

5.3 Measurement of Fiber Volume Fraction

Matrix burn-out technique was used to measure the fiber volume fractions. Sections of composite pipes were accurately weighted (3 specimens for each type of composite tube). The materials placed in ceramic pots were subjected to 650^{o}C for 1 hour to remove the matrix by burning. The remaining glass debris was then re-weighted. In practice, this provided a weight fraction but since the density of each component is known and void content was assumed to be negligible, the weight fraction allows derivation of an approximate volume fraction as below.

$$\vee_f = \frac{V_f}{V_f + V_m} \times 100 = \frac{(\frac{m_f}{\rho_f})}{(\frac{m_f}{\rho_f} + \frac{m_m}{\rho_m})} \times 100 \qquad (5.1)$$

where v_f is volume fraction, V_f and V_m are volume of fiber and matrix, m_f and m_m are mass of fiber and matrix and ρ_f and ρ_m are density of fiber and matrix, respectively.

5.4 Water Uptake Measurements of The Composite Pipes and Neat Polymers

The composite tubes were cut down to specified length of the test specimens to measure the specific water uptakes. The length and the inner diameter of the test specimens were 40 and 85 mm, respectively. In addition, the neat polymer samples (polyester, epoxy, graphite particles added epoxy) were prepared to replicate the polymer matrix. The neat polymer samples were casted in a metallic mold and cured following with a post-curing based on the conditions similar to composite pipe processing. The specimens were cut into 8 mm length for mechanical testing and durability experiments. Both the composites and neat polymers were left in distilled water tank (70^{o}C) and continuously flowing geothermal fluid bath (84^{o}C) to measure the weight gains of specimens until they were saturated to water absorption (Figure 5.6). The geothermal fluid was taken from B-10 well at Balçova Geothermal Field.

(a) **(b)**

Figure 5.6 (a) Distilled water tank and (b) geothermal fluid bath with continuous flow.

The water uptake values (M_t) were calculated from the equation (5.2). The water uptake values were plotted as a function of time as shown in Figure 5.7 and the exposure of the specimens were ended as the values reach to the saturation. The saturated specimens were carried to mechanical testing from geothermal bath to compression test machine, which took thirty minutes.

$$M_t = \frac{m - m_o}{m_o} \times 100 \qquad (5.2)$$

where M_t is water content percentage, m_o and m are weight of dry and wet specimens, respectively.

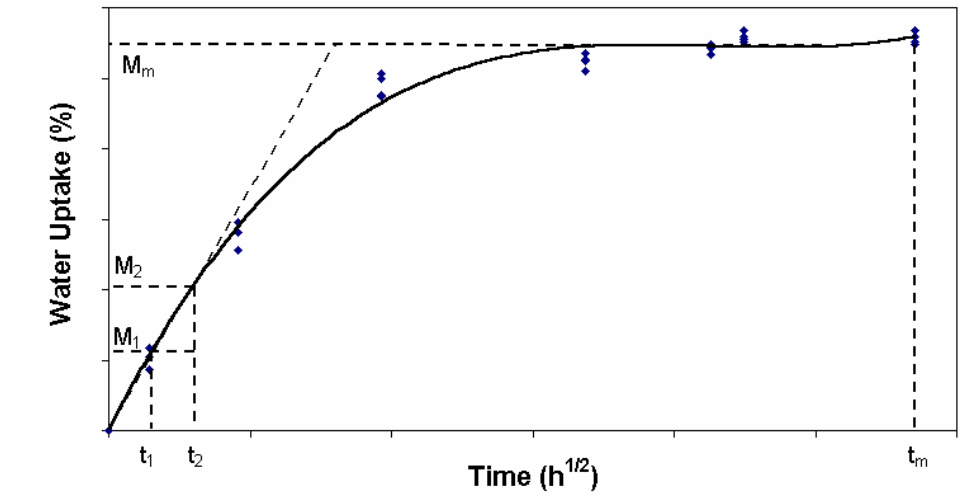

Figure 5.7 Example of water uptake percentage vs square root of time graph.

5.5 Determination of Diffusion Coefficient

It was assumed that the specimens are made in the form of a thin plate so that the water enters predominantly through the cross-section surfaces of the plate. The

value of maximum water content is constant when the specimens are fully submerged in a liquid. As seen from Figure 5.7, initially, the curve is straight line, the slope being proportional to the diffusivity of the material. The diffusion coefficient D was obtained from the initial slope of the M_m versus square root of time (Equation 5.3) [71].

$$D = \pi.\left(\frac{h}{4.M_m}\right)^2.\left(\frac{M_2 - M_1}{t_2 - t_1}\right)^2 \tag{5.3}$$

where h is thickness of the specimen, M_m is the maximum water content.

5.6 Mechanical Testing

The dry and wet specimens exposed to liquid environments were subjected to compressive mechanical testing. Firstly, two specimens for filament wound composite and three specimens for tube rolled composite were prepared for each test. The composite specimens were compressed to failure in axial and radial directions between parallel plates using a Schimadzu Universal test machine. The cross-head speeds were 3 mm/min and 5 mm/min, for axial and radial loading respectively. The test specimens under loading of various stroke values are shown in Figure 5.8 and 5.9.

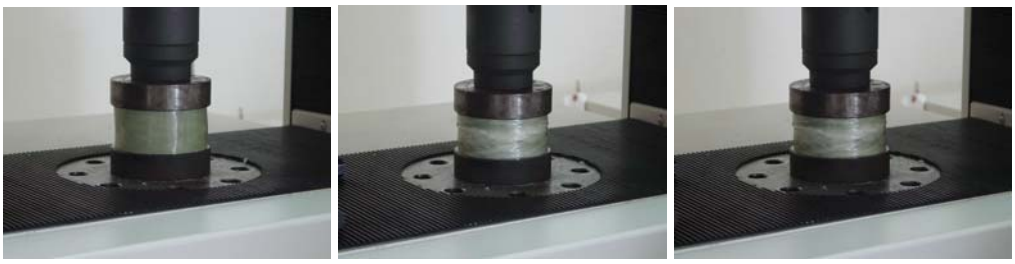

(a) x = 0 mm (b) x = 1.5 mm (c) x = 4 mm

Figure 5.8 Dry E-Glass/Epoxy composite pipe specimens under compressive loading in axial loading.

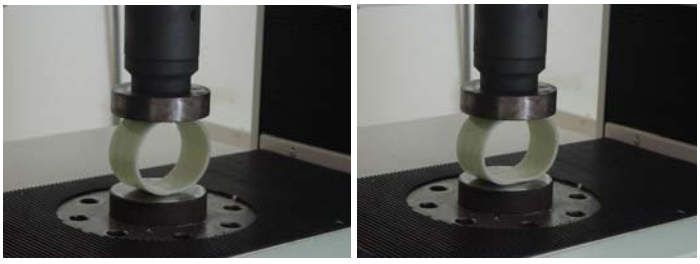

(a) x = 0 mm (b) x = 10.2 mm

Figure 5.9 Dry E-Glass/Epoxy composite pipe specimens under compressive loading in radial loading.

During the tests, the load-stroke values were acquired continuously and later stress-strain behaviors were obtained for specimens loaded in axial direction. The stress values were calculated from the applied load and cross-sectional area of the samples and the strain values from the initial length of the specimen and instantaneous cross-head displacements. Figure 5.10 illustrates the example of load-stroke and stress-strain graphs. The elastic modulus value is measured based on the slope of the initial linear portion of the stress-strain graphs. The fracture strength was defined as the peak stress value. Moreover, from the load-stroke graphs, the absorbed specific energies were calculated using the following equation (5.4) for compression under axial loading.

$$E_s = \frac{\int_0^{\delta f} p(\delta)\,d\delta}{A\rho\delta_f} \qquad \text{(J/kg)} \qquad (5.4)$$

where E_s is specific energy, A is the cross-sectional area of pipe, $P(\delta)$ is applied load, ρ is the material density and δ_f is the final crush displacement. Also, the absorbed energies were calculated by measuring areas under the load-stroke curves for compression under radial loading.

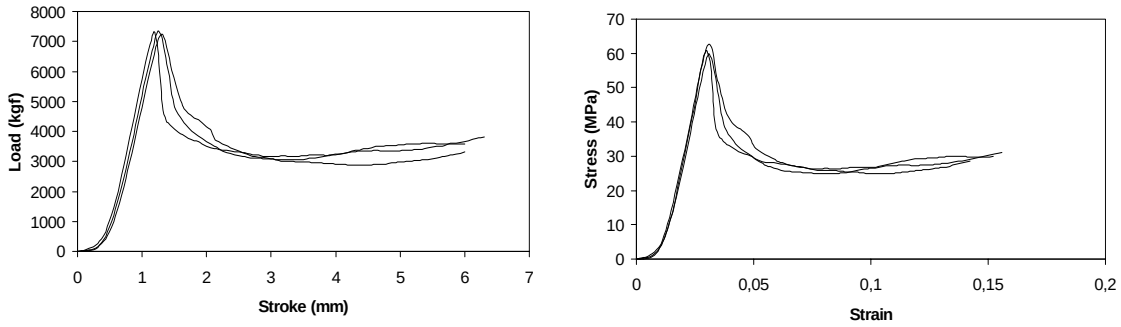

Figure 5.10 Typical load-stroke and stress-strain graphs for composite tubes compressed under axial loading.

In addition to tubular composites, model matrix materials were prepared to measure the compressive stress-strain behavior of the matrix polymer. For this purpose, polymers (polyester, epoxy and graphite particles added epoxy) with cubic shape were sectioned from the blocks of the materials. Five specimens were prepared for each test. The specimens were exposed to distilled water (70^{o}C) and continuously flowing geothermal fluid (84^{o}C) located at Balçova Geothermal Field. After saturation of the specimens, the dry and wet specimens were subjected to compressive loading with 3

mm/min cross-head speed, using Schimadzu Universal test machine. During the test, load and stroke values were recorded and then the stress-strain graphs were obtained based on the procedure described for composites. The elastic modulus, stress and strain values at yield were determined.

5.7 Analysis of the Residues on Material Surfaces Exposed to Geothermal Fluid

As a case study, the surfaces of E-Glass/epoxy composite pipe specimens exposed to geothermal fluid and distilled water were analyzed with Scanning Electron Microscopy (SEM) to observe the residual components on composite pipe. The residual components were also investigated using Energy Dispersive X-Ray (EDX spectroscopy). Before the analyses, the specimens were dried to prevent shriveling. The SEM samples were coated with a very thin layer of gold by a sputter coater to provide electrical conductivity on the surface.

5.8 Measurement of Thermal Conductivity

Thermal conductivity (k) of the material is a measure of the ability of a material to conduct heat. It can be defined as the rate of heat transfer through a unit thickness of the material per unit area per unit temperature difference. A large value for thermal conductivity indicates that the material is a good heat conductor and a low value indicates that the material is a poor heat conductor or insulator [77]. To measure the thermal conductivity of composites, hot-wire method with Shotherm QTM machine in Dokuz Eylül University Mechanical Engineering Department was used. Three specimens from each set were prepared in the shape of rectangle prism with dimensions of 50x100x15 mm. In this method, a metal wire, the hot-wire, is immersed in the substance whose properties are to be measured. A constant power is supplied to the heater element and the temperature rise ΔT of the heating wire is measured by a thermocouple and recorded with respect to time during a short heating interval. The thermal conductivity (k) of the sample is calculated from the temperature ± time ($\Delta T \pm \Delta t$) record and power input. The thermal conductivities of various materials used in geothermal piping at room temperature are given in Table 5.2. The thermal conductivities of materials vary over a wide range, as shown in Figure 5.11.

Table 5.2 Average thermal conductivity values for common piping and insulating materials used in geothermal direct use applications [77].

Material	k (W/m.K)
Carbon Steel	63.9
Stainless Steel	15.1
Polyurethane Foam	0.026
Fiberglass Coat	0.036
Soil	0.52

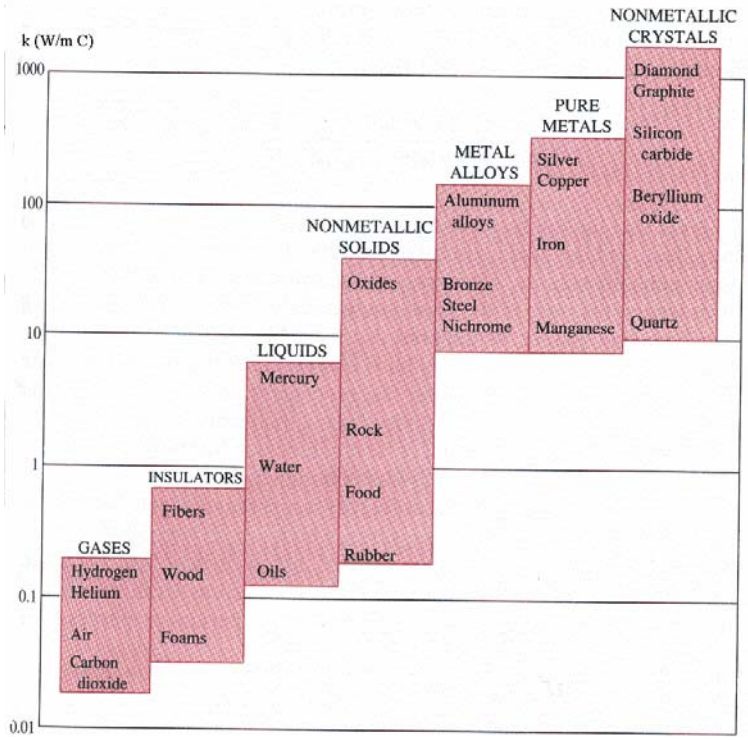

Figure 5.11 The range of thermal conductivity of various materials at room temperature [77].

5.9 Analysis of the Temperature Distributions Within the Pipes and Calculation of Heat Losses

In Balçova Geothermal District Heating System, pre-insulated carbon steel pipes, which are buried underground at 1.5-2 m depth, are used to transport the geothermal fluid. Insulation material is polyurethane and cover material is E-glass reinforced composite. Three types of composite pipes developed for geothermal applications were compared with steel pipe, which has been used in Balçova Geothermal District Heating System based on their thermal performance.

Heat is lost from a hot water pipe to the surroundings in the radial direction and thus heat transfer from a long pipe is very nearly one-dimensional. The wall of the pipe, whose thickness is rather small, separates two fluids at different temperatures and thus the temperature gradient in the radial direction will be relatively large. Further, if the fluid temperatures inside and outside the pipe remain constant, heat transfer through the pipe can be modeled as steady and one-dimensional. The temperature of the pipe in this case will depend on one-dimensional only which can be expressed as T=T(r). This situation is approximated in practice in long cylindrical pipes. The heat losses of pipes were calculated by using general heat loss equation (W/m) for one-dimensional system shown in Equation 5.5 based on Figure 5.12, which shows cross-section of pipe with insulation.

$$Q = \frac{T_f - T_1}{\left(\frac{1}{2.\pi.r_1.h_f} + \frac{\ln(\frac{r_2}{r_1})}{2.\pi.k_p} + \frac{\ln(\frac{r_3}{r_2})}{2.\pi.k_f} + \frac{\ln(\frac{r_4}{r_3})}{2.\pi.k_c}\right)} \quad \text{(W/m)} \qquad (5.5)$$

where h is the heat transfer coefficient and k is thermal conductivity.

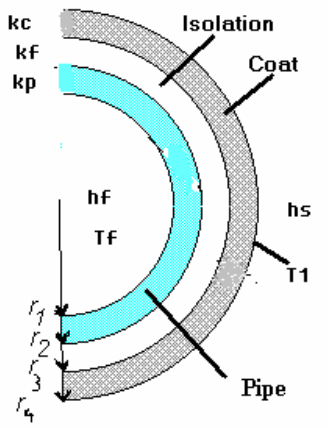

Figure 5.12 Cross-section of pipe with insulation.

Figure 5.13 shows a two-dimensional pipe buried in semi-infinite medium and Equation 5.6 gives the heat loss equation for this pipe. Assuming that Equation 5.5 and 5.6 are equal, the outer surface temperature of the pipe can be determined (Equation 5.7).

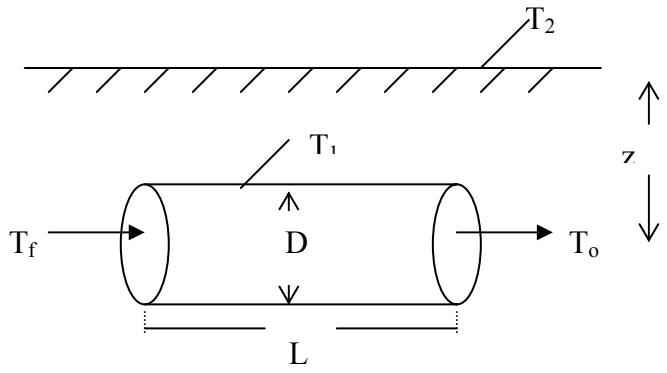

Figure 5.13 Schematic picture of a two-dimensional pipe buried in semi-infinite medium

$$Q = S.k.\Delta T_{1-2} \quad \text{(W/m)} \qquad S = \frac{2.\pi}{\ln(4z/D)} \tag{5.6}$$

$$T_1 = \frac{T_f + (\frac{1}{2.\pi.r_1.h_f} + \frac{\ln(\frac{r_2}{r_1})}{2.\pi.k_p} + \frac{\ln(\frac{r_3}{r_2})}{2.\pi.k_f} + \frac{\ln(\frac{r_4}{r_3})}{2.\pi.k_c}).S.k.T_2}{(\frac{1}{2.\pi.r_1.h_f} + \frac{\ln(\frac{r_2}{r_1})}{2.\pi.k_p} + \frac{\ln(\frac{r_3}{r_2})}{2.\pi.k_f} + \frac{\ln(\frac{r_4}{r_3})}{2.\pi.k_c})S.k + 1} \quad (^0\text{C}) \tag{5.7}$$

To find out the temperature dropdown in the longitudinal direction of a long pipe caused by heat loss can be calculated using Equation 5.8.

$$Q = \frac{m.c_p.\Delta T}{L} = \frac{m.c_p.(T_f - T_o)}{L} \qquad \text{(W/m)} \tag{5.8}$$

where c_p is the specific heat capacity of fluid. The actual data from Balçova Geothermal District Heating System and some assumptions, which were used on calculations, are given below.

- Radiative heat transfer was neglected.
- Fluid inlet temperature to pipe is 84^0C, which was experimental temperature.
- Inner flow convective heat transfer coefficient was calculated as 8107 W/m^{2}K for 84^0C saturated water [77].
- Thermal performance calculations are conducted for actual pipe installation conditions in Balçova Geothermal District Heating System.
- Burial depth of the pipe was taken as 2 m. [78].
- Fluid velocity was 2 m/s [78].
- Cover material and thickness was taken as E-glass reinforced composite (k=0.036 W/mK) [78] and 3 mm, respectively.

- Insulation material was polyurethane foam (k=0.026 W/mK) [78].
- Pipe inner and outer diameters were 0.085 m and 0.093 m, respectively, which were manufactured composite pipe diameters.
- Ground surface was assumed as 0^0C, which is the outer design temperature for Izmir [79].
- Mass flow rate of geothermal fluid calculated for 2 m/s velocity was 10.995 kg/s and specific heat was 4200 J/kgK for saturated water at 84^{o}C [77].

In addition, the temperature distributions within the uninsulated pipe cross-sections were analyzed using LUSAS software program. It is assumed that the pipe is installed on the above ground surface. The objective of the analysis is determination of temperature gradient along the cross-section of the pipe that reaches during continual pumping of the fluid. Figure 5.14 shows the mesh construction used in the analysis. In the program, firstly, material parameter is defined. Then, environmental variable and temperatures are defined. All parameters and data, which were used for one and two-dimensional buried pipe, are the same data used in LUSAS, except for heat transfer coefficient of outer environment. It was taken as 18 W/m^{2}C [77].

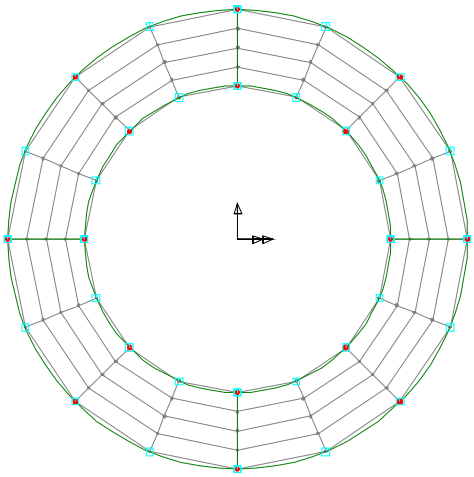

Figure 5.14 The mesh construction of the pipe used in LUSAS software program.

CHAPTER VI
RESULTS AND DISCUSSION

6.1 Composite Processing

A variety of E-glass reinforced polymer matrix composite pipes were produced by employing filament winding and tube rolling methods. In this study, E-glass fibers in the form of continuous filament and $0/90^0$ woven fabrics with polyester, epoxy and graphite particles added epoxy materials were used. Table 6.1 shows the characteristics of the pipes fabricated within the study. Figure 6.1 shows the photos of typical pipes produced with mentioned techniques.

Table 6.1 Characteristics of the produced pipes.

Composite Pipe	Filament Wound	Tube Rolled
Inner Diameter (mm)	85	85
Outer Diameter (mm)	93	93
Angle (^{o})	67^o (Winding Angle)	$0/90^0$ (Woven fabric)
Fiber	E-Glass (Continuous)	E-Glass (Woven)
Resin	Epoxy Epoxy-C Polyester	Epoxy Epoxy-C Polyester

(a) **(b)**

Figure 6.1 The photos of the composite pipes fabricated by (a) filament winding and (b) tube rolling methods.

The specifications of the composite and neat polymer specimens are given in Appendix Table A1, A2 and A3.

6.2 Fiber Volume Fraction by Burn-out

The fiber volume fractions of the produced composites were measured by burn-out technique and the results are shown in Table 6.2.

Table 6.2 Fiber volume fraction of the composite specimens.

Filament Wound Composite Pipe	Fiber Volume Fraction (V_f)	Tube Rolled Composite Pipe	Fiber Volume Fraction Percentages (W_f)
Polyester	47 %	**Polyester**	45 %
Epoxy	46 %	**Epoxy**	40 %
Epoxy-C	40 %	**Epoxy-C**	42 %

6.3 Water Absorption and Diffusion Coefficients of The Composites and Neat Polymers

6.3.1 Water Absorption of The Composites and Neat Polymers

The composite pipe and neat polymer specimens were exposed to distilled water (70^oC) and geothermal fluid bath (84^oC) to measure the water uptake of specimens until they were saturated. The weights of specimens were measured at predetermined times to measure weight gains. Figure 6.2 and 6.3 show the water uptake percentage vs square root of time for filament wound tubes exposed to distilled water and geothermal fluid, respectively.

As it can be seen from the figures, the water uptakes of polyester matrix composite pipes are much greater than for epoxy and graphite particles added epoxy matrix composite pipes. The weight gain at saturation for each specific pipe was about the same under distilled water and geothermal fluid exposure. The saturation values for the polyester composites reached to 0.19 % in distilled water and 0.18 % in geothermal fluid. This value for epoxy and graphite particles added epoxy composite pipes was 0.1 and 0.06 % in distilled water and 0.09 and 0.05 % in geothermal fluid, respectively. As it is indicated the water uptake was much less for graphite particles added epoxy composite pipes as compared to other matrix materials. It seems that graphite particles prevented water absorption into the composite structure. In addition, the time to reach to

saturation was shorter for specimens in distilled water than for those in the geothermal fluid. This might be due to the presence of a surface layer formed from the residue of geothermal fluid.

Figure 6.4 shows the water uptake percentage vs time for tube rolled composites exposed to geothermal fluid. As it can be seen from the Figure 6.4, similar to filament wound tubes, the water uptakes of polyester matrix composite pipes are much greater than for epoxy and graphite particles added epoxy matrix composite pipes for tube rolled composite pipes. The saturation values for the polyester composites reached to 0.22 % in geothermal fluid. This value for epoxy and graphite particles added epoxy composite pipes was 0.15 and 0.07 % in geothermal fluid, respectively. Similar to filament wound pipes, it is seen the water uptake was much less for graphite particles added epoxy composite pipes as compared to other matrix materials.

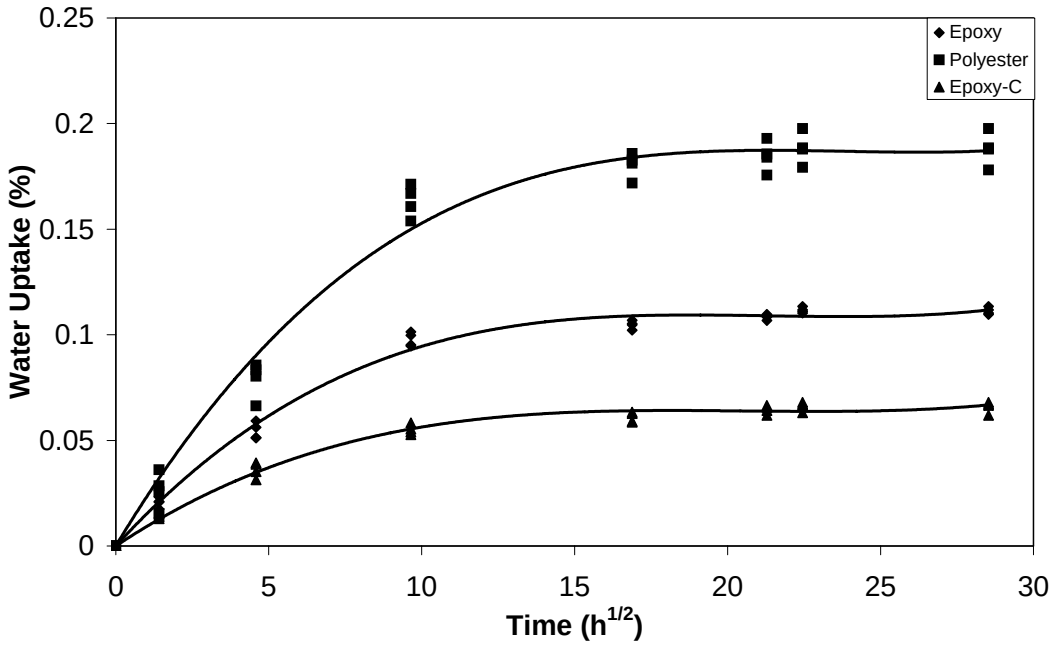

Figure 6.2 Water uptake vs time graphs for three types of filament wound composite tubes exposed to distilled water.

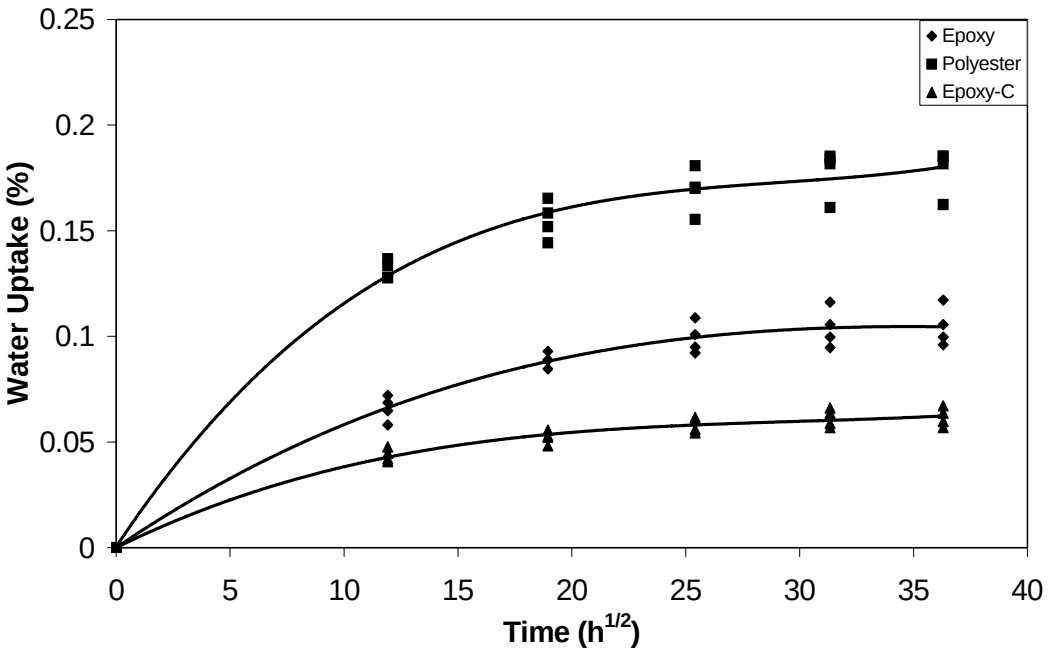

Figure 6.3 Water uptake vs time graphs for three types of filament wound composite tubes exposed to geothermal fluid.

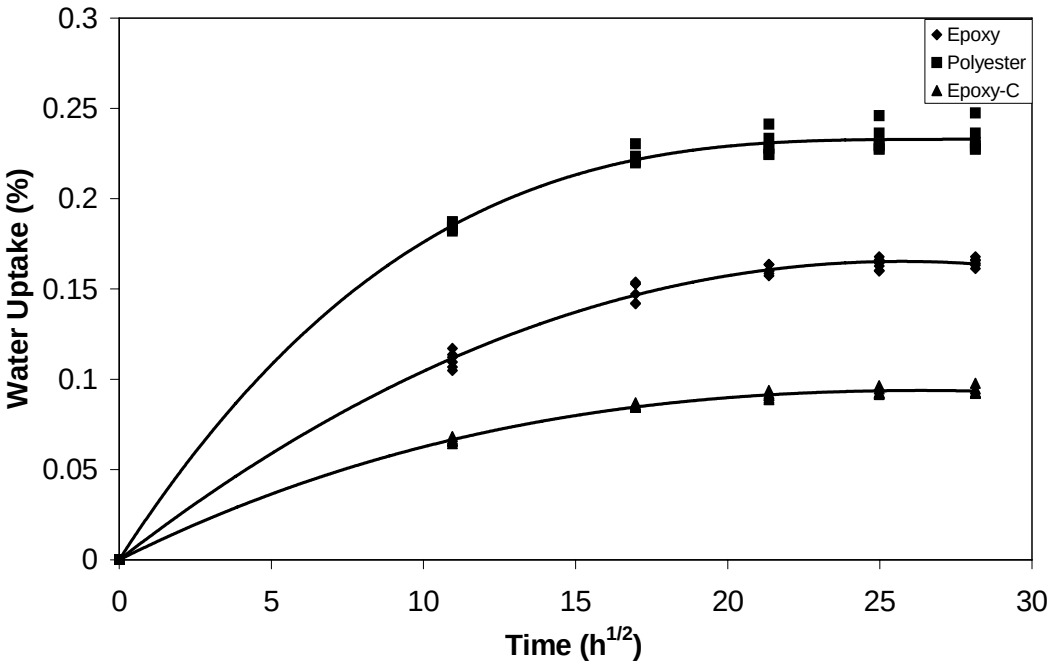

Figure 6.4 Water uptake vs time for three types of tube rolled composite tubes exposed to geothermal fluid.

As seen from the graphs, the composite tubes, which were produced by tube rolling method, absorbed slightly higher amount of water than filament wound composite tubes in geothermal fluid. This may be related to the usage of the woven fabric and the voids on the surface produced within the tube rolling process.

Figures 6.5 and 6.6 illustrate the water uptake percentage vs time for neat polymers exposed to distilled water and geothermal fluid.

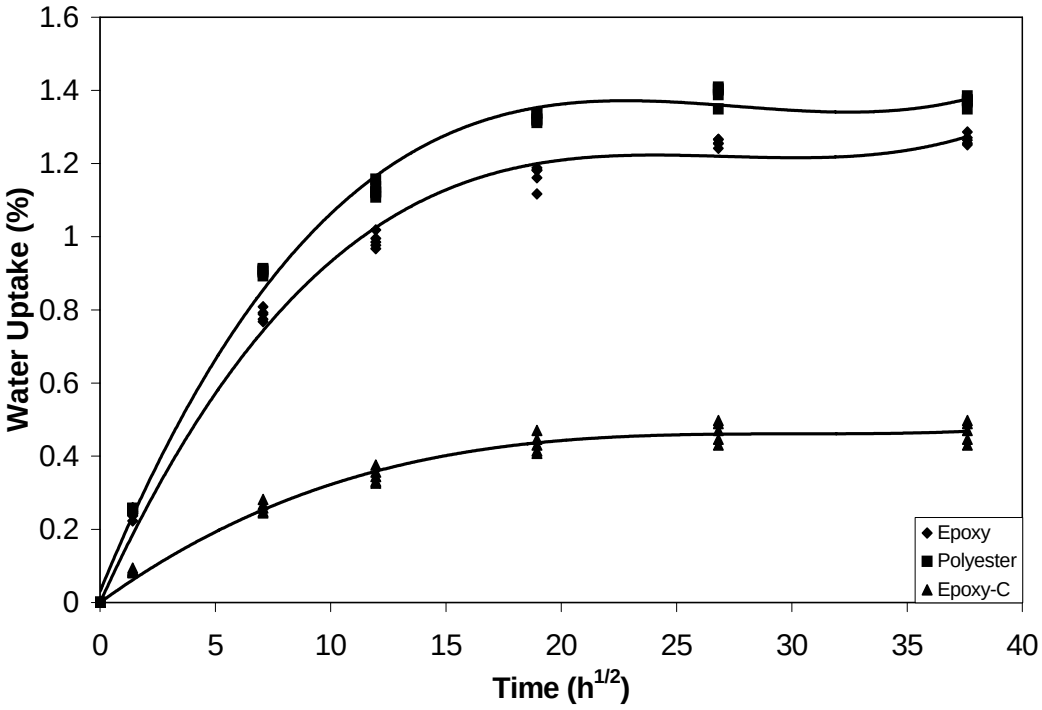

Figure 6.5 Water uptake vs time graphs for three types of neat polymers exposed to distilled water.

As it can be seen from figures, the water uptakes of neat polyester specimens are much greater than for neat epoxy and graphite particles added epoxy in both distilled water and geothermal exposure. The weight gain at saturation for each neat polymer was about the approximately same under distilled water and geothermal fluid exposure. The saturation values for the polyester specimens reached to 1.3 % in distilled water and 1.5 % in geothermal fluid. This value for neat epoxy and graphite particles added epoxy was 1.2 and 0.4 % in distilled water and 1.3 and 0.45 % in geothermal fluid,

respectively. It is seen that the water uptake was much less for neat graphite particles added epoxy as compared to other matrix materials.

Also, it was found that the water absorption values of the neat polymer are much greater than composite specimens. Although it is known that water absorption of the fibers is insignificant, the relatively high water absorption of the neat polymers may be related to the larger surface area involved in the diffusion of water.

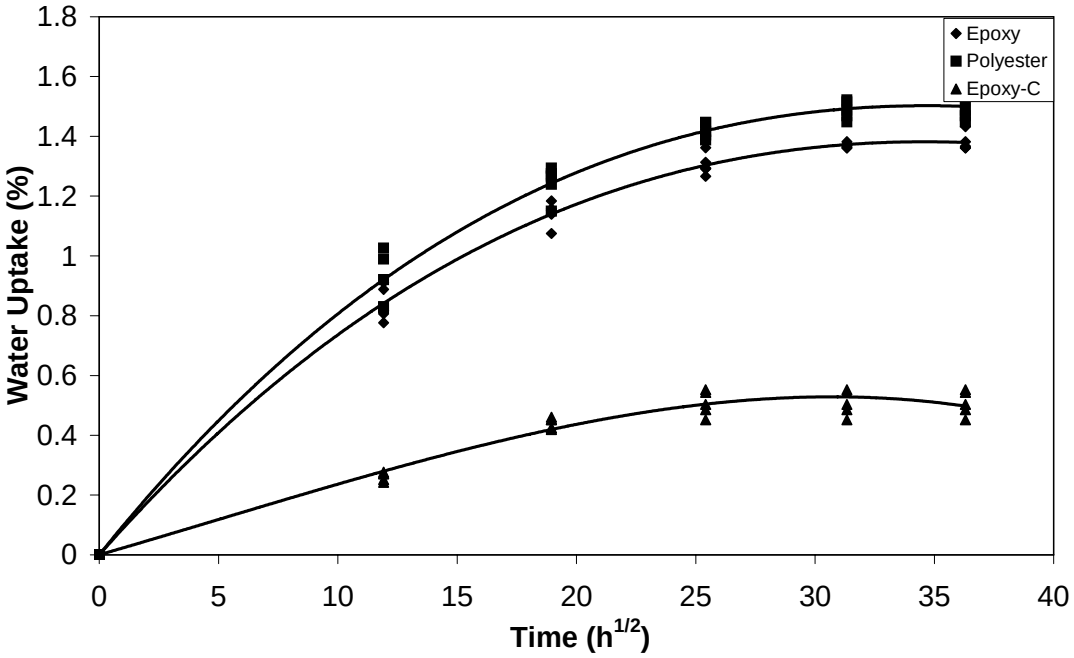

Figure 6.6 Water uptake vs time graphs for three types of neat polymers exposed to geothermal fluid.

6.3.2 Diffusion Coefficients of The Composites and Neat Polymers

Based on Figures 6.2 to 6.4, the diffusion coefficients of various matrix material composites were determined, as shown in Table 6.3. In addition Table 6.4 shows the maximum water absorption percentages for various matrix material composites and neat polymers. In addition, based on the results shown in Figures 6.5 and 6.6, the diffusion coefficients of various neat polymers were determined using Equation 6.1 [81]. It was assumed that specimens were in the shape of sphere.

$$\frac{M_t}{M_m} = 1 - \frac{6}{\pi^2}\sum_{n=1}^{\infty}\frac{1}{n^2}\exp(-Dn^2\pi^2 t/a^2) \qquad (6.1)$$

where M_t is water uptake percentage at time t and a is the radius of specimen.

Table 6.3 Diffusion coefficients (10^{-13} m^2 s^{-1}) of various matrix material composites and neat polymers.

	Filament Wound		Tube Rolled	Neat Polymer	
	Geothermal	**Distilled**	**Geothermal**	**Geothermal**	**Distilled**
Polyester	33.3	55.6	55.6	73.1	65.5
Epoxy	27.7	69.4	30.6	68.7	54.9
Epoxy-C	33.3	44.4	47.2	44.3	35.9

Table 6.4 The maximum water absorption percentages for various matrix material composites and neat polymers.

	Filament Wound		Tube Rolled	Neat Polymer	
	Geothermal	**Distilled**	**Geothermal**	**Geothermal**	**Distilled**
Polyester	0.18	0.19	0.22	1.5	1.3
Epoxy	0.09	0.1	0.15	1.3	1.2
Epoxy-C	0.05	0.06	0.07	0.45	0.4

6.4 Compressive Mechanical Properties of Composite Tubes and Neat Polymers

Compressive mechanical behavior of composite tubes with various matrix polymers under dry condition and after exposure to wet environments (distilled water and geothermal fluid) was investigated. For wet environments, once the water uptake in the specimens reached to saturation, they were carried to mechanical testing to measure the degradation of the properties as compared to dry specimens. For this purpose, load and stroke values for all specimens were measured. Additionally, the stress-strain behaviors, strain and stress at maximum, modulus at elasticity for composites under axial loading and yield stress and strain, modulus at elasticity for neat polymers were determined. Moreover, specific energy absorption during mechanical loading was calculated.

6.4.1 Filament Wound Composite Tubes

6.4.1.1 Mechanical Behavior Under Dry Environment

Figures 6.7 and 6.8 show load vs stroke and stress vs strain graphs for filament wound composites with different matrix materials compressed under axial loading in dry environment, respectively. As it can be seen from the figures, the stress values initially increases linearly with strain and reaches a highest value. At highest value, the failure of the material occurs and the stress values drops suddenly. It was found that the strength of the composite under axial loading was the highest for polyester matrix

composite. The strength values were about 100 and 40 MPa for polyester and epoxy matrix composites. Moreover, the fracture in polyester matrix occurred in a more brittle manner although the epoxy matrices exhibited yield behavior near to the maximum values. The drop of the stress at the maximum was also less for epoxy matrices.

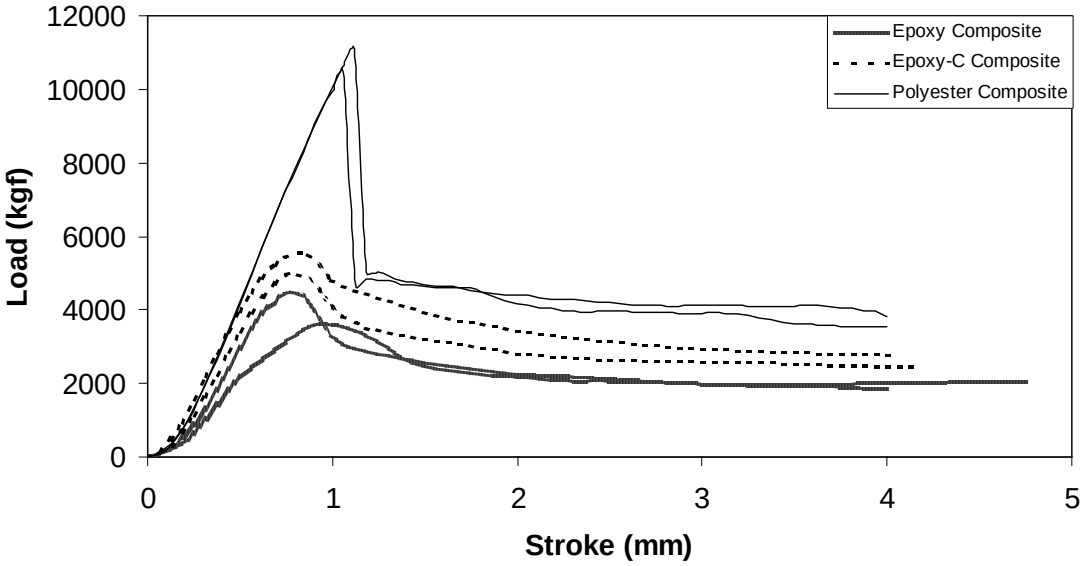

Figure 6.7 Load vs stroke graph of filament wound E-glass composite pipes with three different matrix material compressed under axial loading in dry environment.

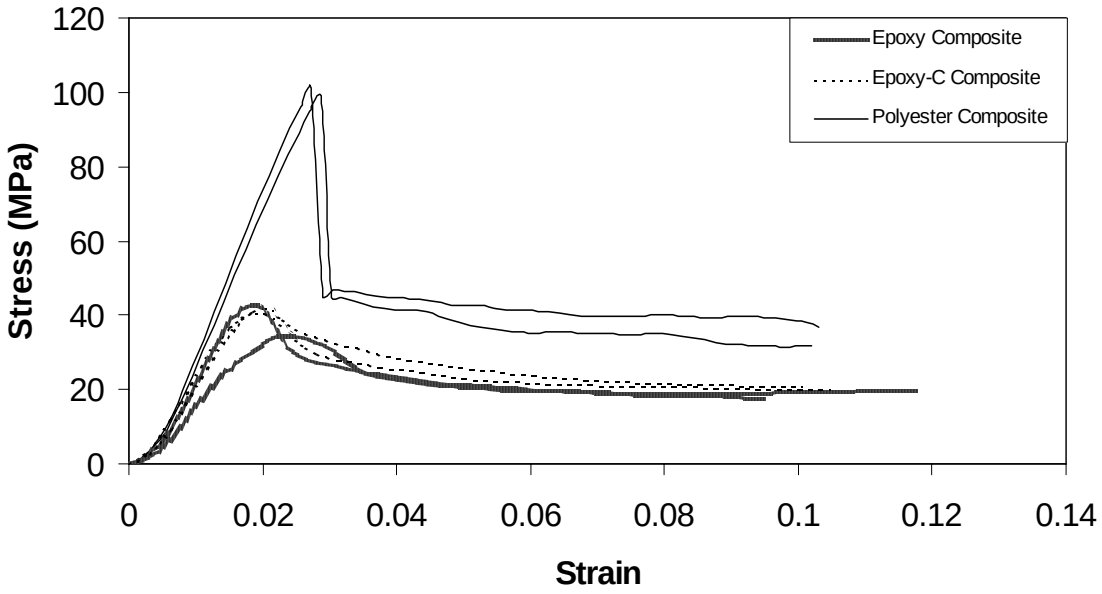

Figure 6.8 Stress vs strain graph of filament wound E-glass composite pipes with three different matrix material compressed under axial loading in dry environment.

Figure 6.9 shows load vs stroke graph of three types of filament wound E-glass composite pipes with three different matrix material compressed under radial loading in dry environment. As it can be seen, all of the tubes showed progressive type failure under radial loading and polyester matrix tubes fractured in a more brittle manner although epoxy and graphite particles added epoxy tubes showed more progressive fracture. Moreover, polyester tubes exhibited the highest load values as compared to epoxy and graphite particles added epoxy tubes. Also, note that graphite particles added epoxy matrix tubes have a considerably higher strength values than epoxy matrix.

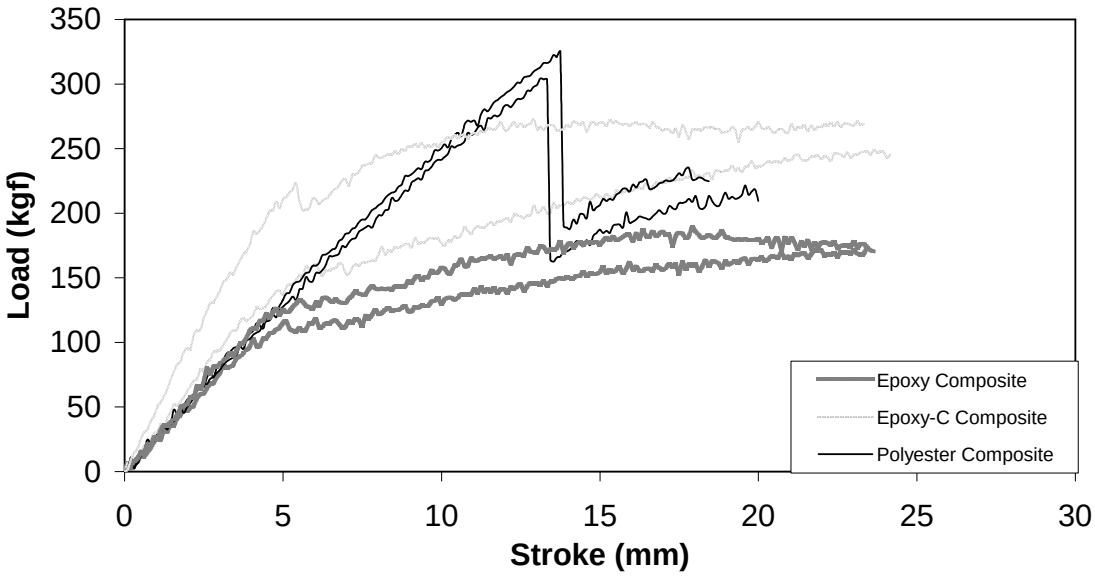

Figure 6.9 Load vs stroke graph of filament wound E-glass composite pipes with three different matrix material compressed under radial loading in dry environment.

6.4.1.2 Mechanical Behavior Under Wet Environments

Figures 6.10 to 6.18 illustrate the load vs stroke and stress vs strain responses for E-glass fiber reinforced composite tubes fabricated with various matrix polymers. The composite specimens were exposed to dry, distilled water and geothermal fluid and subjected to compressive mechanical loading along axial and radial directions. For loading along axial direction, stress-strain responses of all of composites are almost linear up to a maximum stress level at which damage initiates. Above the maximum level, there is a drop of stress. In case of epoxy and graphite particles added epoxy matrix, some specimens exhibited yield behavior prior to maximum level at which initiation of deformation may occur.

Moreover, Figures 6.19 and 6.20 show stress and strain at maximum, respectively for composites made with various matrix materials and loaded along the axial direction.

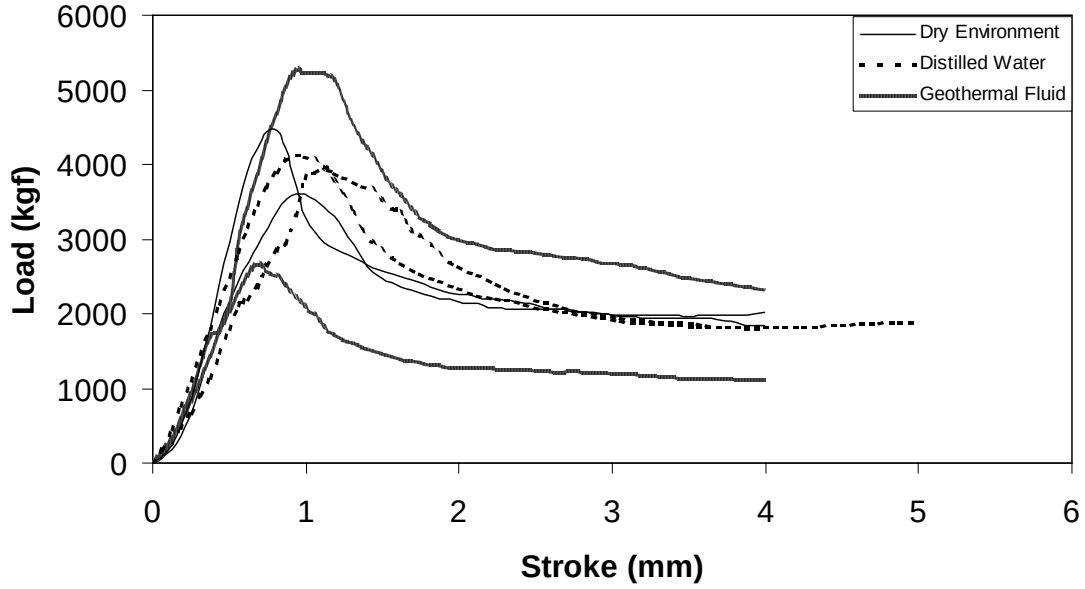

Figure 6.10 Load vs stroke graph of E-glass / epoxy filament wound composite tube exposed to various environments and subjected to compressive loading in axial direction.

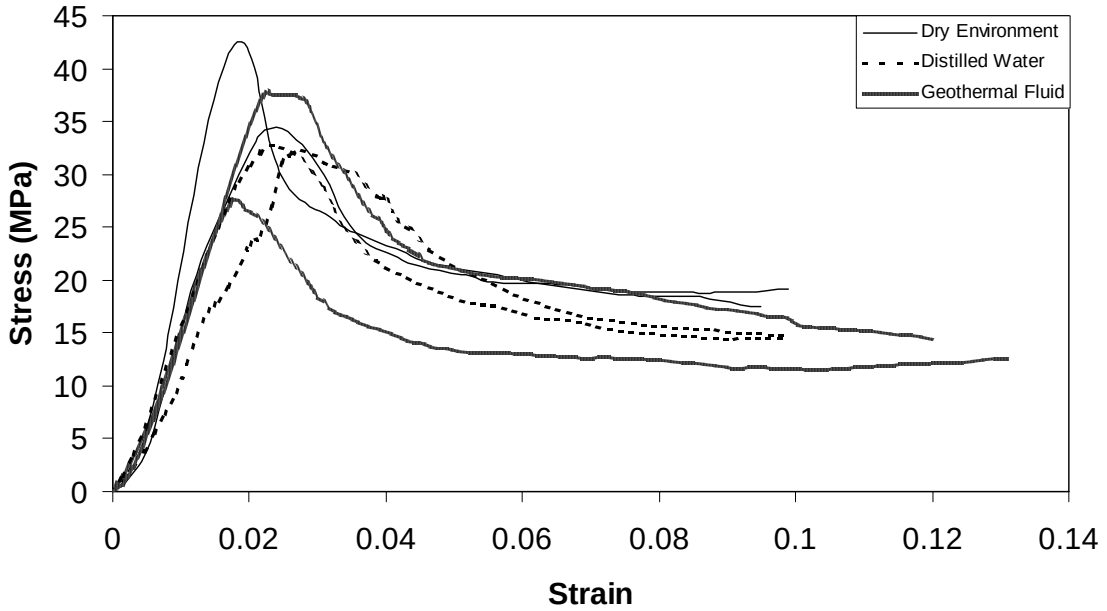

Figure 6.11 Stress vs strain graph of E-glass / epoxy filament wound composite tube exposed to various environments and subjected to compressive loading in axial direction.

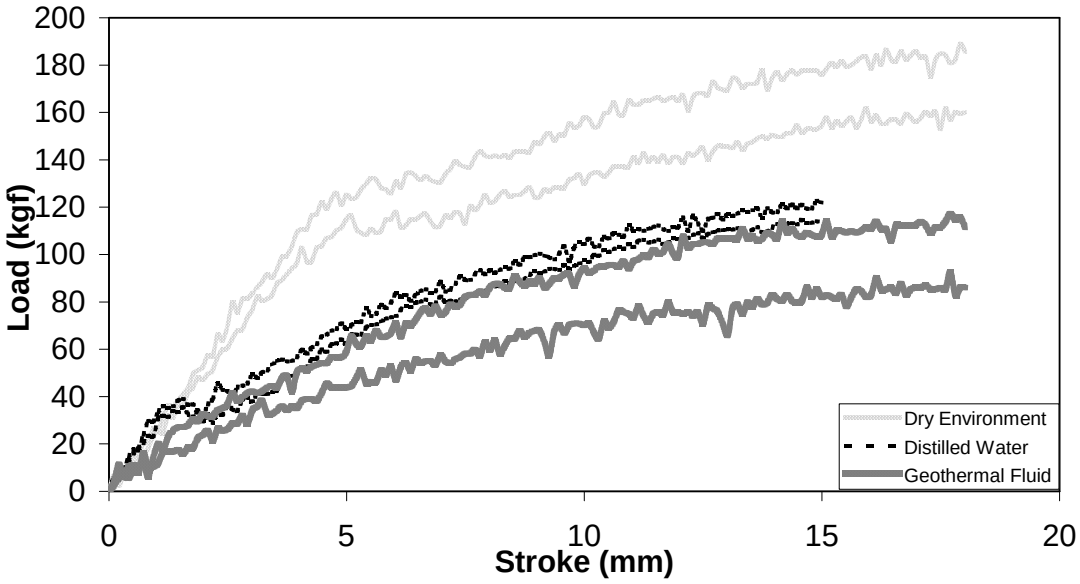

Figure 6.12 Load vs stroke graph of E-glass / epoxy filament wound composite tube exposed to various environments and subjected to compressive loading in radial direction.

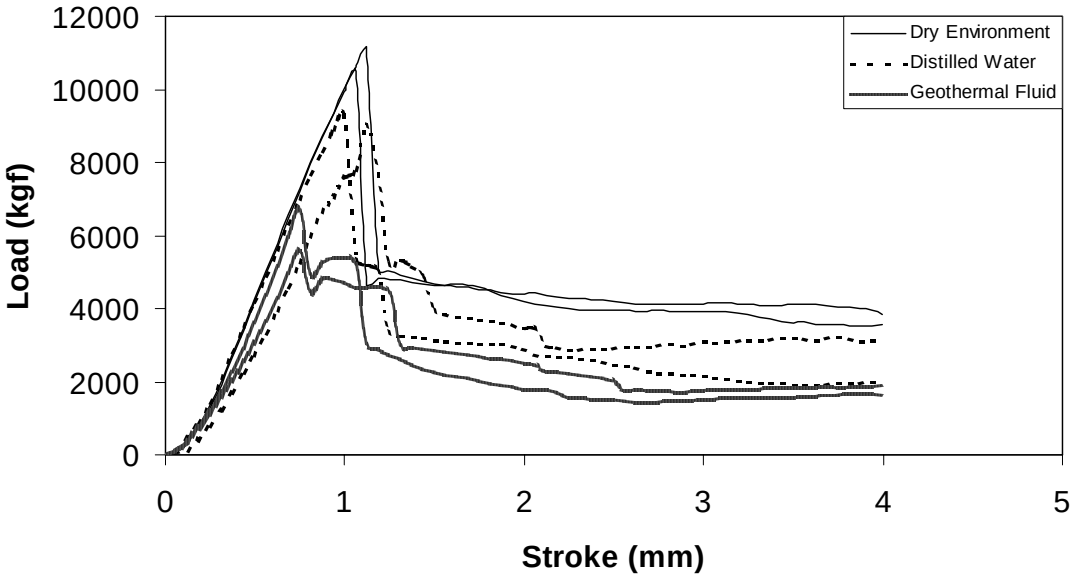

Figure 6.13 Load vs stroke graph of E-glass / polyester filament wound composite tube exposed to various environments and subjected to compressive loading in axial direction.

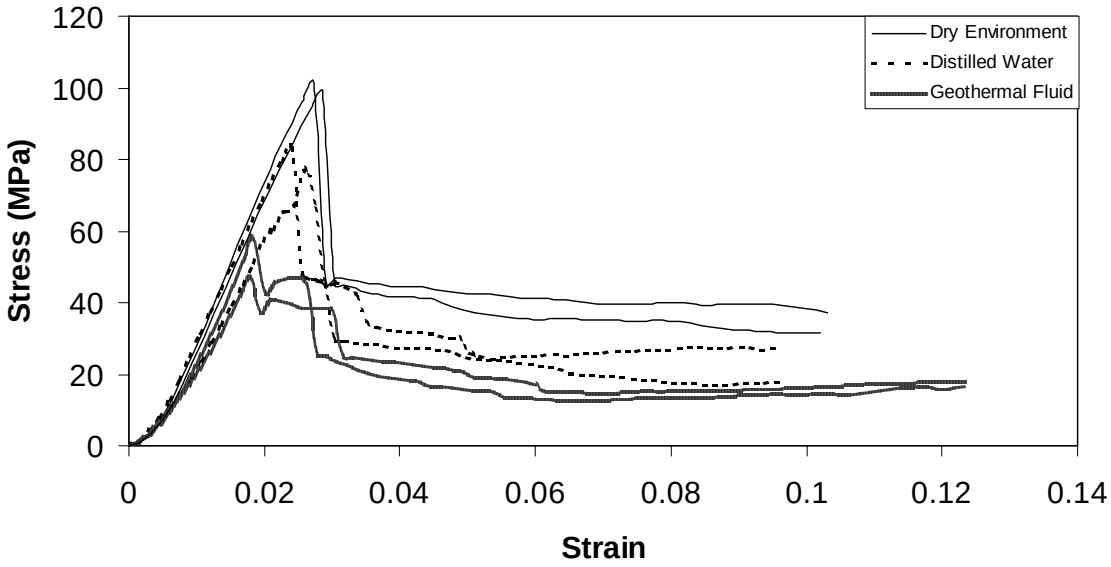

Figure 6.14 Stress vs strain graph of E-glass / polyester filament wound composite tube exposed to various environments and subjected to compressive loading in axial direction.

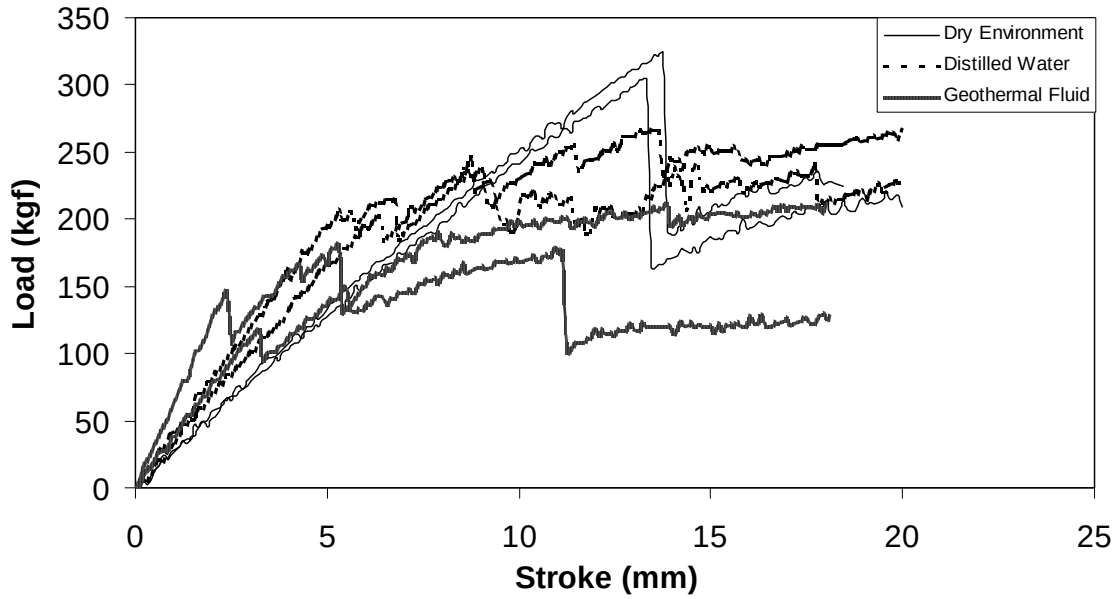

Figure 6.15 Load vs stroke graph of E-glass / polyester filament wound composite tube exposed to various environments and subjected to compressive loading in radial direction.

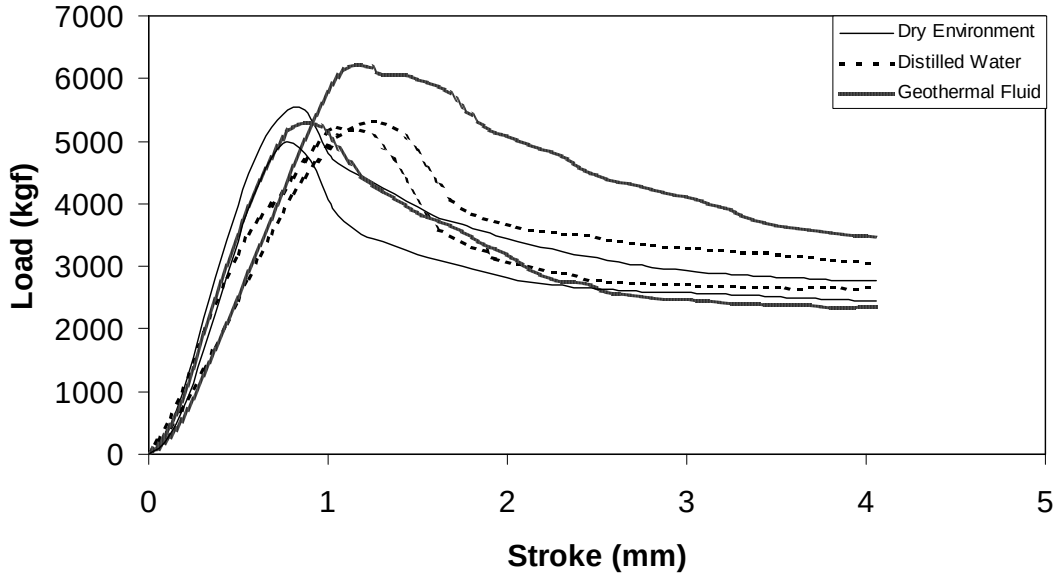

Figure 6.16 Load vs stroke graph of E-glass / graphite particle added epoxy filament wound composite tube exposed to various environments and subjected to compressive loading in axial direction.

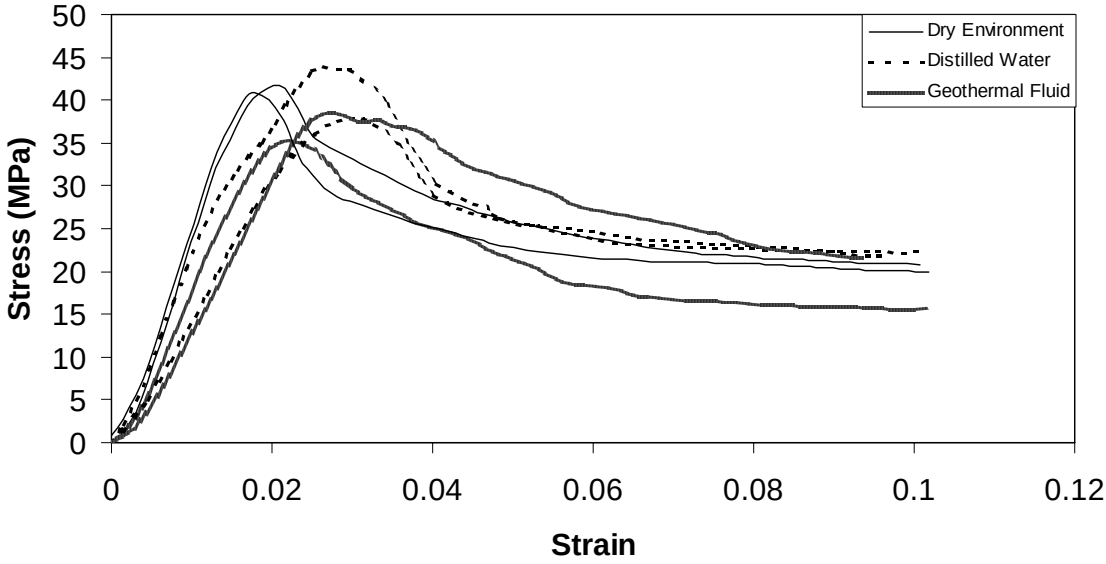

Figure 6.17 Stress vs strain graph of E-glass / graphite particle added epoxy filament wound composite tube exposed to various environments and subjected to compressive loading in axial direction.

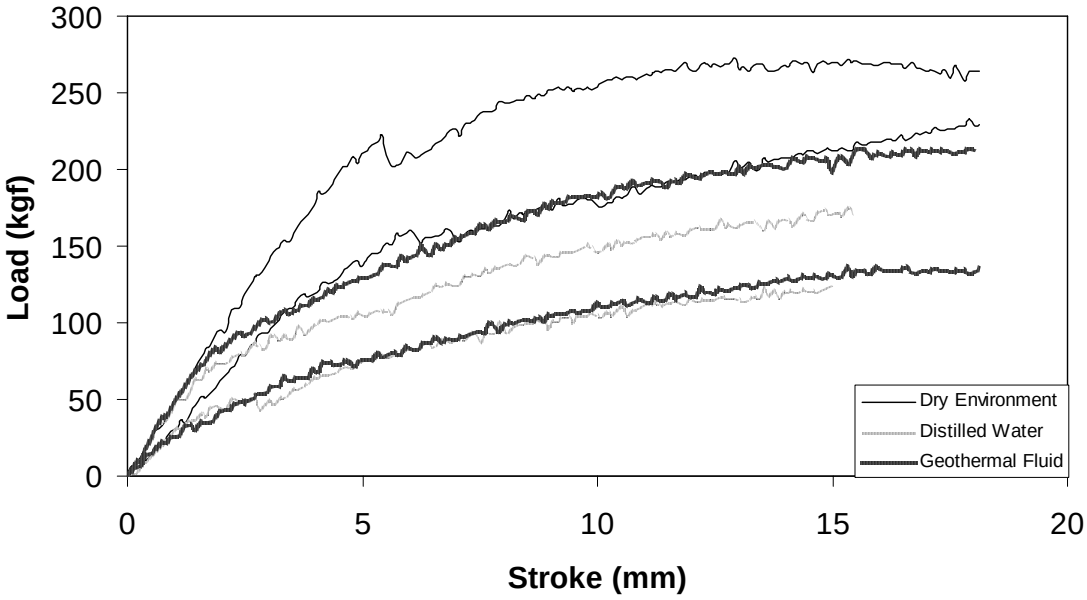

Figure 6.18 Load vs stroke graph of E-glass / graphite particle added epoxy filament wound composite tube exposed to various environments and subjected to compressive loading in radial direction.

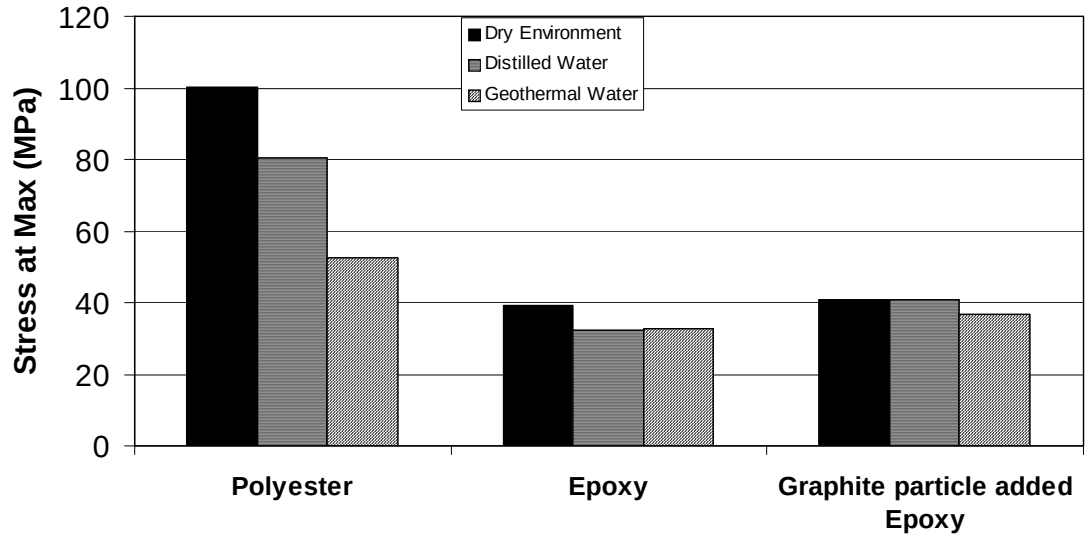

Figure 6.19 Stress at max values of three types of filament wound composite tubes exposed to various environments and subjected to compressive loading in axial direction.

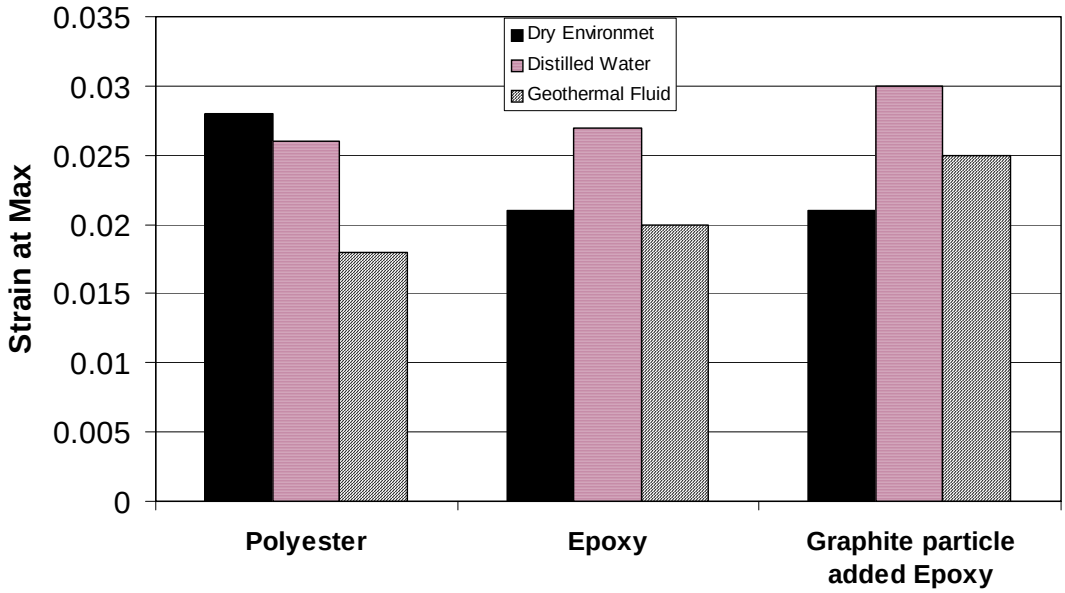

Figure 6.20 Strain at max values of three types of filament wound composite tubes exposed to various environments and subjected to compressive loading in axial direction.

As shown in Figures 6.19 and 6.20, it was found that the polyester composite pipe has the highest strength values in all type of environments. The average strength values are in the range of 100 and 40 MPa for polyester and epoxy matrices, respectively, for dry conditions. At dry condition, the strain at maximum value is 0.027 for polyester composite tube and 0.021 for epoxy and graphite particle added epoxy composite tubes. The results show that there is a considerable decrease of strength and strain at maximum values for polyester matrix composites due to the exposure to wet environments. Moreover, the decrease of the values is more extensive in the case of geothermal fluid. On the other hand, the drop of the strength values in wet environments for epoxy matrix is almost negligible as compared to polyester matrix. The strain at maximum values for graphite added epoxy is slightly higher than for polyester matrix. Moreover, there is a significant increase of strain values for both epoxy matrices under distilled water exposure. The increase of strain values in geothermal fluid is considerably less.

The results reveal that although the polyester matrix exhibited the highest strength values, the degradation of the properties of graphite particles added epoxy composite tube is less as compared to other two. The extensive degradation of polyester may be associated with the highest water absorption. The loss of mechanical properties

may be related to the plasticization of the matrix and by the degradation of the fiber/matrix interface properties. The progress of water molecules may swell the matrix, generating internal stresses and inducing loss of resilience. Since the graphite particle added epoxy tube absorbs the least amount of water, a less degradation may be expected.

Figure 6.21 shows the modulus of elasticity values of three types of filament wound composite tubes exposed to various environments and subjected to compressive loading in axial direction.

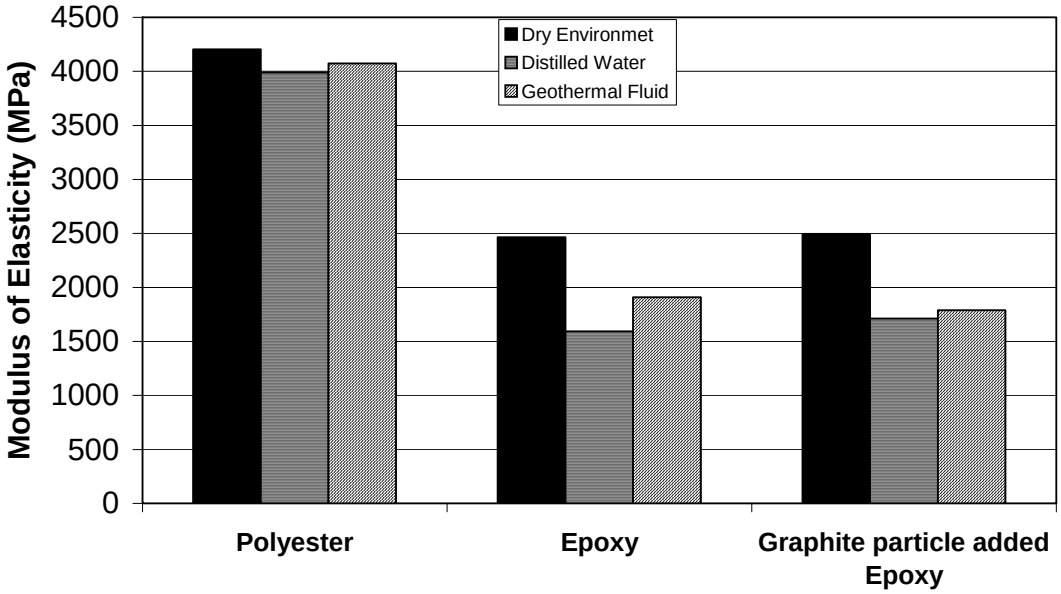

Figure 6.21 Modulus of elasticity values of three types of filament wound composite tubes exposed to various environments and subjected to compressive loading in axial direction.

It was also found that the modulus of elasticity values are about 4200 MPa for polyester composite tube and 2500 MPa for epoxy and graphite particle added epoxy composite tubes for dry condition. The modulus values for polyester matrix do not change significantly due to wet environment. On the other hand, modulus values for epoxy and graphite particle added epoxy composite tubes were considerably reduced due to exposure to wet environments.

For loading along radial direction, all type of filament wound composites exhibited a progressive type failure beginning at relatively small stroke values. As seem in Figures 6.12, 6.15 and 6.18, the load values approaches to about 170, 280 and 200

kgf for epoxy, polyester and graphite particle added epoxy, respectively, for dry environment. On the other hand, a considerable degradation of mechanical properties under radial loading was observed for all type of composites due to the exposure to wet environments.

Figure 6.22 illustrates the typical fracture mode of filament wound composite pipes loaded along axial direction. The fracture mode is due to collapse in transverse shearing mode and matrix fracture along the fiber winding angle direction in all the specimens. In Figure 6.22 (c), the change of color is due to the residues from geothermal fluid. The red color on the surface may be from iron and the yellow from sulfur.

(a) **(b)** **(c)**

Figure 6.22 Photos of the mechanical testing specimens of filament wound E-glass composite tubes loaded along axial direction and exposed to (a) dry environment (b) distilled water and (c) geothermal fluid.

Figure 6.23 also shows the typical modes of failure for specimen loaded along the radial direction. In all the specimens, no visible macro-failure mechanism within the applied stroke was observed. However, micro-failure modes such as fiber failure, fiber/matrix interface debonding matrix microcracking, *etc*. may occur during the loading.

(a) **(b)** **(c)**

Figure 6.23 Photos of the mechanical testing specimens of filament wound E-glass composite tubes loaded along radial direction and exposed to (a) dry environment (b) distilled water and (c) geothermal fluid.

6.4.1.3 Energy Absorption

The energy absorption during mechanical loading of composite tubes along axial and radial directions was also determined. Figure 6.24 and 6.25 show the absorbed energies as a function of stroke for composites made of various matrix materials and loaded along axial and radial directions, respectively. As seen in the figures, in general the absorbed energy increases with the increase of stroke. The energy is the highest for the polyester matrix under axial loading as compared to epoxy and graphite particle added epoxy. However, under radial loading the energy for polyester and graphite particle added epoxy seem to be in the same range.

Figure 6.26 to 6.31 show the absorbed energy as a function of stroke for composites made of various matrix material exposed to various environments and loaded along axial and radial directions, respectively. Under exposure to wet environments, as shown in Figure 6.26 and 6.27, epoxy matrix exhibited some decrease of energy absorption capability under radial loading. For the same case, under axial loading, no change of energy values was observed between the distilled water exposure and dry environment, however, the data was scattered for geothermal fluid exposure. For polyester matrix, the energy absorption capability, as shown in Figure 6.28 and 6.29, was decreased significantly due to exposure to wet environments although it was not considerably changed under radial loading condition. For graphite particle added epoxy matrix, the absorbed energies were not affected by wet environments under axial loading, however, the same decay on the radial loading values were observed, as shown in Figure 6.30 and 6.31.

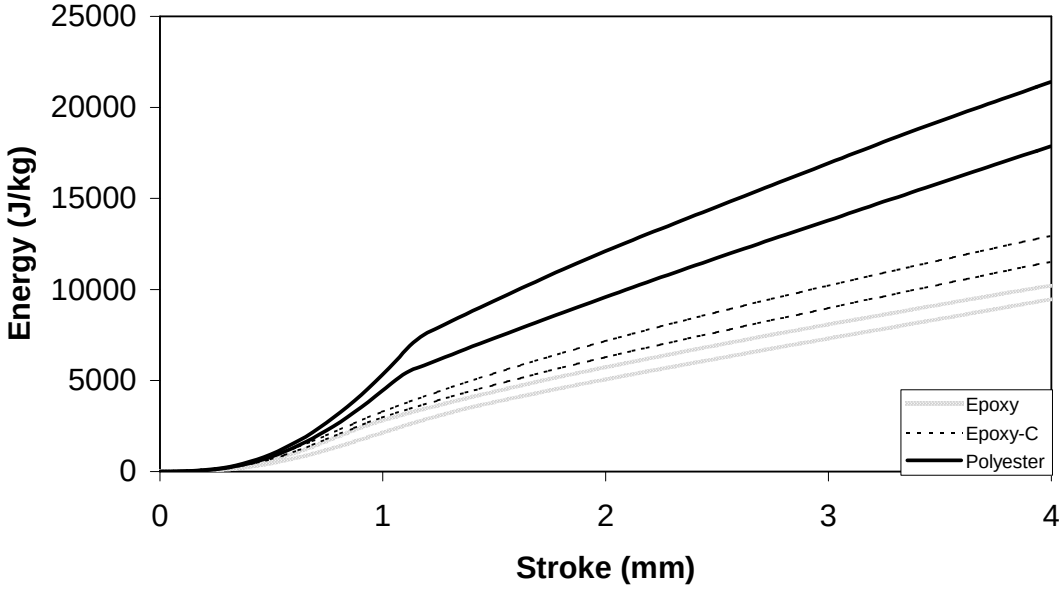

Figure 6.24 Specific energy absorption graph of filament wound E-glass fiber composite tubes with various matrix polymers and compressed along axial direction.

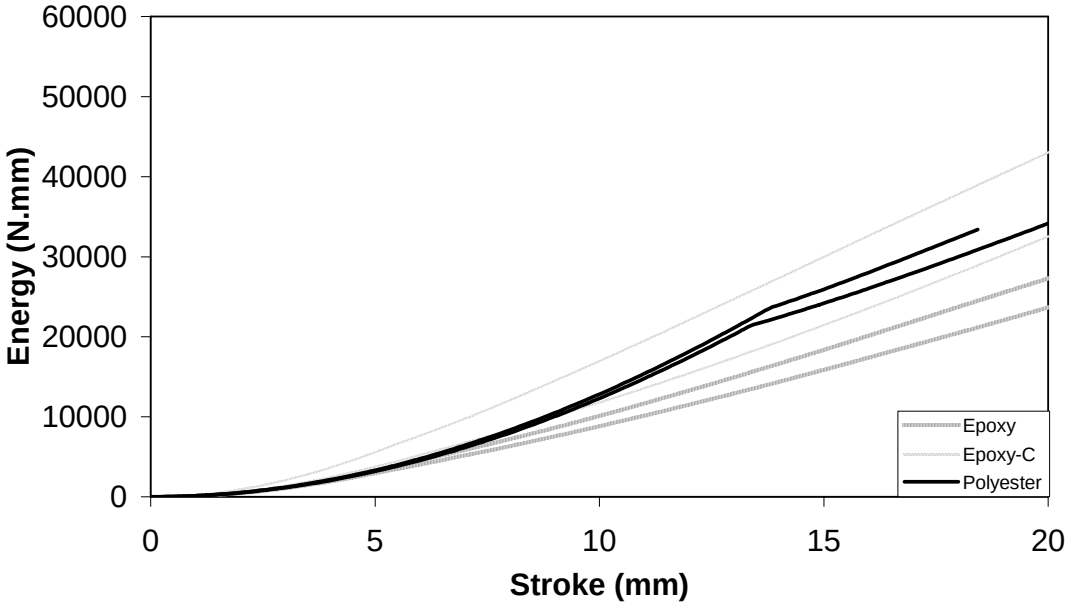

Figure 6.25 Energy absorption graph of filament wound E-glass fiber composite tubes with various matrix polymers and compressed along radial direction.

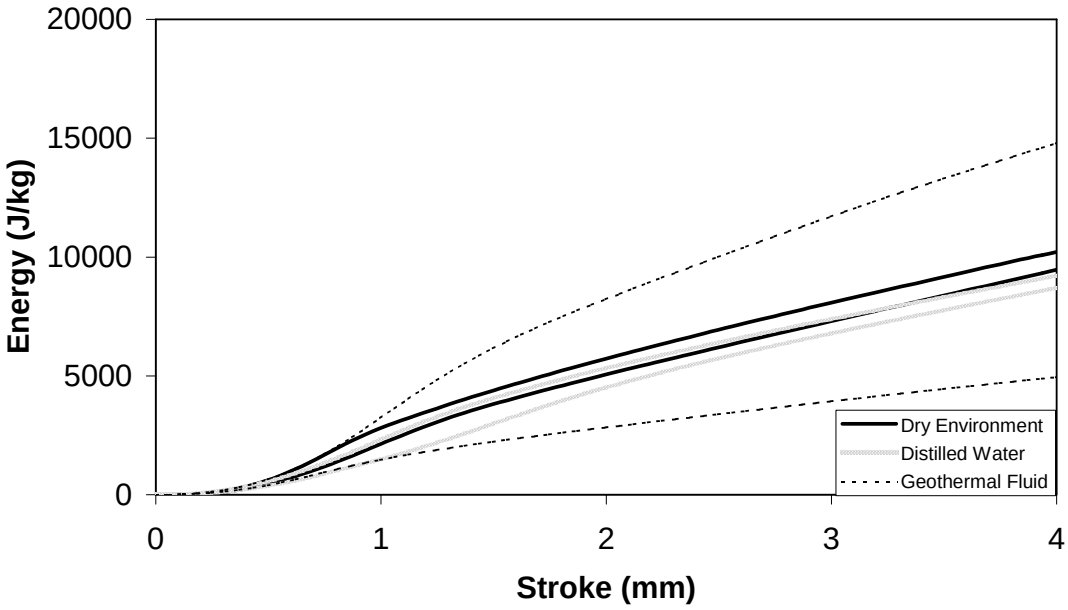

Figure 6.26 Specific energy absorption graph of E-glass / epoxy filament wound composite tube exposed to various environments subjected to compressive loading in axial direction.

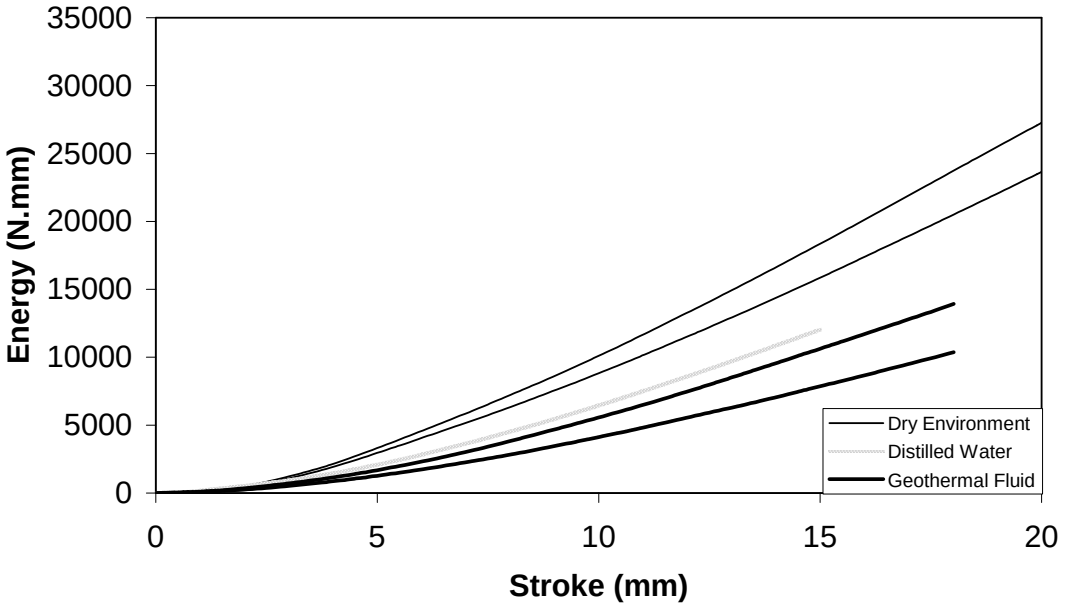

Figure 6.27 Energy absorption graph of E-glass / epoxy reinforced wound composite tube exposed to various environments subjected to compressive loading in radial direction.

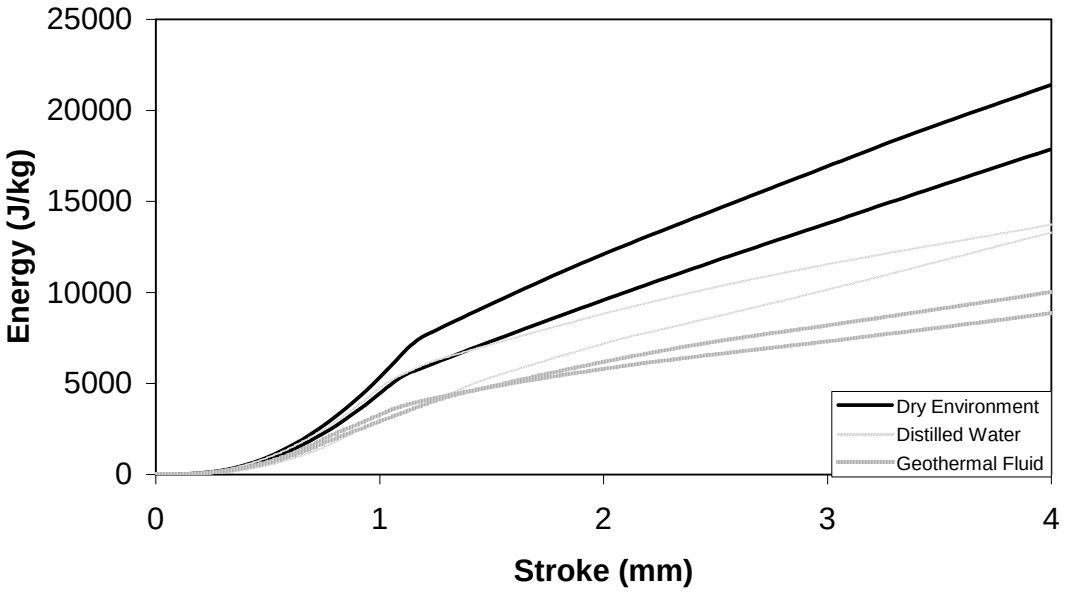

Figure 6.28 Specific energy absorption graph of E-glass / polyester filament wound composite tube exposed to various environments subjected to compressive loading in axial direction.

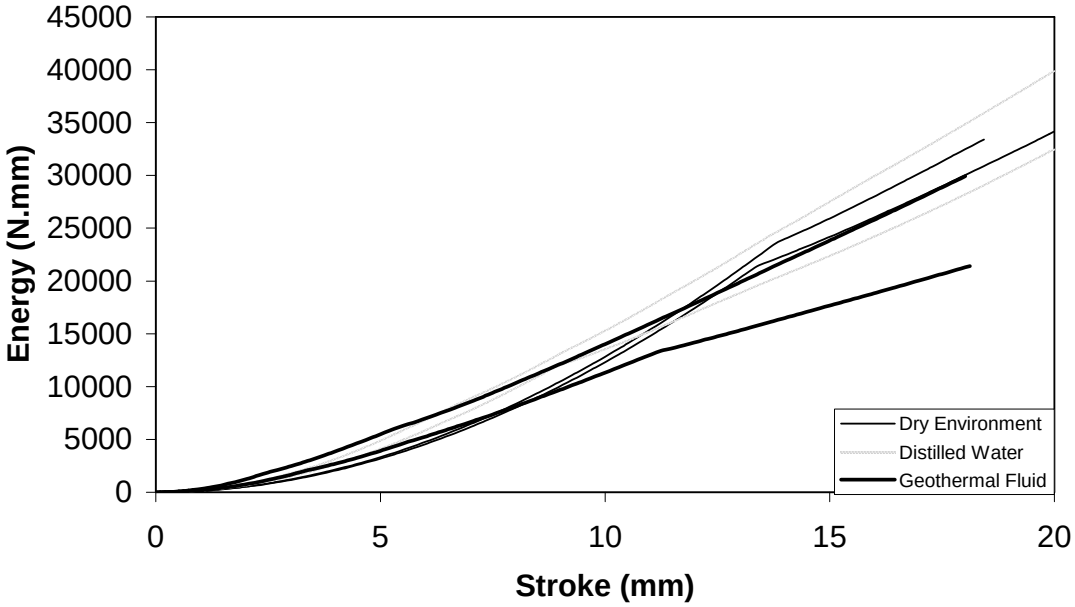

Figure 6.29 Energy absorption graph of E-glass / polyester filament wound composite tube exposed to various environments subjected to compressive loading in radial direction.

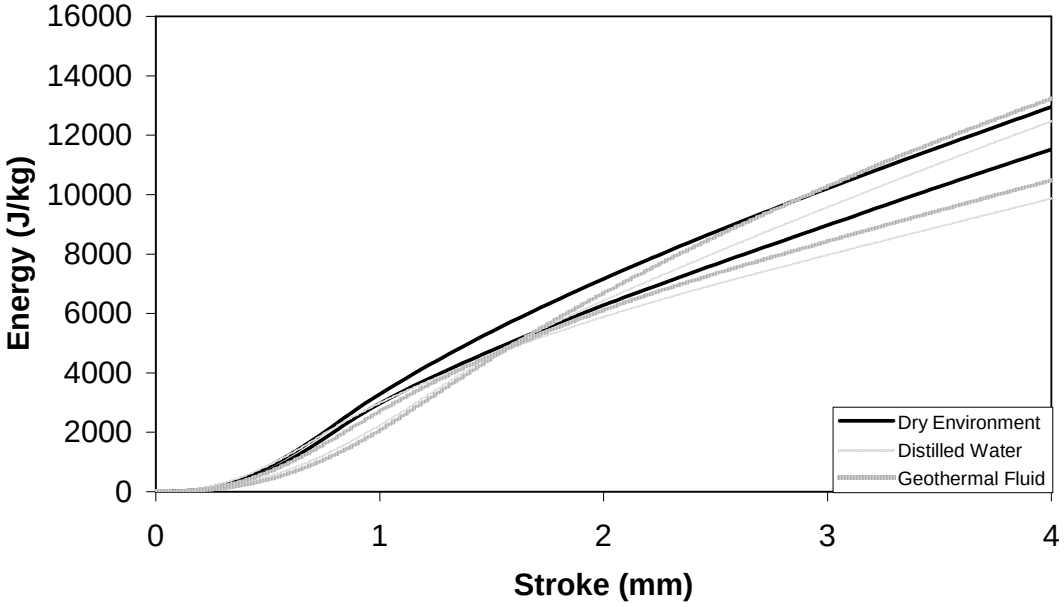

Figure 6.30 Specific energy absorption graph of E-glass / graphite particles added epoxy filament wound composite tube exposed to various environments subjected to compressive loading in axial direction.

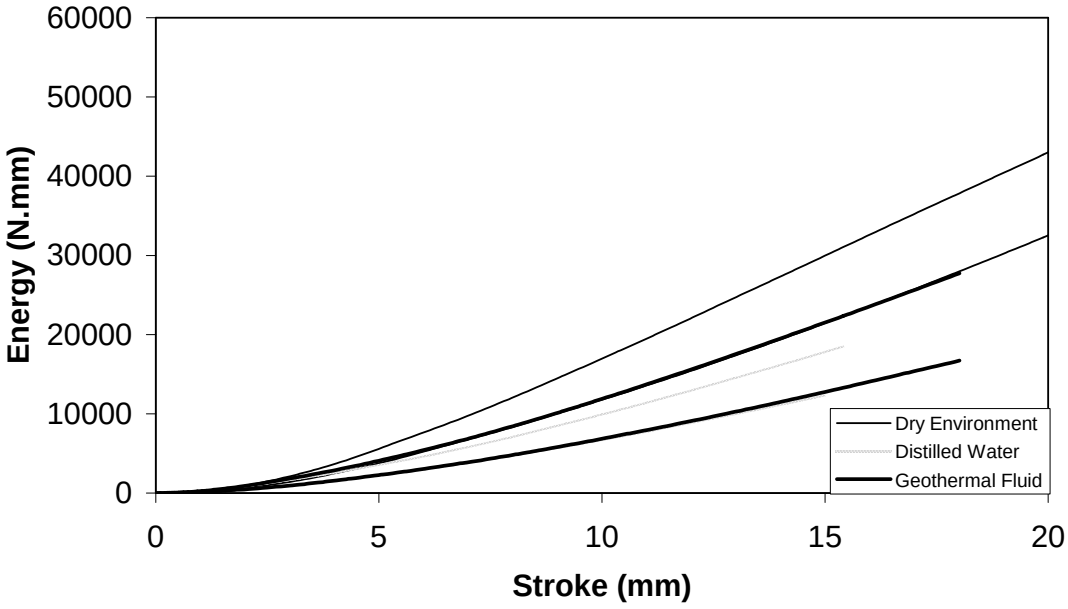

Figure 6.31 Energy absorption graph of E-glass / graphite particles added epoxy filament wound composite tube exposed to various environments subjected to compressive loading in radial direction.

6.4.2 Tube Rolled Composite Tubes

6.4.2.1 Mechanical Behavior Under Dry Environment

Figures 6.32 and 6.33 show load vs stroke and stress vs strain graphs for tube rolled composite with different matrix material compressed under axial loading in dry environment, respectively.

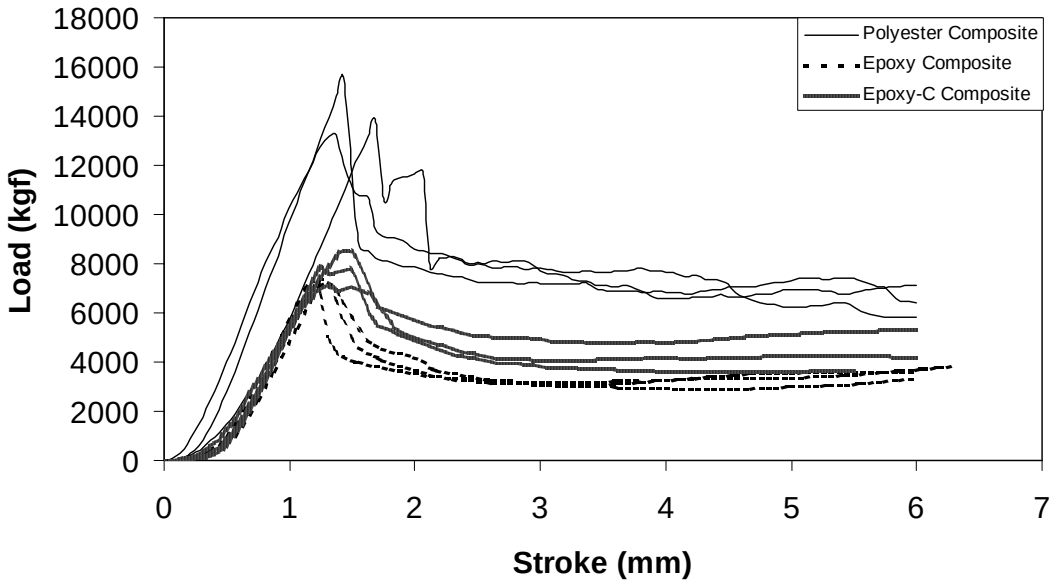

Figure 6.32 Load vs stroke graph of tube rolled composite pipes with three different matrix materials compressed under axial loading in dry environment.

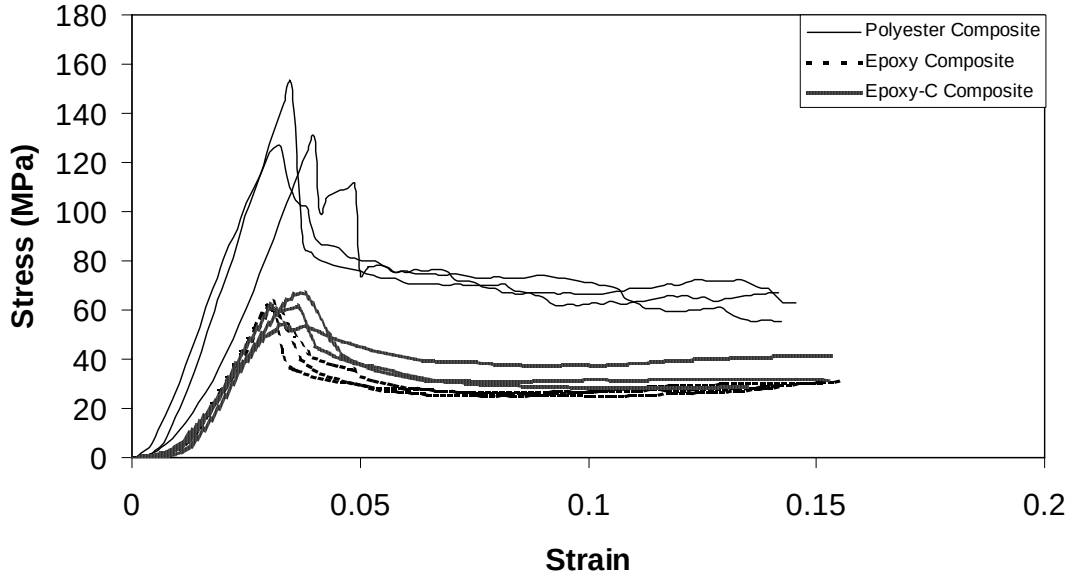

Figure 6.33 Stress vs strain graph of tube rolled composite pipes with three different matrix materials compressed under axial loading in dry environment.

As it can be seen from the figures, similar to filament wound composite pipes, the stress values in the initial part increase linearly with strain and reach a highest value. At highest value, the failure of the material occurs and the stress values drops suddenly. It was found that the strength of the composites under axial loading was the highest for polyester matrix composite. The strength values were about 130 and 60 MPa for polyester and epoxy matrix composite. Similar to like filament wound composite pipes, the fracture in polyester matrix occurred in a more brittle manner although the epoxy matrices exhibited yield behavior near to the maximum values. The drop of the stress of the maximum was also less for epoxy matrices.

Figure 6.34 shows load vs stroke graph of three types of tube rolled composite pipes compressed under radial loading in dry environment. As it can be seen, epoxy and graphite particles added epoxy tubes showed progressive type failure under radial loading but polyester matrix tubes fractured in a more brittle manner. Moreover, polyester tubes exhibited the highest load value as compared to epoxy and graphite particles added epoxy tubes. Also, similar to filament wound composite pipe, graphite particles added epoxy matrix tubes exhibited a considerably higher strength values than epoxy matrix.

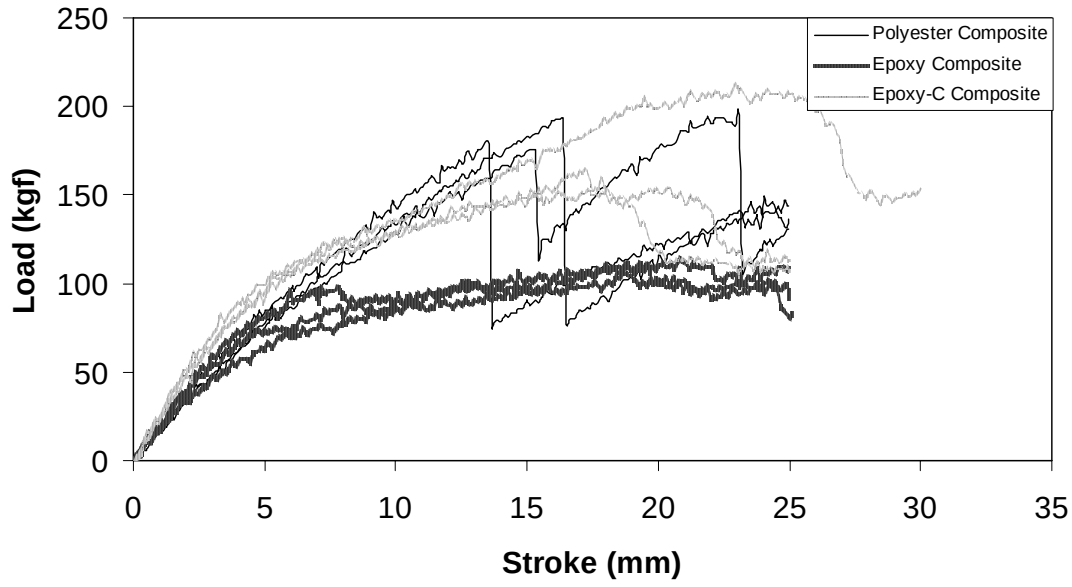

Figure 6.34 Load vs stroke graph of tube rolled composite pipes with three different matrix materials compressed under radial loading in dry environment.

6.4.2.2 Mechanical Behavior Under Wet Environments

Figures 6.35 to 6.43 show the load vs stroke and stress vs strain responses for tube rolled composites made of various matrix polymers. Similar to filament wound pipes, the composite specimens were exposed to dry, distilled water and geothermal fluid and subjected to compressive mechanical loading along axial and radial directions. The stress-strain response of all type of composites is almost linear up to a maximum stress level at which damage initiates. In case of epoxy and graphite particles added epoxy matrix, some specimens exhibited yield behavior prior to maximum level at which deformation may initiate.

Figures 6.44 and 6.45 show stress and strain at maximum for tube rolled composite pipes, respectively.

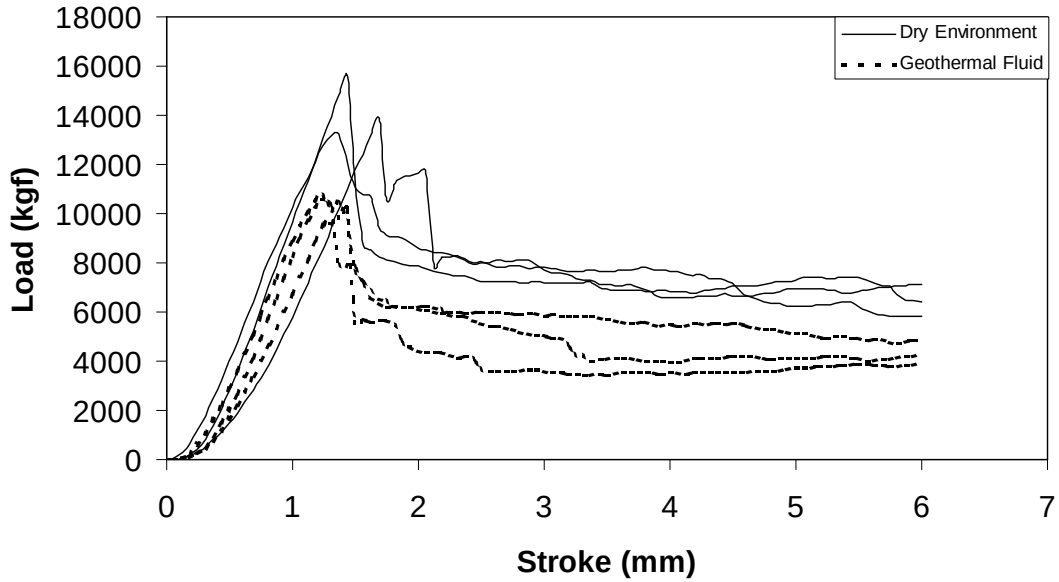

Figure 6.35 Load vs stroke graph of E-glass / polyester tube rolled composite tube exposed to two environments and subjected to compressive loading in axial direction.

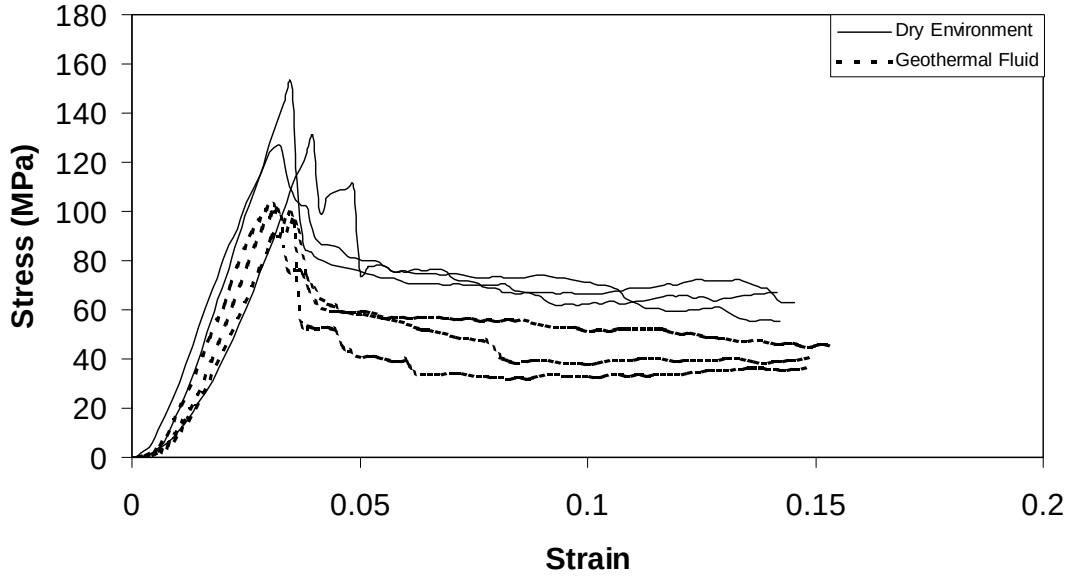

Figure 6.36 Stress vs strain graph of E-glass / polyester tube rolled composite tube exposed to two environments and subjected to compressive loading in axial direction.

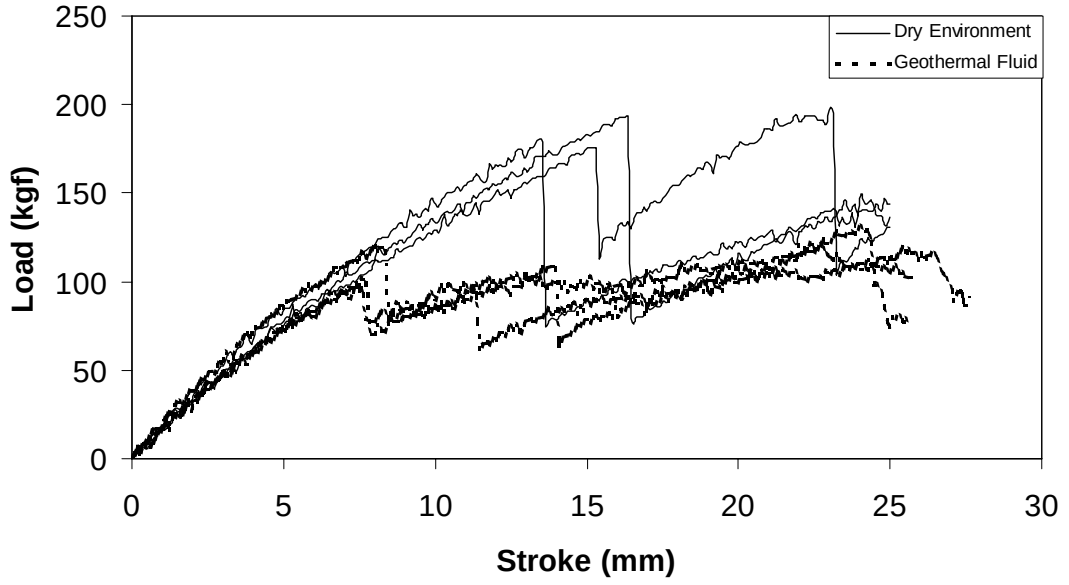

Figure 6.37 Load vs stroke graph of E-glass / polyester tube rolled composite tube exposed to two environments and subjected to compressive loading in radial direction.

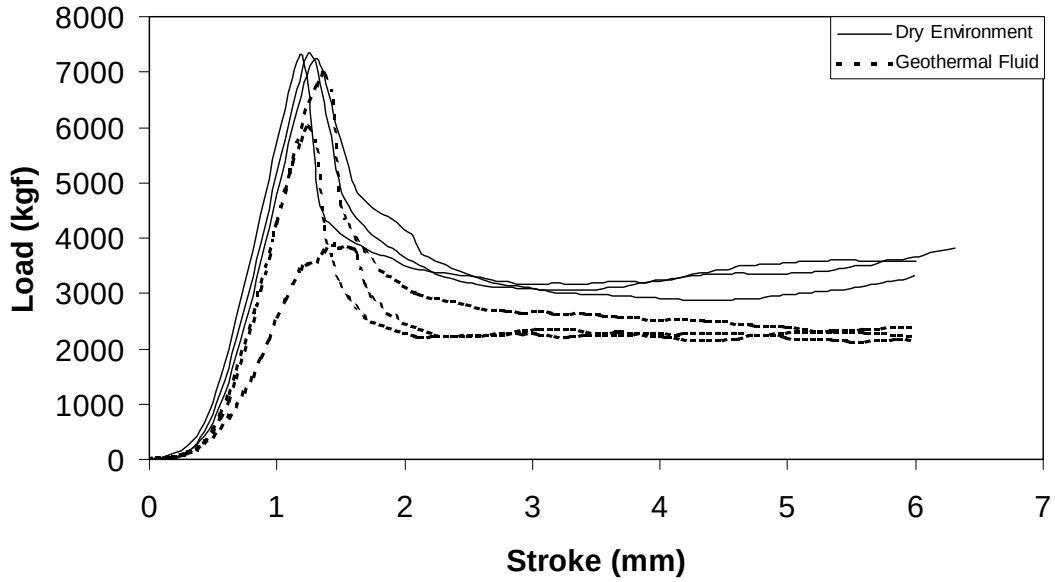

Figure 6.38 Load vs stroke graph of E-glass / epoxy tube rolled composite tube exposed to two environments and subjected to compressive loading in axial direction.

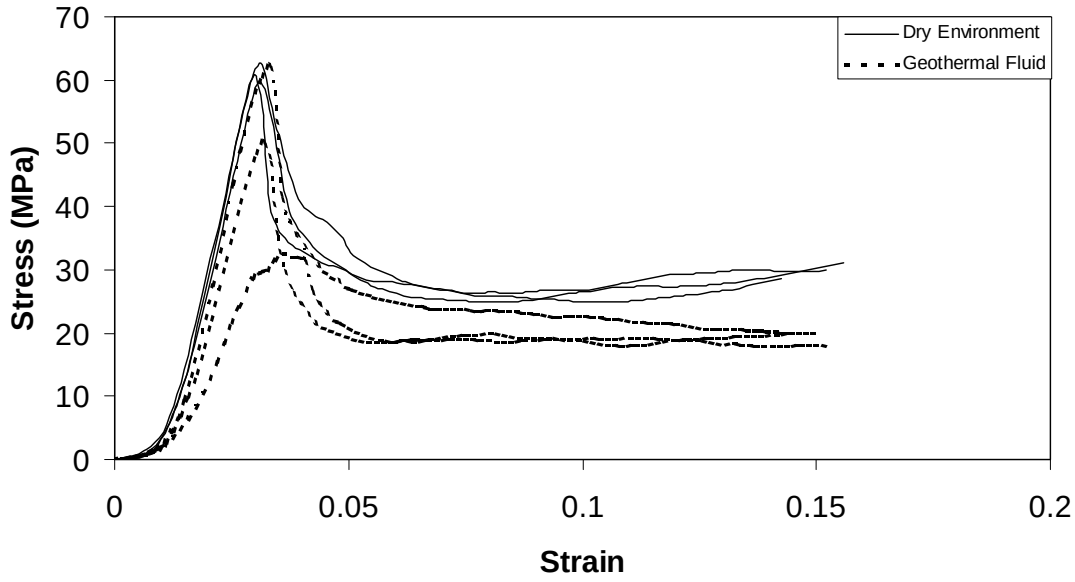

Figure 6.39 Stress vs strain graph of E-glass / epoxy tube rolled composite tube exposed to two environments and subjected to compressive loading in axial direction.

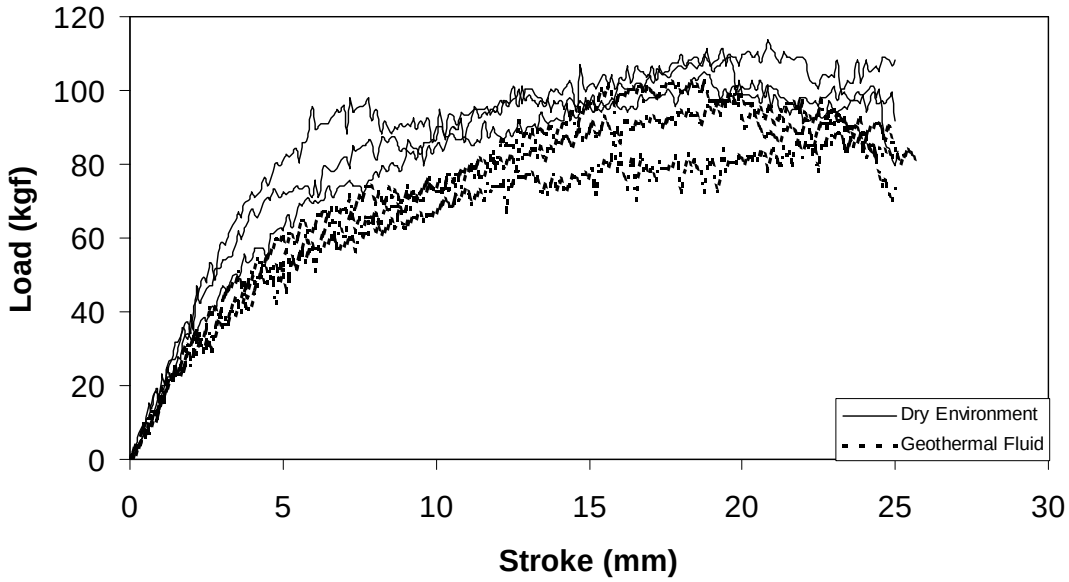

Figure 6.40 Load vs stroke graph of E-glass / epoxy tube rolled composite tube exposed to two environments and subjected to compressive loading in radial direction.

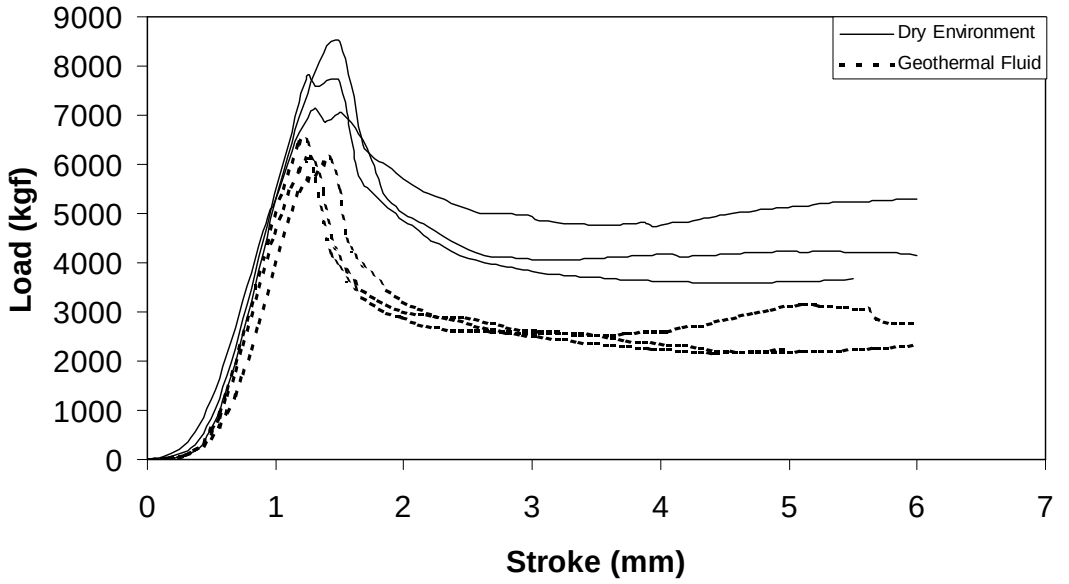

Figure 6.41 Load vs stroke graph of E-glass / graphite particle added epoxy tube rolled composite tube exposed to two environments and subjected to compressive loading in axial direction.

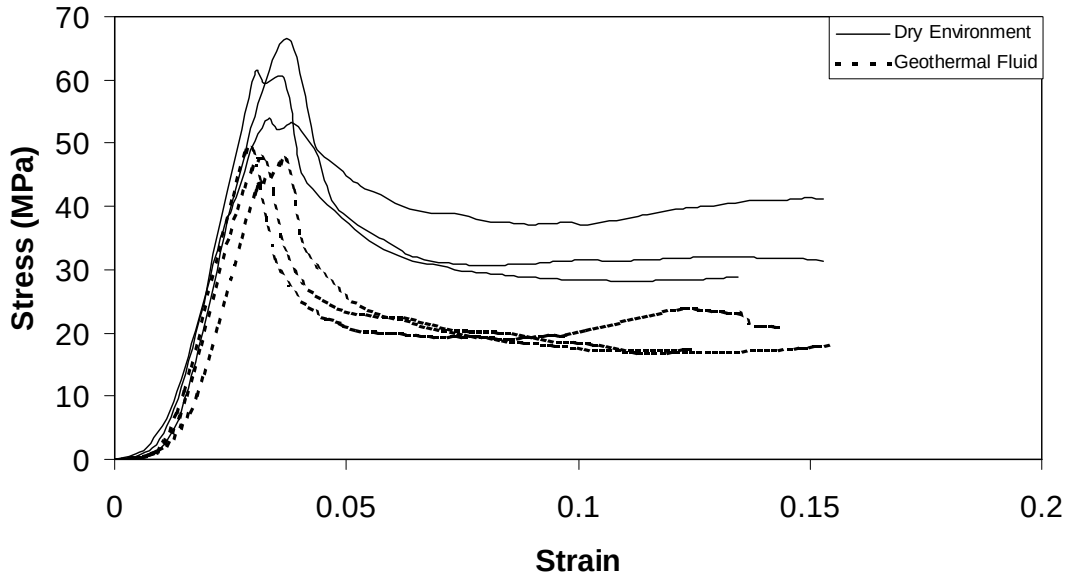

Figure 6.42 Stress vs strain graph of E-glass / graphite particle added epoxy tube rolled composite tube exposed to two environments and subjected to compressive loading in axial direction.

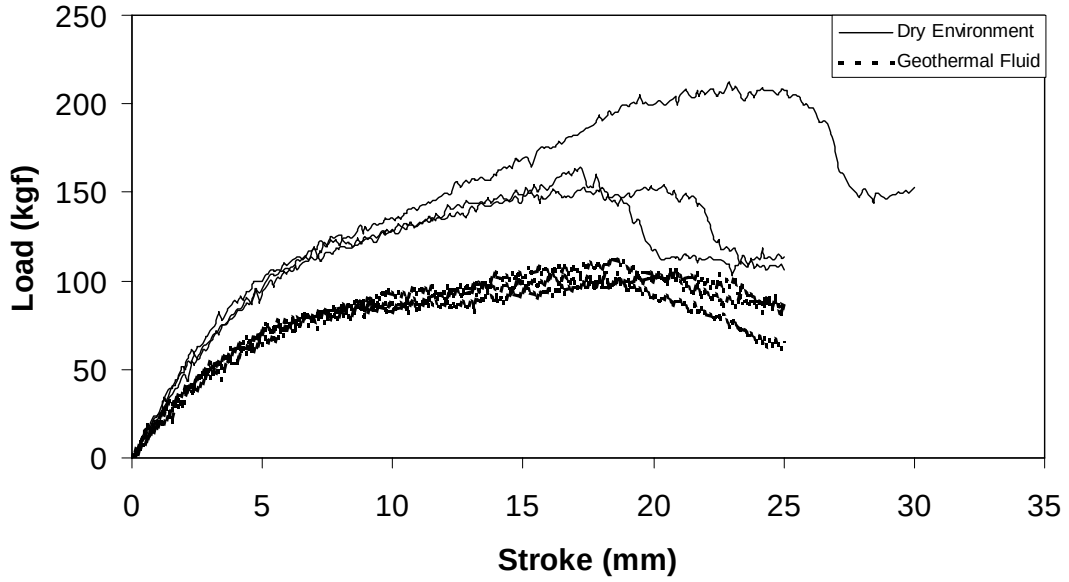

Figure 6.43 Load vs stroke graph of E-glass / graphite particle added epoxy tube rolled composite tube exposed to two environments and subjected to compressive loading in radial direction.

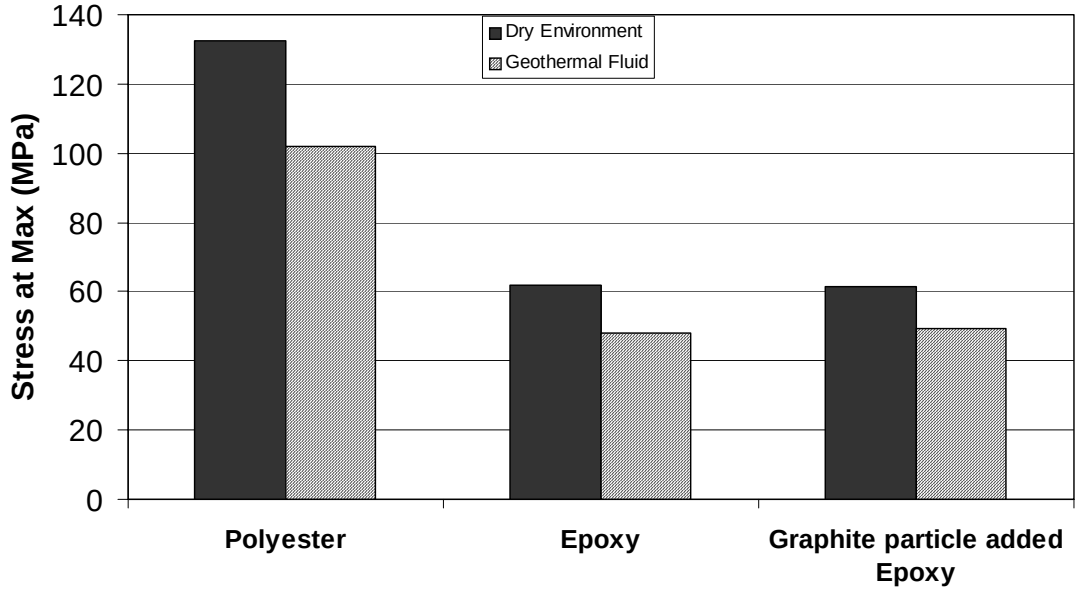

Figure 6.44 Stress at max values of three types of tube rolled composite tubes exposed to two environments and subjected to compressive loading in axial direction.

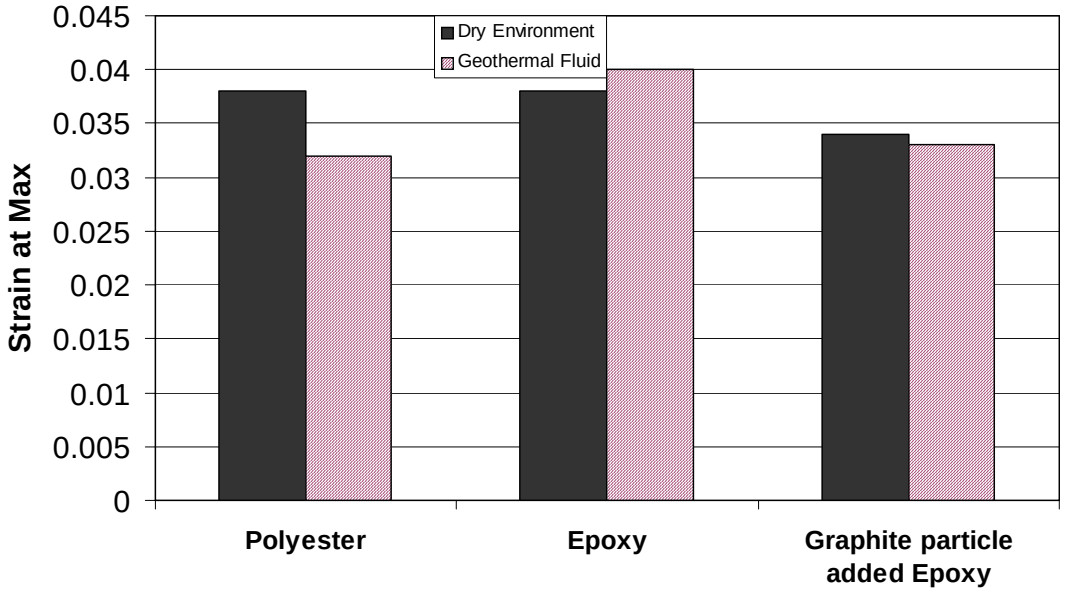

Figure 6.45 Strain at max values of three types of tube rolled composite tubes exposed to two environments and subjected to compressive loading in axial direction.

It was found that, similar to filament wound composite pipe, the polyester composite pipe has the highest strength values in both environments. The average strength values are in the range of 130 and 60 MPa for polyester and epoxy matrices, respectively, for dry conditions. At dry condition, the strain at maximum value is 0.037 for polyester composite tube and epoxy and 0.034 for graphite particle added epoxy composite tubes. The results show that there is a considerable decrease of strength and strain at maximum values for polyester matrix composites due to the exposure to geothermal fluid. The strain at maximum values for three types of composite pipes are almost the same. Moreover, there is a considerable increase of strain values for epoxy matrix under geothermal fluid exposure.

Although the polyester matrix exhibited the highest strength values, the degradation of the properties of epoxy and graphite particles added epoxy composite tube is less as compared to polyester matrix. Similar to filament wound composite pipes, the extensive degradation of composite may be associate with water absorption. From the same reason, the loss of mechanical properties may be related to the plasticization of the matrix and by the degradation of the fiber/matrix interface properties.

Figure 6.46 shows the modulus of elasticity values of three types of tube rolled composite tubes exposed to both environments and subjected to compressive loading in axial direction. It was found that the modulus of elasticity values are about 3700 MPa for polyester and 3000 MPa for epoxy and 2600 MPa for graphite particle added epoxy composite tubes for dry condition. In addition, modulus values for polyester and epoxy composite tubes were considerably reduced due to exposure to geothermal fluid.

For loading along radial direction, similar to filament wound composite pipes, all type of tube rolled composites exhibited a progressive type failure beginning at relatively small stroke values. As seen in Figures 6.37, 6.40 and 6.43, the load values approaches to about 170, 110 and 150 kgf for polyester, epoxy and graphite particle added epoxy, respectively, for dry environment. On the other hand, a considerable degradation of mechanical properties under radial loading was observed for all type of composites due to the exposure to geothermal fluid.

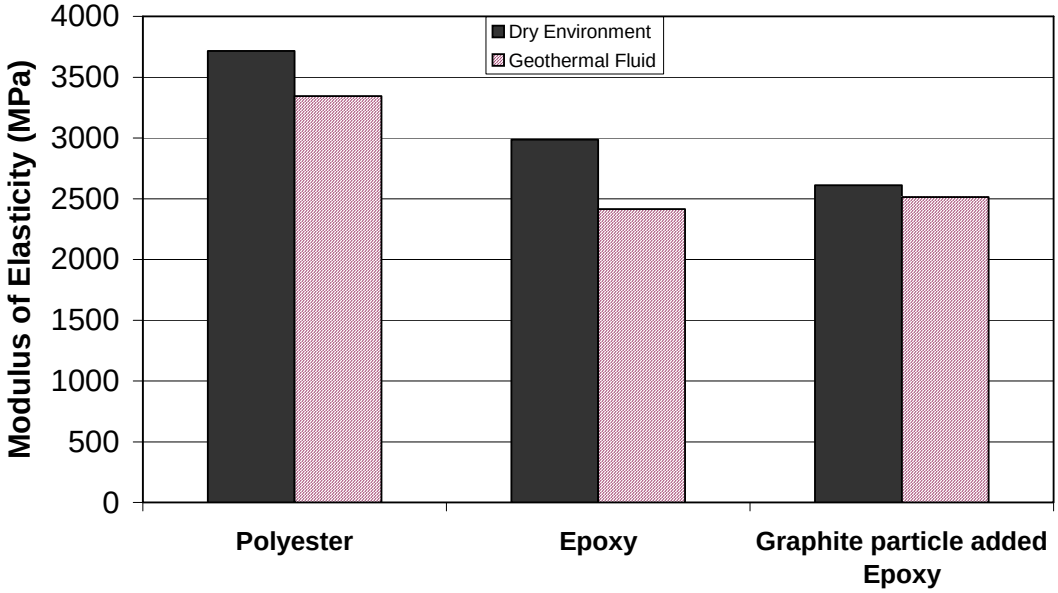

Figure 6.46 Modulus of elasticity values of three types of tube rolled composite tubes exposed to two environments and subjected to compressive loading in axial direction.

Figure 6.47 shows the typical fracture mode of tube rolled composite pipes loaded along axial direction. The fracture mode is due to fiber microbuckling, diamond shaped buckling and matrix fracture. Similar to filament wound composite tubes, the color change shown in Figure 6.47 (b) is due to the residues from geothermal fluid.

(a) **(b)**

Figure 6.47 Photos of the mechanical testing specimens of tube rolled composite tubes loaded along axial direction and exposed to (a) dry environment (b) geothermal fluid.

Figure 6.48 also shows the typical modes of failure for tube rolled specimen loaded along the radial direction. In all the specimens, no visible macro-failure mechanism within the applied stroke was observed. However, micro-failure modes such as fiber failure, fiber/matrix interface debonding matrix microcracking etc. may occur during the loading.

(a) **(b)**

Figure 6.48 Photos of the mechanical testing specimens of tube rolled composite tubes loaded along radial direction and exposed to (a) dry environment (b) geothermal fluid.

6.4.2.3 Energy Absorption

The energy absorption during mechanical loading of tube rolled composite tubes along axial and radial directions was determined. Figures 6.49 and 6.50 show the absorbed energy as a function of stroke for composites made of various matrix materials and loaded along axial and radial directions, respectively. From the figures, the absorbed energy increases with the increase of stroke. Similar to filament wound composite tubes, the energy is the highest for the polyester matrix under axial loading as compared to epoxy and graphite particle added epoxy. However, under radial loading the energy for polyester and graphite particle added epoxy seem to be in the same range.

Figures 6.51 to 6.56 show the absorbed energy as a function of stroke for tube rolled composites made of various matrix material exposed to various environments and loaded along axial and radial directions, respectively.

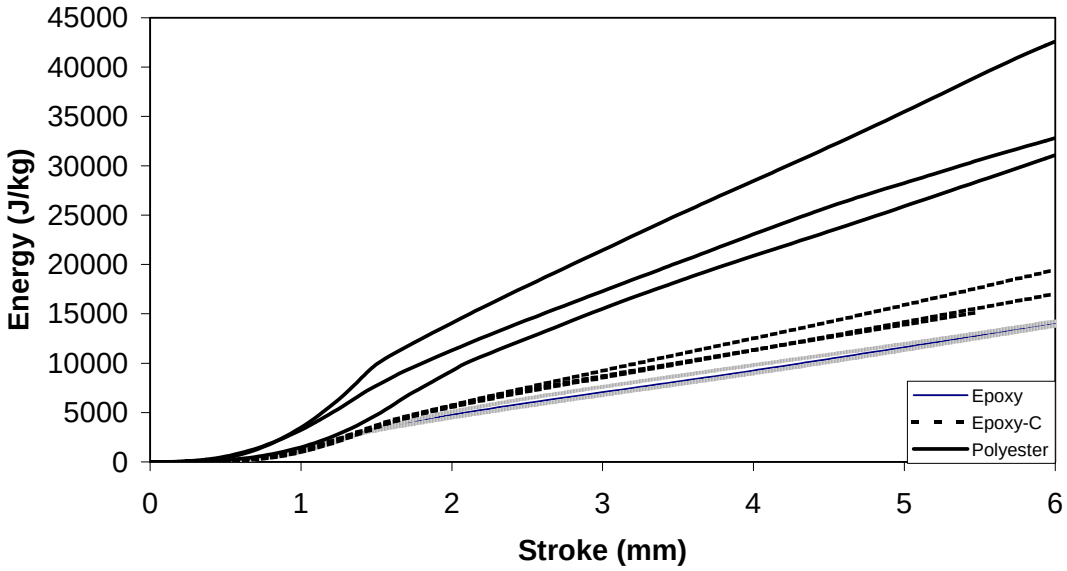

Figure 6.49 Specific energy absorption of three types of tube rolled composite tubes with various matrix polymers and compressed along axial direction.

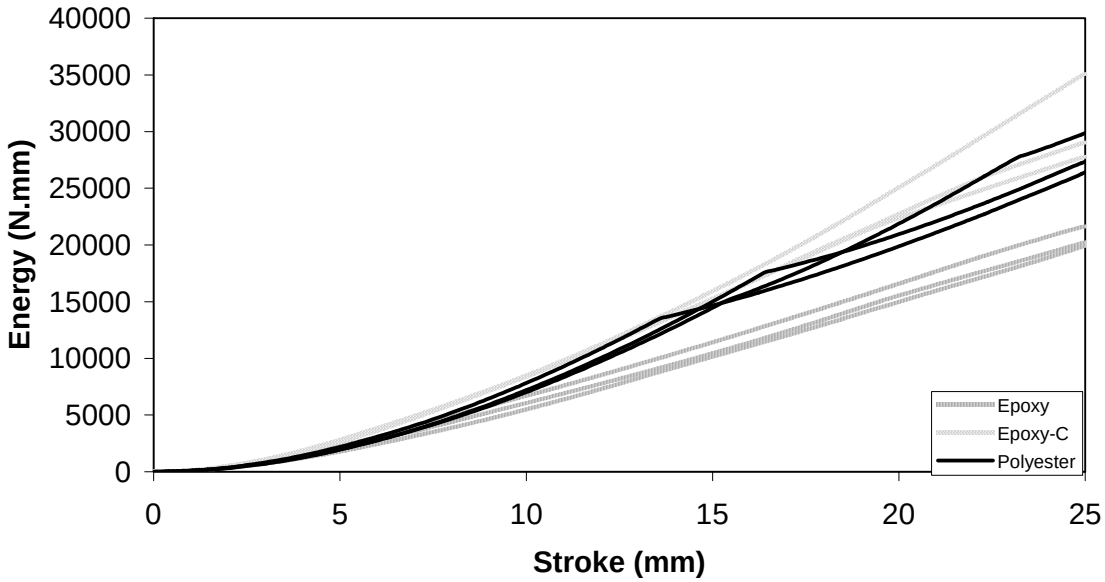

Figure 6.50 Energy absorption of three types of tube rolled composite tubes with various matrix polymers and compressed along radial direction.

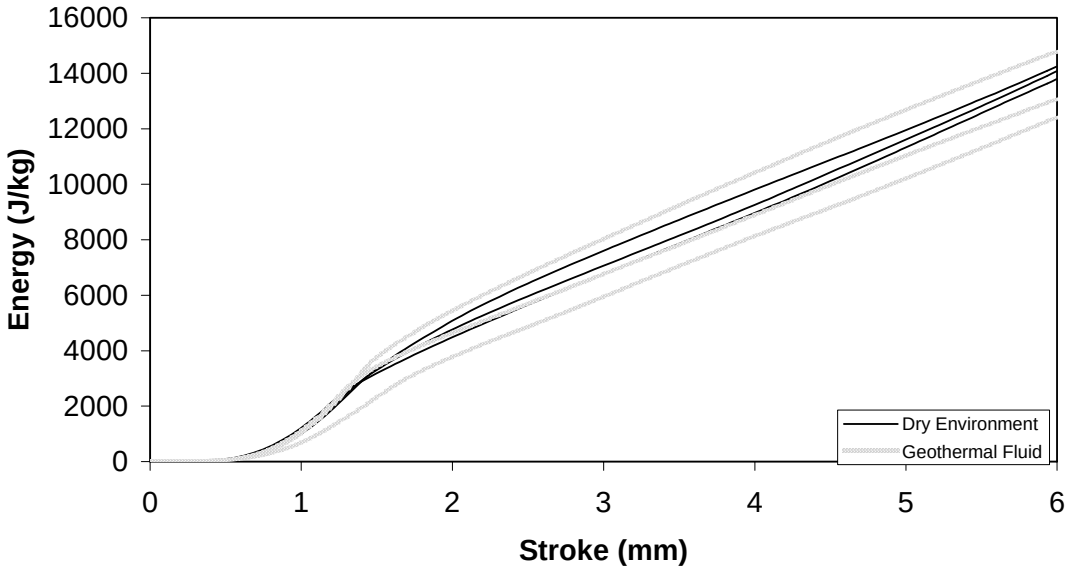

Figure 6.51 Specific energy absorption of E-glass / epoxy tube rolled composite tube exposed to two environments compressed in axial loading.

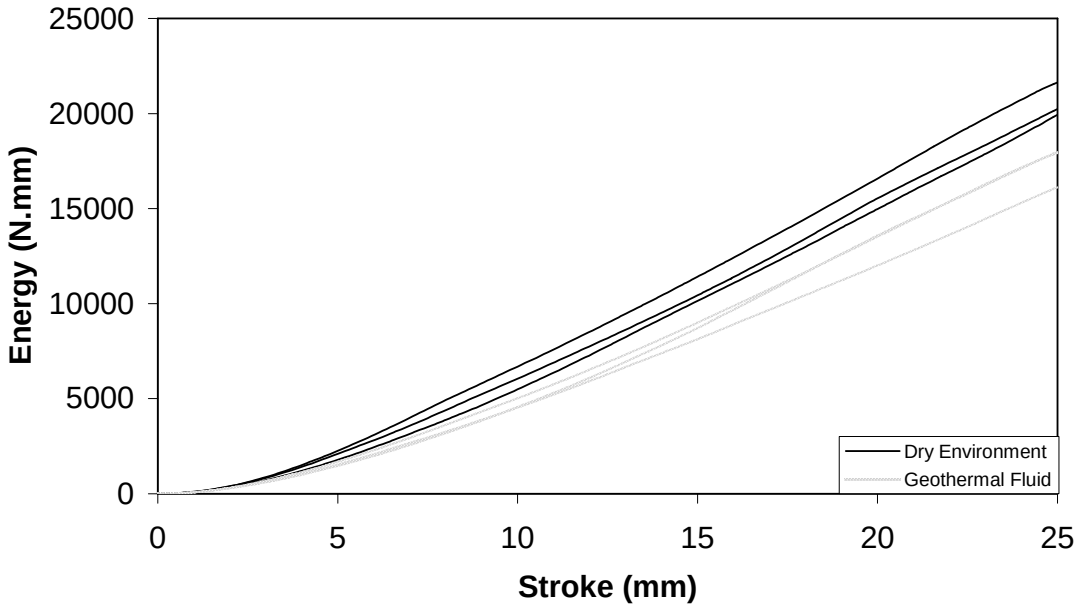

Figure 6.52 Energy absorption of E-glass / epoxy tube rolled composite tube exposed to two environments compressed in radial loading.

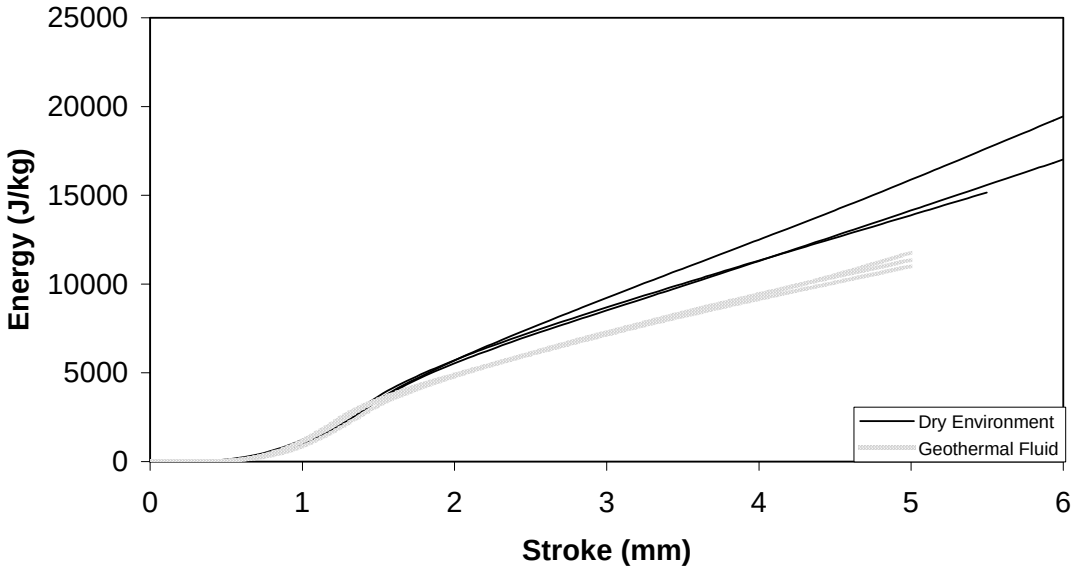

Figure 6.53 Specific energy absorption of E-glass / graphite particles added epoxy tube rolled composite tube exposed to two environments compressed in axial loading.

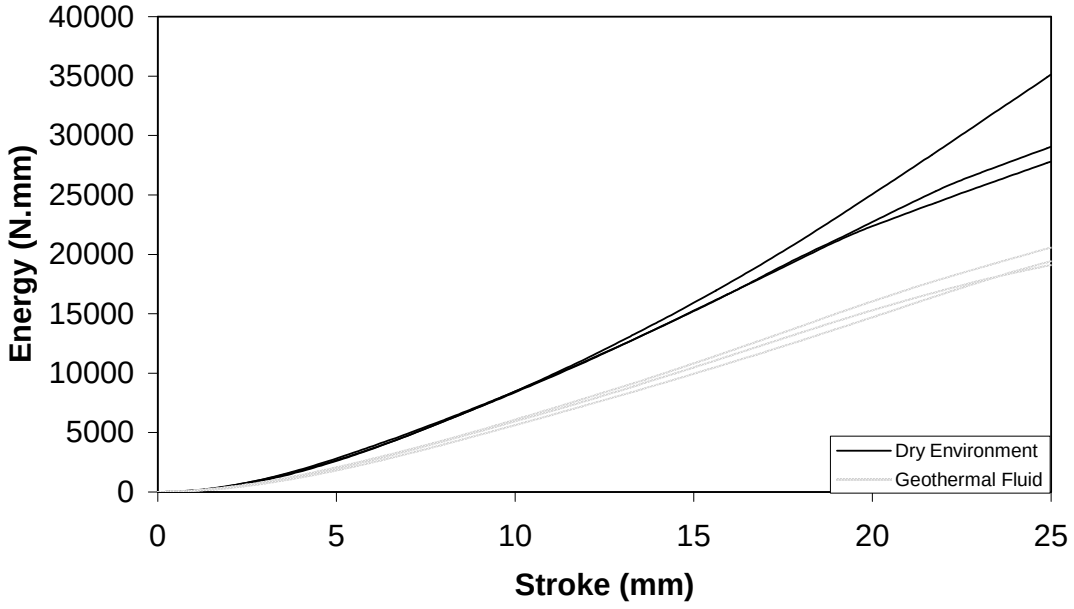

Figure 6.54 Energy absorption of E-glass / graphite particles added epoxy tube rolled composite tube exposed to two environments compressed in radial loading.

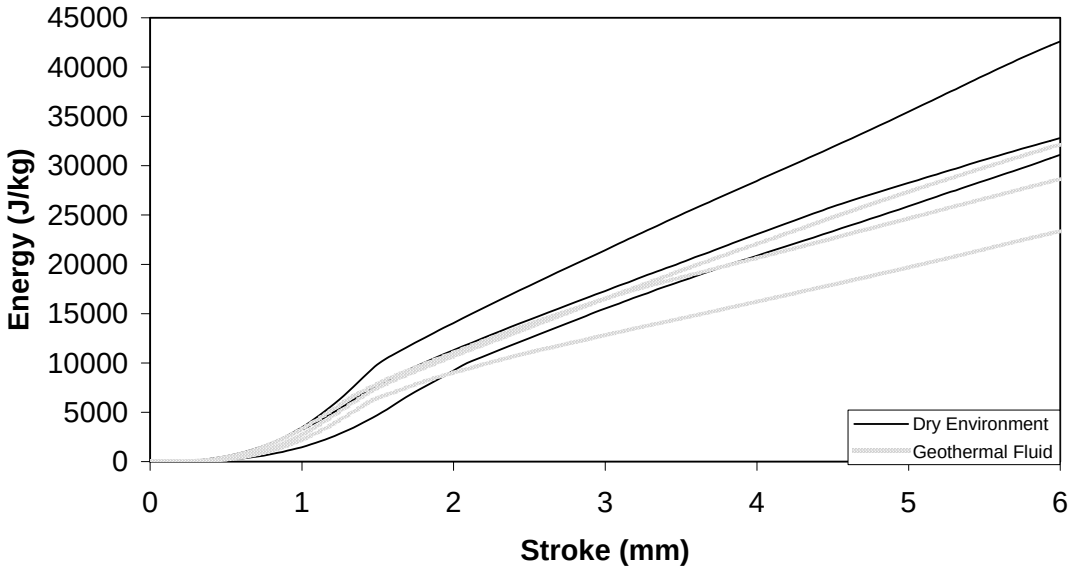

Figure 6.55 Specific energy absorption of E-glass / polyester tube rolled composite tube exposed to two environments compressed in axial loading.

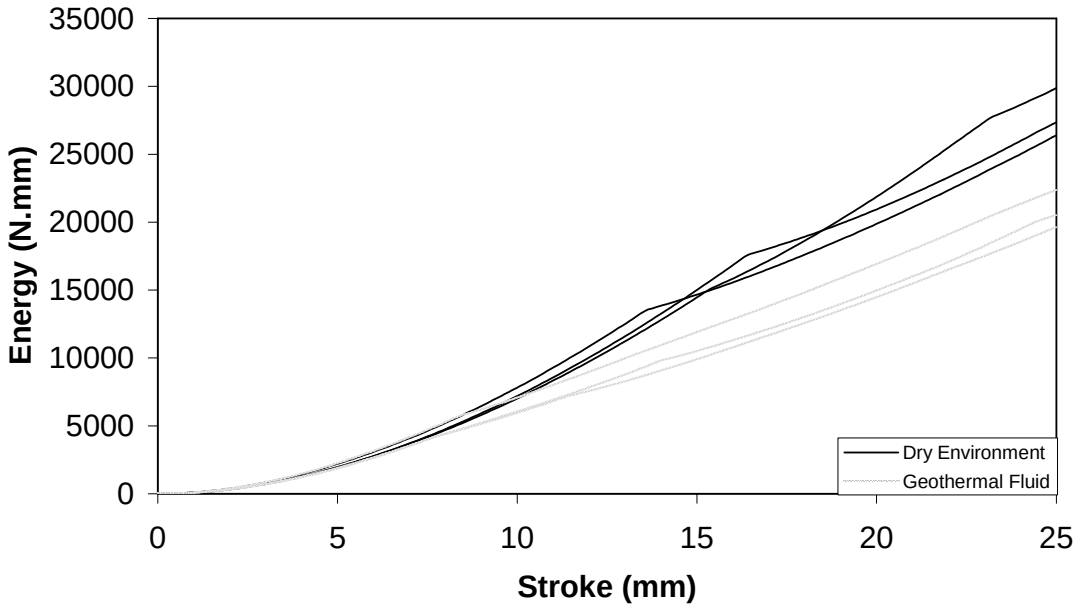

Figure 6.56 Energy absorption of E-glass / polyester tube rolled composite tube exposed to two environments compressed in radial loading.

From Figures 6.51 and 6.52, epoxy matrix exhibited some decrease of energy absorption capability under radial loading under exposure to wet environments. For the same case, under axial loading, no change of energy values was observed between the geothermal fluid exposure and dry environment. For graphite particle added epoxy matrix, the absorbed energies were decreased significantly due to exposure to geothermal fluid under both axial and radial loading conditions as shown in Figure 6.53 and 6.54. For polyester matrix, similar to graphite particle added epoxy matrix, the energy absorption capability, shown in Figure 6.55 and 6.56, was also decreased significantly due to exposure to geothermal fluid under radial loading condition, however, no change of energy values was observed between the geothermal fluid exposure and dry environment under axial loading.

6.4.3 Neat Polymers

6.4.3.1 Mechanical Behavior Under Dry Environment

The compressive mechanical behavior of neat polymer matrix materials and the effects of various hot-wet environments on the properties were investigated. For this purpose, cubic tests specimens were sectioned from post-cured polymer parts of polyester, epoxy and graphite particle added epoxy and at least five specimens for each set was tested using Schmadizu Universal test machine. Figure 6.57 shows the typical stress vs strain graph of various neat polymers under dry environment. As seen in the figure, the stress value is highest for neat polyester matrix. At the beginning, the stress increases linearly and reaches to maximum point at which yield occurs.

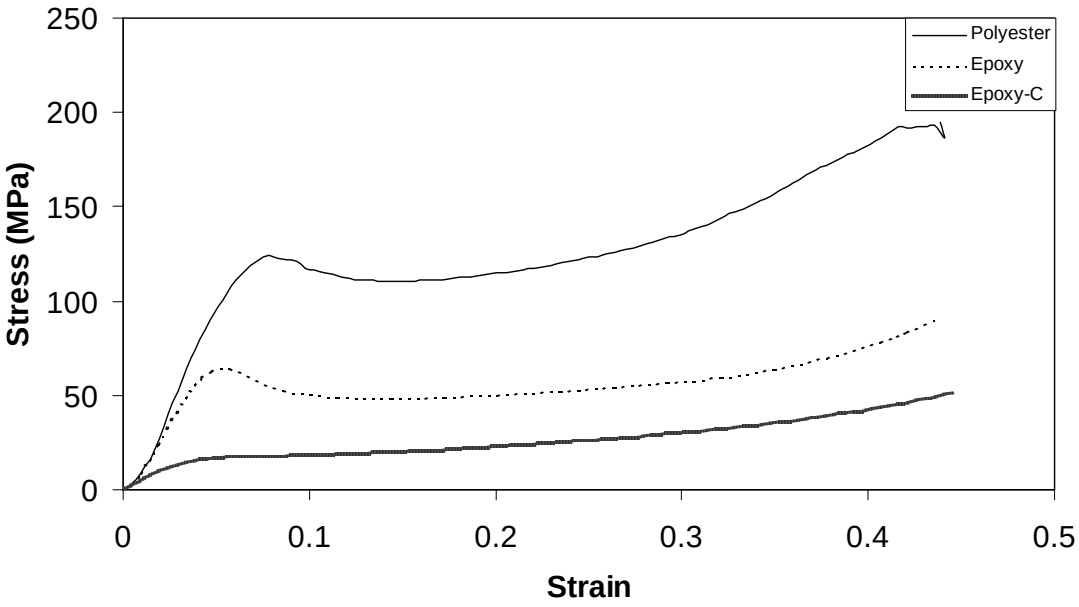

Figure 6.57 Compressive stress vs strain response of various polymers under dry environment.

6.4.3.2 Mechanical Behavior Under Wet Environments

Figure 6.58 to 6.60 shows the typical stress vs strain graphs of the mentioned polymers exposed to dry, distilled water and geothermal fluid, respectively.

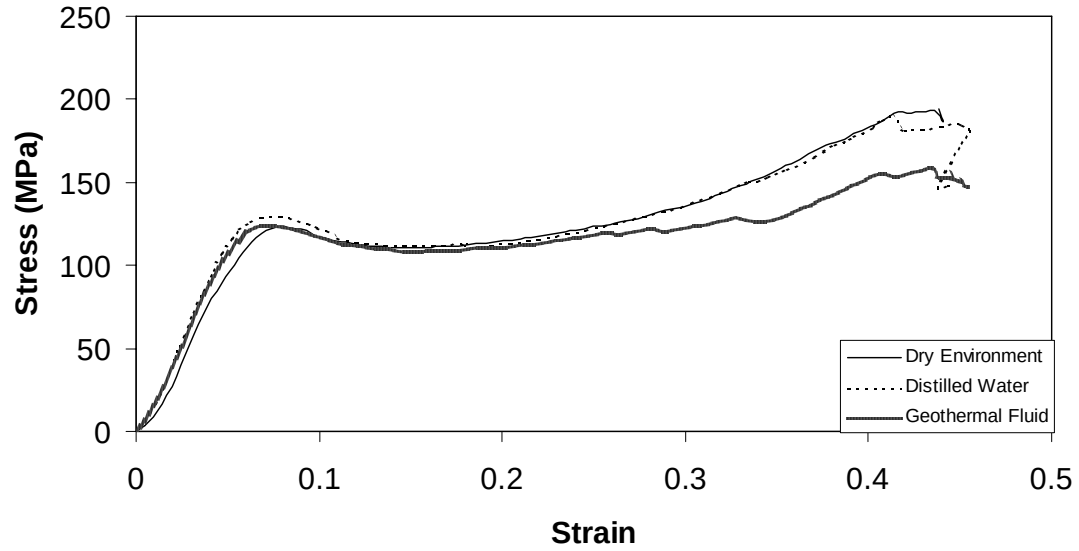

Figure 6.58 Compressive stress vs strain behavior of neat polyester exposed to various environments.

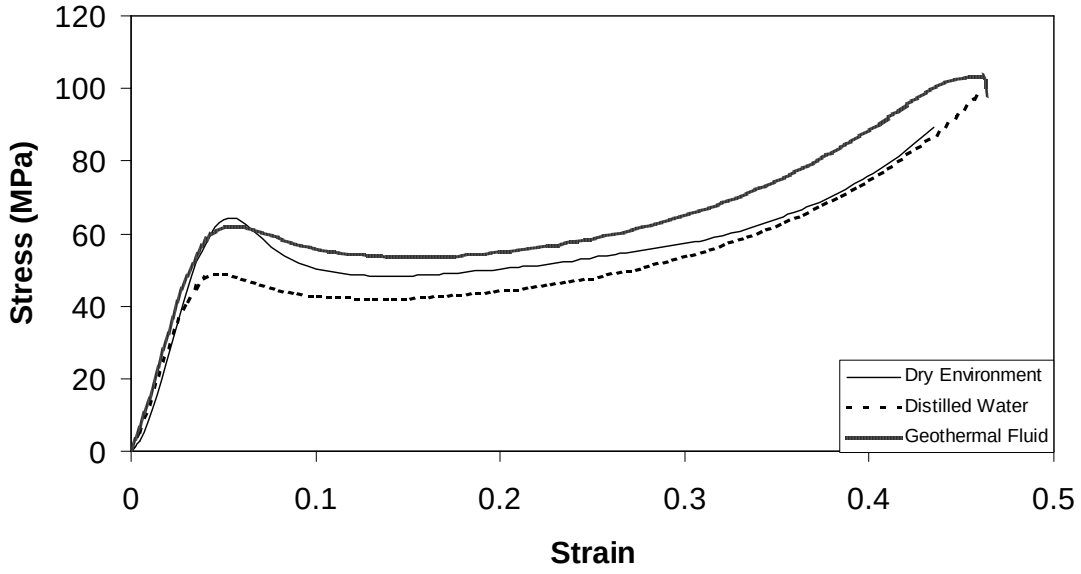

Figure 6.59 Compressive stress vs strain behavior of neat epoxy exposed to various environments.

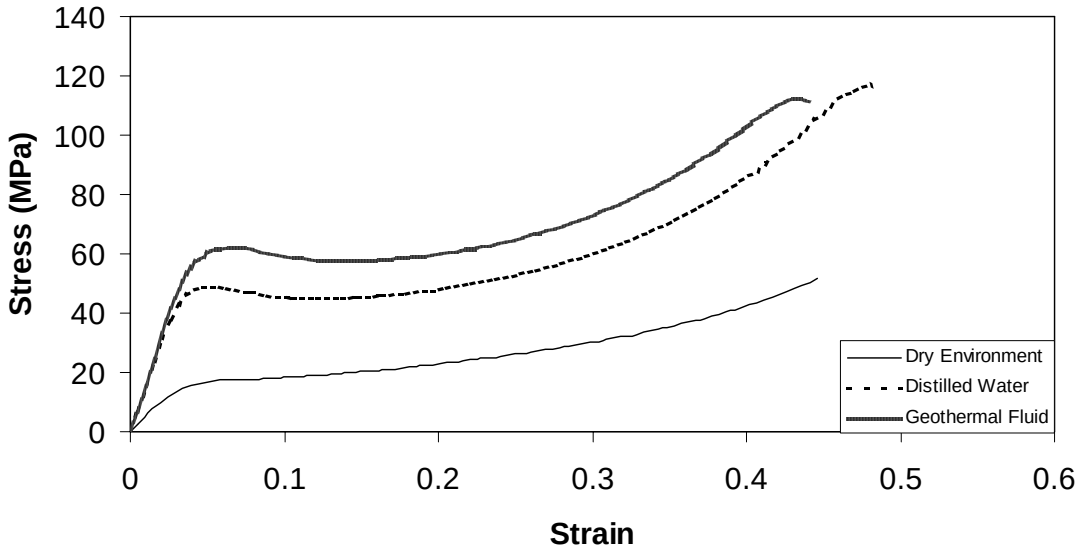

Figure 6.60 Compressive stress vs strain behavior of neat graphite particle added epoxy exposed to various environments.

In general, the stress-strain behavior of all the specimens tested showed linear elasticity up to yield point. The yield point is defined as the point of which deviation was observed in the linear part of stress-strain curve. Above the maximum stress, specimens exhibited significant plastic flow up to high strains. Yield stress, strain at yield and modulus of elasticity values for each specimen were obtained from stress-

strain graphs and average values are plotted in Figures 6.61 to 6.63, respectively. As seen in the figures, polyester exhibited the highest yield stress, strain at yield and modulus of elasticity. Also, it was found that these properties for polyester are not significantly affected by the exposure to hot-wet environments. On the other hand, epoxy and graphite particle added epoxy showed lower yield stress, strain and modulus values. For epoxy, the yield stress and strain values decreased considerably in the distilled water, however, the change was significant in geothermal fluid. The yield stress and modulus values for graphite particle added epoxy was lower as compared to neat epoxy. However, the yield stress, strain and modulus values of graphite particle added epoxy increased by exposure to wet condition and reached to the values of neat epoxy.

The reduced yield stress due to incorporation of graphite particles under dry condition may be associated with the residual stresses and stress concentration by the presence of particles during the loading. The residual stresses may be redistributed and released during hot-wet exposure that took places at elevated temperatures relatively close to the glass transition temperature of the matrix material. In addition, the increase may be related to the progress of cross-linking of polymer network, which may be affected by the presence of graphite particles surfaces.

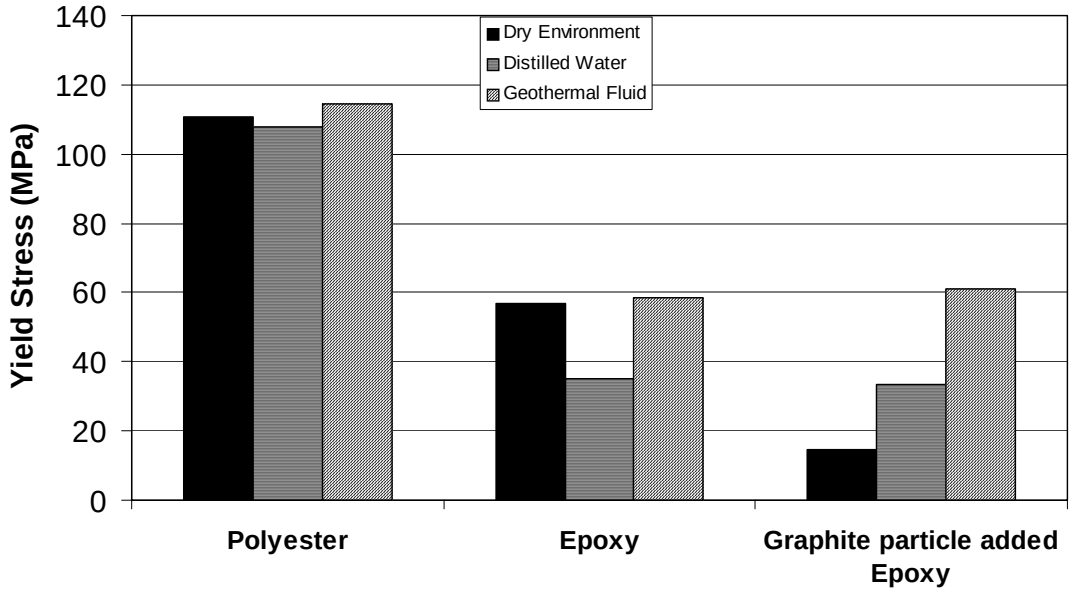

Figure 6.61 Average yield stress values of various types of neat polymers exposed to three different environments.

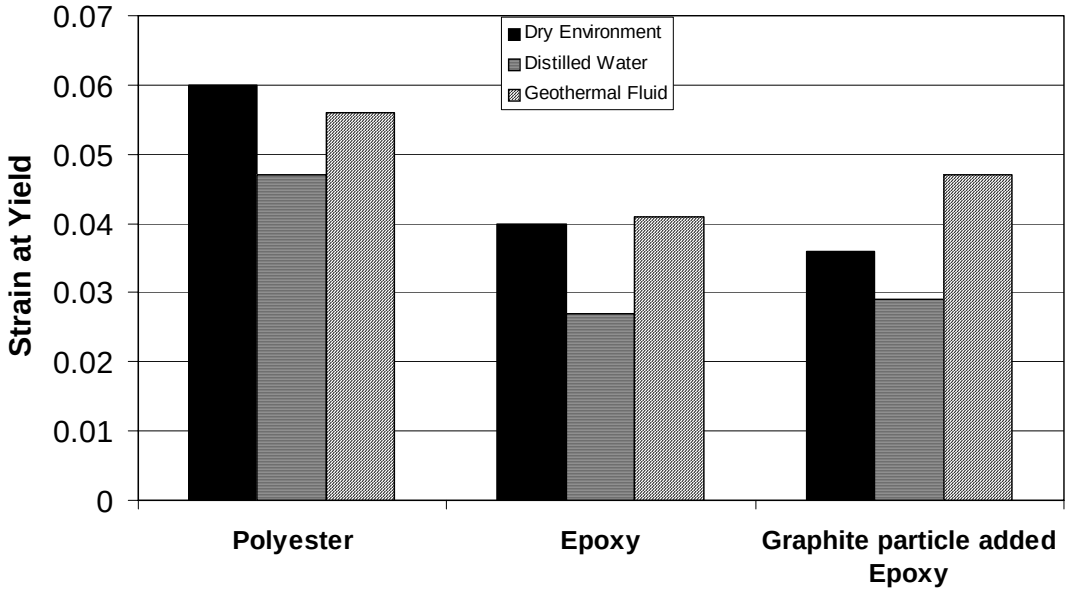

Figure 6.62 Average strain at yield values of various types of neat polymers exposed to three different environments.

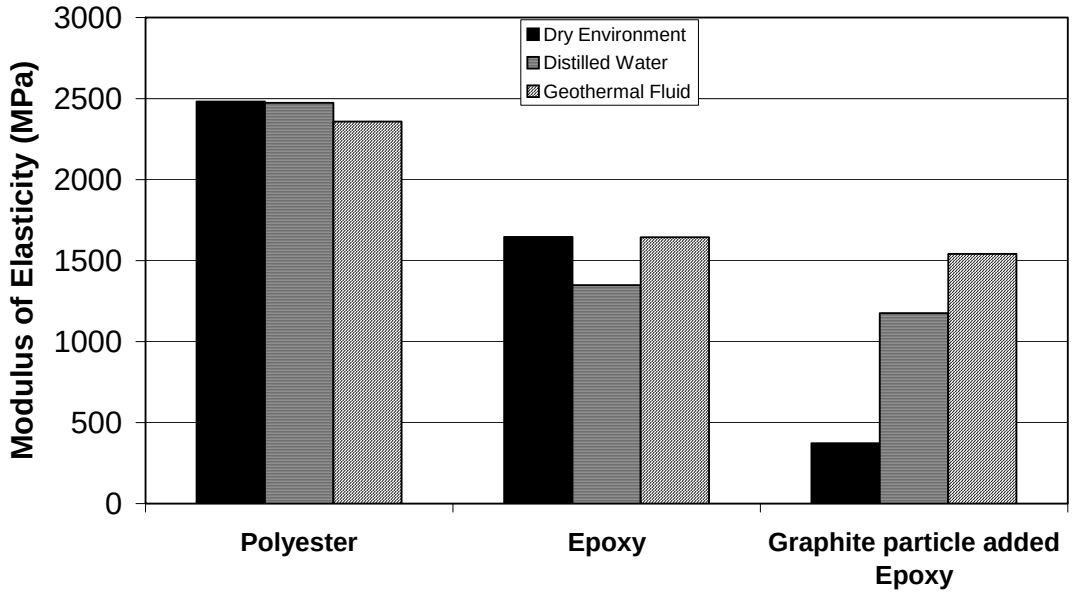

Figure 6.63 Average modulus of elasticity values of various types of neat polymers exposed to three different environments.

6.5 Residues on Composite Surfaces Exposed To Geothermal Fluid and Distilled Water

The surfaces of the E-glass/epoxy composite pipe were analyzed using SEM coupled with EDX analyzer. Figure 6.64 shows SEM micrographs of E-glass/epoxy composite pipe surface exposed to various environments. It was observed that some particles were precipitated on the surface of the pipe exposed to geothermal fluid.

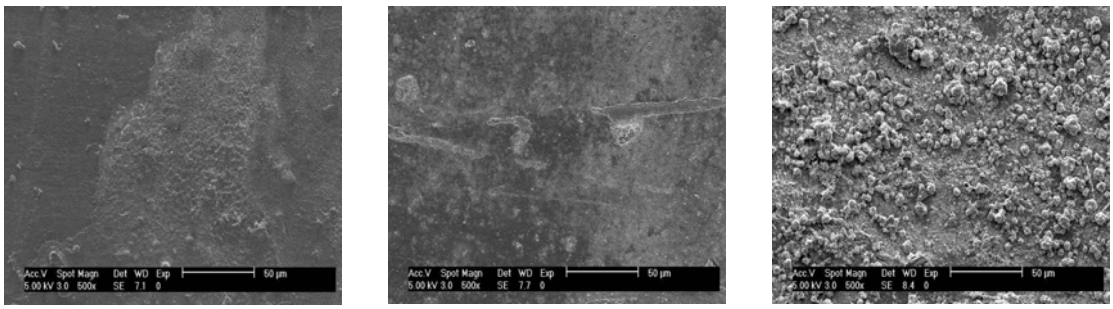

(a) **(b)** **(c)**

Figure 6.64 SEM micrographs of the E-glass/epoxy composite pipe surface; at (a) dry environment, exposed to (b) distilled water and (c) geothermal fluid.

Figure 6.65 gives SEM-EDX results showing the chemical composition of the particles accumulated on the surface of the composite pipes exposed to dry environment, distilled water and geothermal fluid. As it can be seen in the Figure 6.65, the chemical composition of the surface of dry specimen and the one exposed to distilled water is almost similar. On the other hand, on the surface exposed to geothermal fluid, there is a significant increase in oxygen, iron, silica, chloride, aluminum, sulfur and calcium elements resulted by precipitation.

The EDX analysis and chemical analysis of geothermal fluid were modeled and interpreted by Dr. Lutz B. Giese, who is a geochemist, works for Federal Institute Research and Testing (BAM) in Germany. Solution-mineral equilibrium computations software (SOLMINEQ) was used for modeling. The geothermal fluid data of B-10 well was put to an input file, which was first modeled for 25^{o}C temperature, then for 84^{o}C. The results are given in Appendix A.4 and A.5.

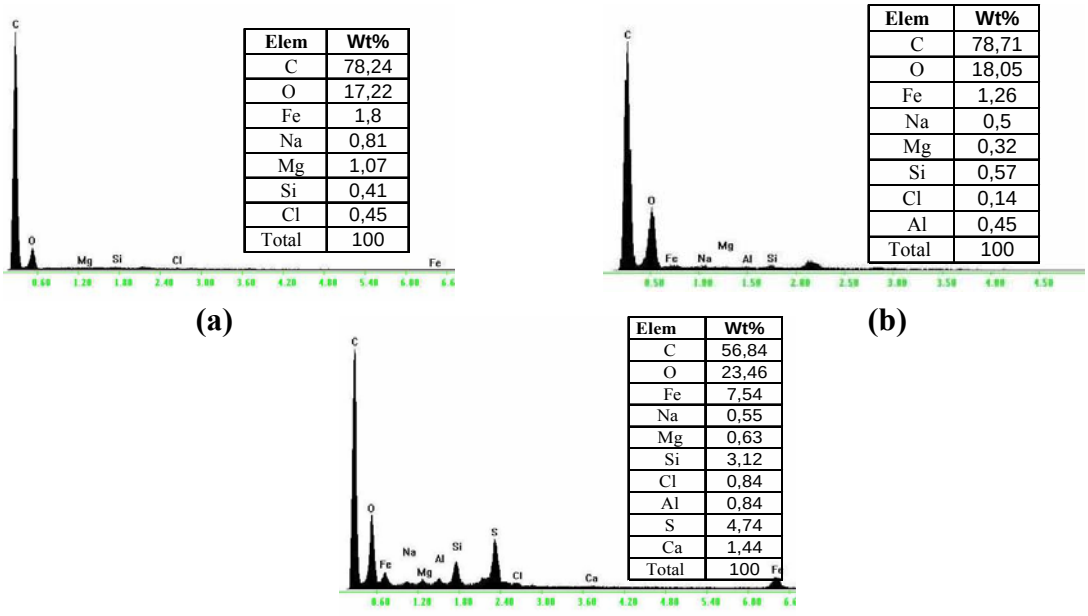

Elem	Wt%
C	78,24
O	17,22
Fe	1,8
Na	0,81
Mg	1,07
Si	0,41
Cl	0,45
Total	100

(a)

Elem	Wt%
C	78,71
O	18,05
Fe	1,26
Na	0,5
Mg	0,32
Si	0,57
Cl	0,14
Al	0,45
Total	100

(b)

Elem	Wt%
C	56,84
O	23,46
Fe	7,54
Na	0,55
Mg	0,63
Si	3,12
Cl	0,84
Al	0,84
S	4,74
Ca	1,44
Total	100

(c)

Figure 6.65 SEM-EDX results showing the chemical composition of the residual particles accumulated on the surface of the composite pipes at (a) dry environment, (b) distilled water and (c) geothermal fluid.

The output of the program gives that;

1) Ion balance is very well.
2) At 84°C temperature, saturation indices of aragonite, calcite, fluorite (CaF_2) and some iron minerals, e.g. goethite (FeO(OH)) and ankerite ($Ca(Fe^{+2})CO_3$) are supersaturated, silica is undersaturated. In Table A.4 and A.5, first vertical line is log (AP), logarithm of ion activity product. This is taken from actual content in the solution. Second is log (KT), which is log of the solubility product (constant factor, depends on T). Third is log (AP/KT) = SI (saturation index), if AP = KT, AP/KT is one, log (AP/KT) is zero, this is saturation, if log (AP/KT)< 0 undersaturation, if > 0 supersaturation.
3) After cooling down to 25°C, saturation indices are undersaturated for aragonite ($CaCO_3$) and calcite ($CaCO_3$), fluorite (CaF_2) and less iron minerals are still supersaturated, but now silica is supersaturated.

According to the EDX results, there are significant peaks of carbon (from composites) and oxygen (belong partly to the plastics). The precipitation seems to bring a bit of calcium, but significantly iron, sulphur and silicon. Oxygen rises (amorphous

SiO_2) whereas carbon decreases because of dilution effect by the scaling to the background. At 84°C, some carbonate ($CaCO_3$), scaling disposes as aragonite and/or calcite, which depends mainly on the temperature. Due to cooling, precipitation stops as the carbonate solubility rises while temperature sinks. Iron minerals also may dispose as oxides or hydroxooxides but also FeS, because of the high sulphur content, which otherwise is difficult to be explained. At low temperature after cooling, amorphous silica precipitates but not carbonate. This may be what is seen mainly on the SEM picture. It is also possible that due to silica precipitation co-precipitation of iron occurs [80]. However, it hasn't been clarified that these residual particles are scaling. They may be some accumulated particles and they may be removed during high flow rate. In Balçova, inhibitors are used to prevent scaling. Scaling in pipes cause reduction in pipe diameter, which reduces flow rate and extracted heat from the fluid.

6.6 Thermal Conductivity of the Composite Pipes

The thermal conductivity of the composite specimens was measured at room temperature using hot-wire method with Shotherm QTM machine. The results are given in Table 6.5.

Table 6.5 Thermal conductivity (k) values for E-glass composites with various matrix polymers.

Materials	k (W/m.K)
E-glass/epoxy Composite	0.310
E-glass/polyester Composite	0.303
E-glass/epoxy-C Composite	0.267

Thermal conductivity values exhibit small difference between E-glass/epoxy and E-glass/polyester composites. On the other hand, E-glass/graphite particles added epoxy composite has the lowest value among three composites. Therefore, it can be said that graphite particles cause reduction in thermal conductivity and they decrease heat loss from the pipe. In general, composite materials have a very low thermal conductivity compared with metals (Table 5.2) and they can be classified as insulators given in Figure 5.11.

6.7 Temperature Distribution and Heat Losses Within the Composite Pipes

To compare the thermal performance of manufactured composite pipes with carbon steel pipe, which is used in Balçova Geothermal District Heating System, using the equations given in Section 5.8, the heat loss per length (Q), the outer surface temperature of pipe (T_1) and temperature dropdown at 1 km distance from the inlet (T_0) for various insulation thickness (0-20 mm) were calculated and given in Table 6.6.

Table 6.6 The outer surface temperature (T_1), heat loss (Q), geothermal fluid temperature at 1 km. distance from the inlet (T_0), temperature difference between inlet temperature (84°C) and temperature at 1 km length (ΔT) for insulation thickness 0-20 mm.

	Pipe Material	T1 (°C)	Q (W/m)	To (°C)	ΔT (°C)
	Polyester	81.16	59.527	82.711	1.289
Without	Epoxy	81.221	59.572	82.71	1.29
Insulation	Epoxy-C	80.795	59.26	82.717	1.283
	Carbon Steel	83.958	61.579	82.666	1.334
	Polyester	49.350	37.533	83.187	0.813
With	Epoxy	49.373	37.351	83.187	0.813
5 mm	Epoxy-C	49.210	37.427	83.190	0.81
Insulation	Carbon Steel	50.409	38.339	83.170	0.83
	Polyester	39.245	30.471	83.340	0.66
With	Epoxy	39.260	30.482	83.340	0.66
10 mm	Epoxy-C	39.154	30.400	83.342	0.658
Insulation	Carbon Steel	39.926	30.999	83.329	0.671
	Polyester	28.367	22.869	83.505	0.495
With	Epoxy	28.375	22.876	83.505	0.495
20 mm	Epoxy-C	28.318	22.829	83.506	0.494
Insulation	Carbon Steel	28.735	23.166	83.498	0.502

Table 6.6 indicates that for uninsulated pipes, heat loss of carbon steel is 3.63 % higher than composite pipes. Increasing insulation thickness decreases the sensitivity on pipe material. For 20 mm insulation thickness, heat loss of carbon steel is only 1.47 % higher than composite pipes. This implies to pipe outer surface temperature as well. For uninsulated pipes, outer surface temperature of carbon steel is almost 84^0C, which is 3^0C higher than composite pipes, but for 20 mm insulation thickness, the temperature difference between carbon steel and composite pipe is 0.3^0C. Figure 6.66 shows the heat loss values with changing insulation thickness. Optimum insulation thickness

corresponds to a minimum combined cost of insulation and heat loss. Since the economic analysis is out of interest of this Thesis, deciding the optimum insulation thickness another parameter should be investigated. This parameter is the temperature dropdown between fluid inlet and exit temperature at 1 km. Recommended temperature dropdown at 1 km length of a pipe, which carries geothermal fluid, is maximum 1^0C [78]. Figure 6.67 shows the temperature difference between inlet and at 1 km. length of the pipe depending on insulation thickness. For maximum 1°C temperature dropdown under the experimental conditions, the required insulation thickness for composite pipes is 2.5 mm, for metal pipe is 3 mm. It can be concluded that, since heat loss is lower in composite pipes, the required insulation thickness is lower which reduces the cost of the pipeline.

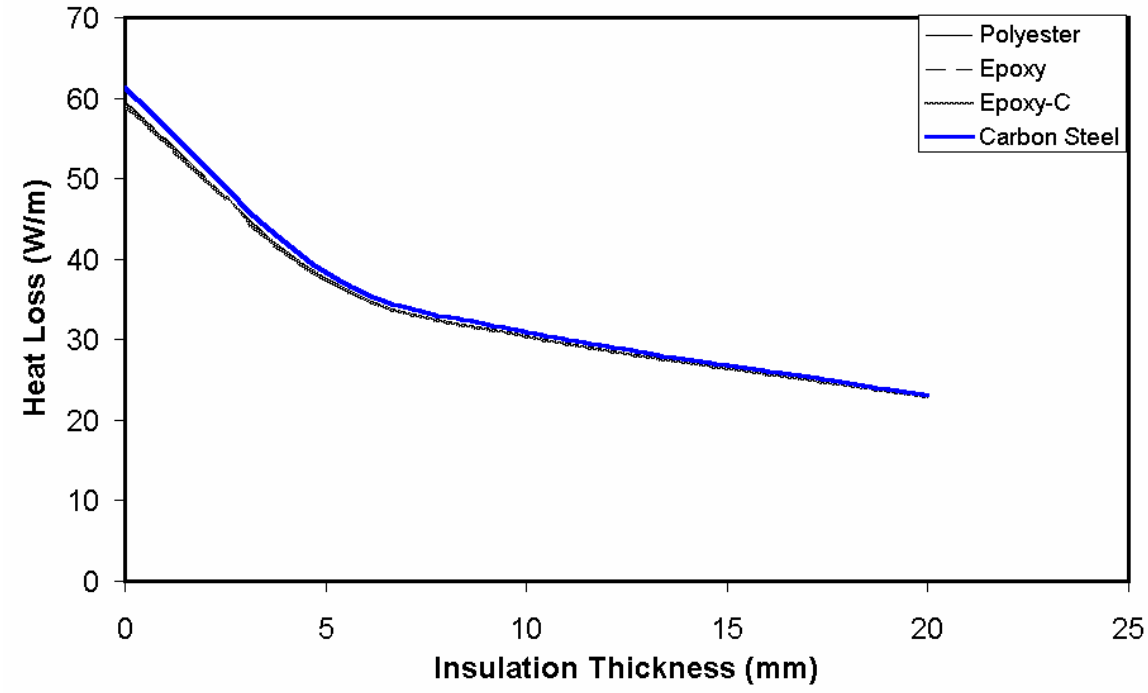

Figure 6.66 The graph of required insulation thickness as a function of heat loss.

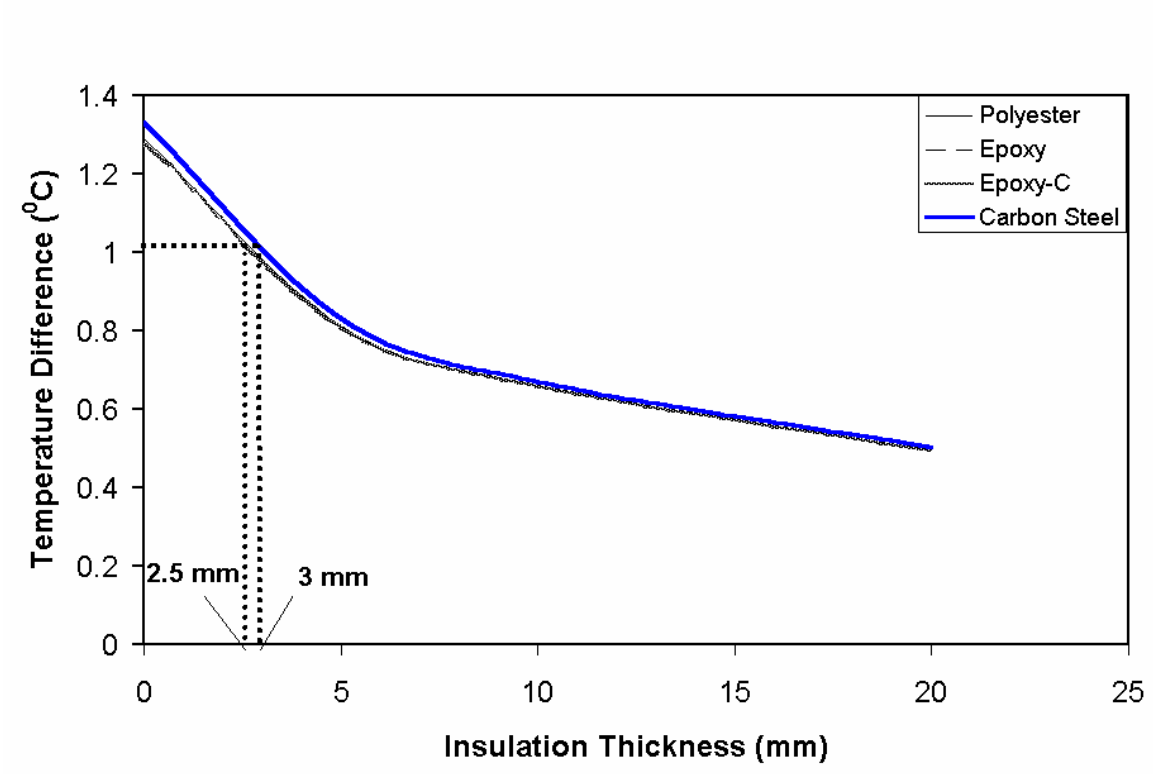

Figure 6.67 The graph of required insulation thickness as a function of temperature difference.

For aboveground installation, outer surface temperatures of three types of composite pipes and carbon steel pipe were calculated by LUSAS software. Figure 6.68, 6.70, 6.72 and 6.74 show the radial temperature distributions of uninsulated geothermal pipes including polyester, epoxy, graphite particle added epoxy composite and carbon steel pipes, respectively. Figure 6.69, 6.71, 6.73 and 6.75 show the time taken to reach the steady state outer surface temperature for the uninsulated geothermal pipes including polyester, epoxy, graphite particle added epoxy composite and carbon steel pipes, respectively. Figure 6.68 gives outer surface temperature of polyester composite pipe as 70.17^0C, which is reached at 150 seconds, as shown in Figure 6.69. Figure 6.70 gives outer surface temperature of epoxy composite pipe as 70.42^0C, which is reached at approximately 150 seconds, as shown in Figure 6.71. Besides, outer surface temperature of graphite particle added epoxy composite pipe is 68.71^0C as shown in Figure 6.72 and it can be seen from Figure 6.73 that the temperature is reached at 155 seconds. Finally, Figure 6.74 gives outer surface temperature of carbon steel pipe as 83.92^0C, which is reached at approximately 20 seconds, as shown in Figure 6.74.

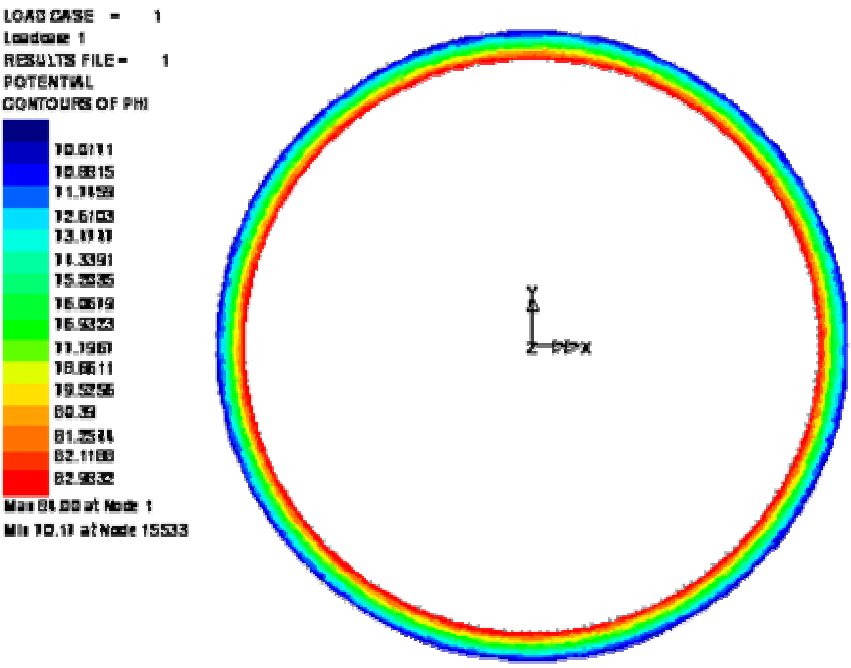

Figure 6.68 The radial temperature distribution of the polyester composite pipe.

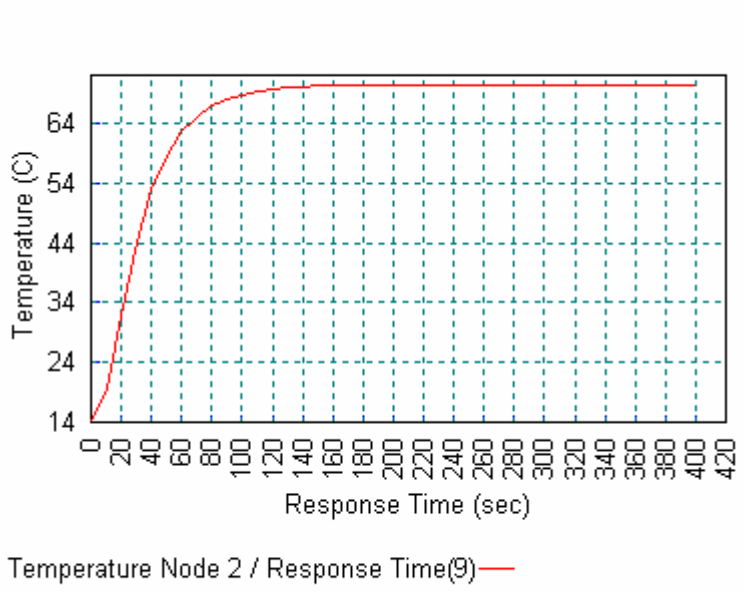

Figure 6.69 Time to reach the steady state condition for polyester composite pipe.

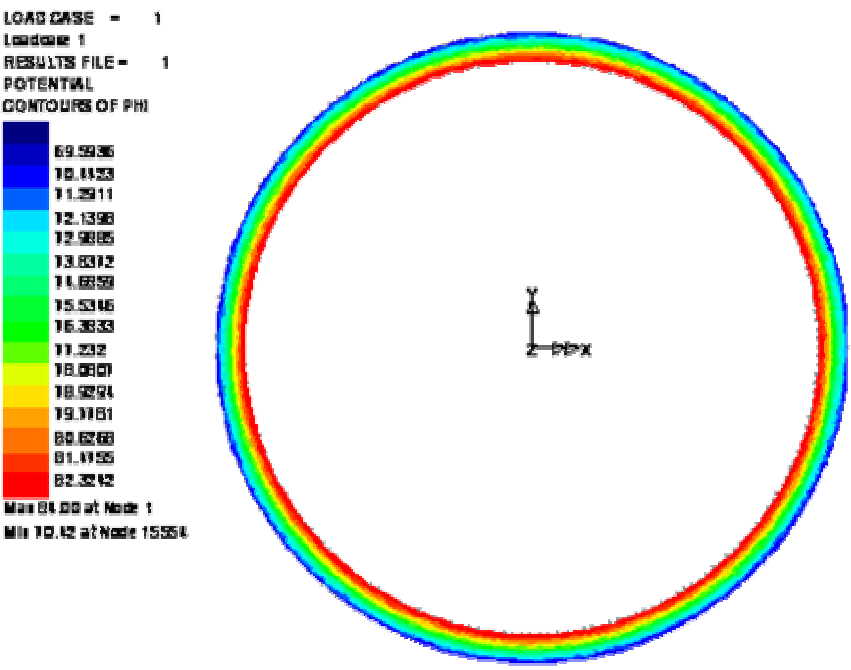

Figure 6.70 The radial temperature distribution of epoxy composite pipe

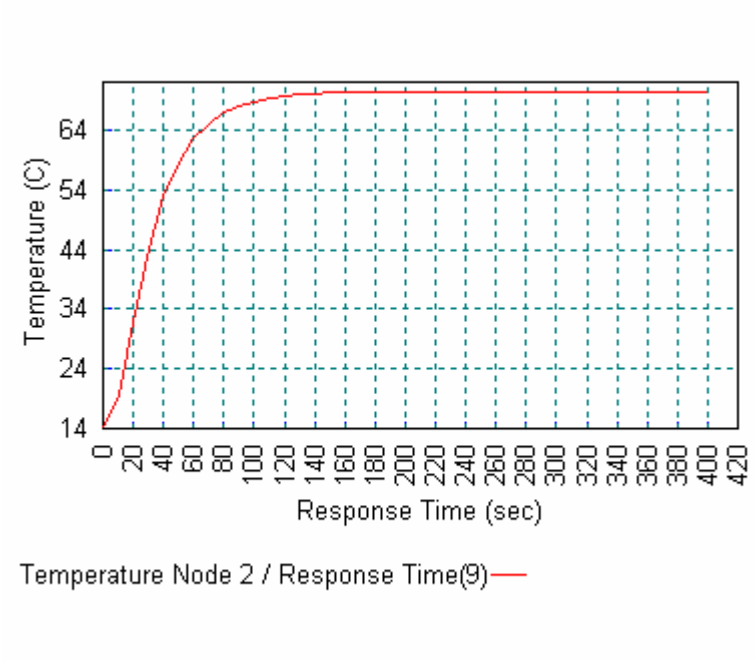

Figure 6.71 Time to reach the steady state condition for epoxy composite pipe.

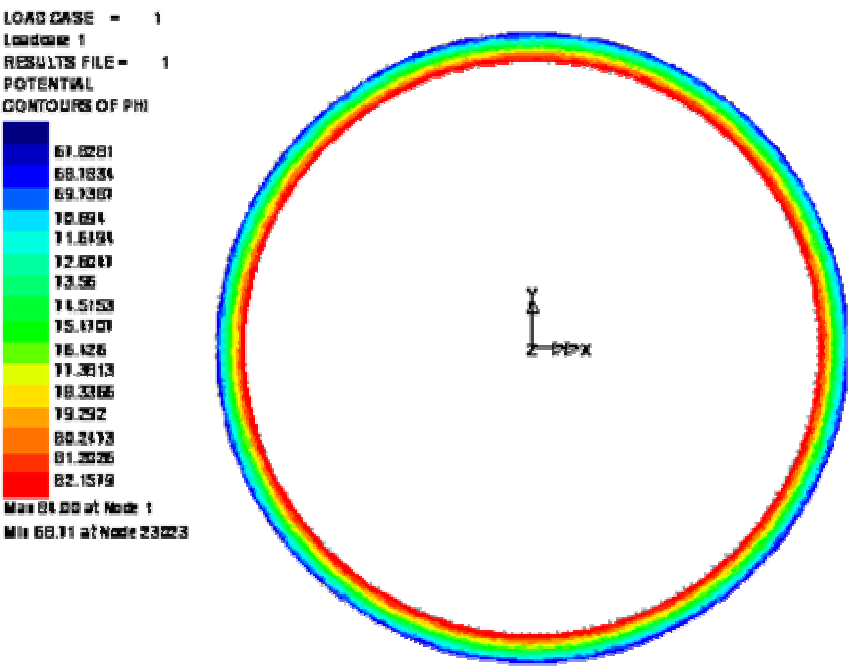

Figure 6.72 The radial temperature distribution of graphite particle added epoxy composite pipe

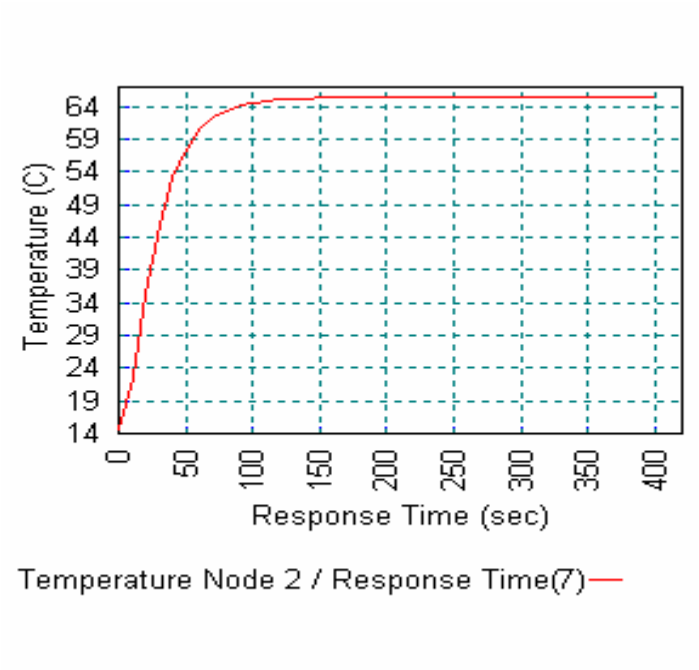

Figure 6.73 Time to reach the steady state condition for graphite particle added epoxy composite pipe.

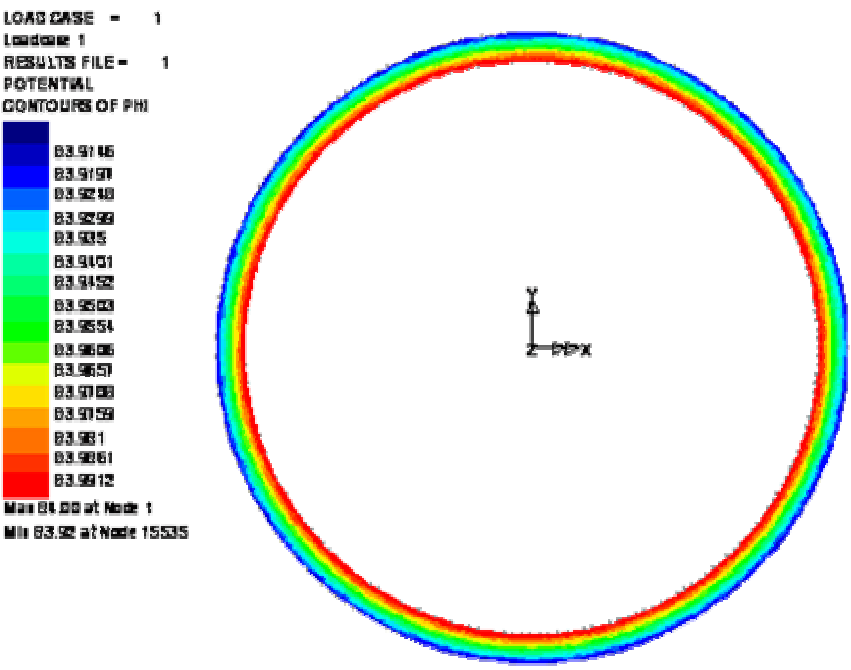

Figure 6.74 The radial temperature distribution of the carbon steel pipe

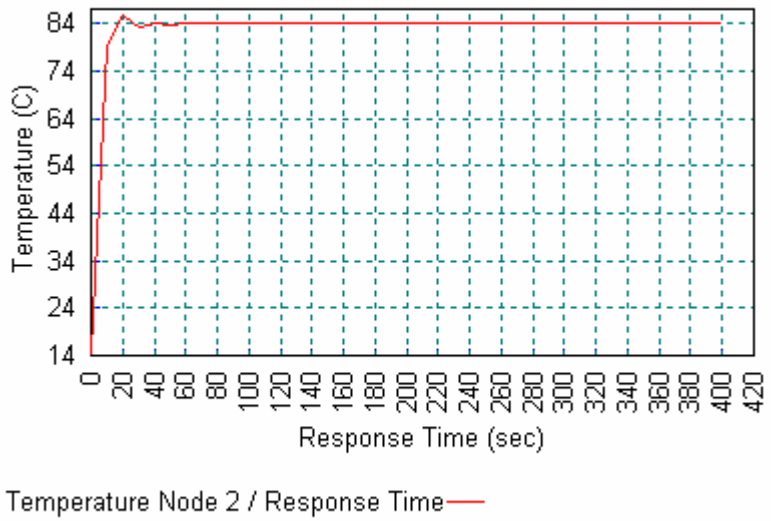

Figure 6.75 The time to reach the steady state condition for carbon steel pipe

CHAPTER VII
CONCLUSIONS AND RECOMMENDATIONS

E-glass fiber reinforced polymer composites were fabricated by employing filament winding and tube rolling techniques with various matrix materials, including polyester, epoxy and graphite particle added epoxy materials. This study focused on investigating interactions between geothermal fluid and the mentioned composite piping materials and the mechanism of degradation in the composites. Water uptake measurements revealed that polyester composite pipes absorb much water than epoxy and graphite particles added epoxy matrix composite pipes. On the contrary, the water uptake values were much less for graphite particles added epoxy composite pipe as compared to epoxy matrix material. Besides, the composite tubes produced by tube rolling method absorbed slightly higher amount of water than filament wound composite tubes in geothermal fluid. This may be related to the usage of the woven fabric and the voids on the surface produced within the tube rolling process. Similar to composites, neat polyester specimens exhibited a higher degree of water absorption than neat epoxy and graphite particles added epoxy polymer specimens As well, the composite tube specimens gained considerably less weight than the neat polymer specimens. It may be related to larger surface area of neat polymers as compared to composite tubes. In addition, the time to reach to saturation was shorter for specimens in distilled water than for those in the geothermal fluid. This might be due to the filling of surface cavities by the residues of geothermal fluid. Based on the water uptake measurements, it was observed that graphite particles prevented water absorption into the composite structure.

According to mechanical testing results, polyester composite pipes exhibited the highest mechanical strength as compared to the other types of composite pipes under both axial and radial loadings. It was found that the mechanical properties of the pipes considerably degrade when they are exposed to geothermal fluid as well as distilled water environments at elevated temperatures. A relatively less degradation for graphite particles added epoxy composite pipes were measured. It was also found that, in dry environment, polyester reinforced tube absorbs the highest amount of energy under axial loading, however, graphite particles added epoxy reinforced composite pipes absorbs the highest amount of energy under radial loading. Similar to mechanical

behaviors, the energy absorption capabilities of composite pipes decreased after they had been exposed to geothermal fluid. It was observed that the fracture mode of filament wound composite pipes is collapse in transverse shearing mode and matrix fracture occurred along fiber winding angle direction under axial loading. There is no visible macro-failure mechanism within the applied stroke and micro-failure mechanisms (fiber failure, fiber/matrix interface debonding etc.) may operate under radial loading. On the other hand, the fracture modes of tube rolled composite tubes are fiber microbuckling, diamond shaped buckling and matrix fracture in axial loading. Similar to filament wound composite tubes, there is no visible macro-failure mechanism under radial loading. The damage process may be initiated by means of microcracking, either in the form of matrix cracking in fiber-free zones or transverse cracking initiated at the porosity combined with fiber/matrix debonding and there might be delamination between the different plies. When the specimens were exposed to geothermal fluid of B-10 well in Balçova Geothermal Field, some residues accumulated on the surface of composite pipes due to geothermal fluid were detected. These residual particles were investigated using SEM-EDX. It hasn't been clarified that these residual particles are scaling. For the surfaces exposed to geothermal fluid, there is a significant increase of the oxygen, iron, silica, chloride, aluminum, sulfur and calcium resulted by the accumulation of the residues depending on the fluid chemistry of the source.

Thermal conductivity coefficient measurements showed that the conductivity of the composites is the lowest as compared to metals. Also, the incorporation of graphite particles into epoxy system caused further reduction in the value of thermal conductivity. Therefore, the calculated heat loss from graphite particles added epoxy composite pipe without insulation was found to be less than other types of composite pipes, however, when the isolation is used, heat loss is not sensitive to pipe material. Optimum insulation thickness corresponds to a minimum combined cost of insulation and heat loss. Since the economic analysis is out of interest of the Thesis, deciding the optimum insulation thickness another parameter should be investigated. The economic analyses of the pipe materials and optimum isolation thickness may be the future works. Therefore, it was calculated that for maximum 1°C temperature dropdown under the experiment conditions, the required insulation thickness for composite pipes is 2.5 mm, for metal pipe is 3 mm. Furthermore, an important parameter for choosing the insulation material is the thermal expansion. If the thermal expansion value of insulation material is not suitable with the pipe material, there may be some cracks in insulation and the

insulation might not perform its service. For these types of composite pipes, polyurethane foam should be used as an insulator.

To our knowledge, there is not much work reported in the literature about the filament wound composites with polymer matrices containing particulates. As summarized before, addition of these particles affected the water up take values, mechanical behavior and thermal properties. Therefore, investigation of the effects of particle addition on the performance of composites with different materials may be a future work. Moreover, the comparison of scaling and corrosion performance of composite and metallic pipes might be another future work.

REFERENCES

1. Lund J., Lienau Paul, Lunis B., "Geothermal Direct-use Engineering and Design Guidebook", Geo-Heat Center, Oregon Institute of Technology
2. Stahl G., Patzay G., Weiser L., Kalman E., "Study of Calcite Scaling and Corrosion Processes in Geothermal Systems", Geothermics 29 (2000) 105-119
3. Bai J., Seeleuthner P., Bompard P., "Mechanical Behaviour of ± 55^0 Filament-Wound Glass-Fibre/Epoxy-Resin Tubes: I. Microstructural Analyses, Mechanical Behaviour and Damage Mechanisms of Composite Tubes Under Pure Tensile Loading, Pure Internal Pressure and Combined Loading" Composites Science and Technology 57 (1997) 141-153
4. Kaynak C., Mat O., "Uniaxial Fatigue Behavior of Filament-wound Glass-fiber/epoxy Composite Tubes", Composites Science and Technology 61 (2001) 1833-1840
5. Perreux D., Suri C., " A Study of the Coupling Between the Phenomena of Water Absorption and Damage in Glass/Epoxy Composite Pipes", Composite Science and Technology 57 (1997) 1403-1413
6. Bai J., Seeleuthner P., Bompard P., "Mechanical Behaviour of ± 55^0 Filament-Wound Glass-Fibre/Epoxy-Resin Tubes: II. Micromechanical Model of Damage Initiation and The Competition Between Different Mechanisms" Composites Science and Technology 57 (1997) 155-164
7. Bond I., Hucker M., Weaver P., Bleay S., Haq S., "Mechanical Behaviour of Circular and Triangular Glass Fibres and Their Composites", Composites Science and Technology
8. Kugler D., Moon T.," A Technique for Compression Testing of Composite Rings", Composites: Part A 33 (2002) 507-514
9. Harte A., Fleck N., "Deformation and Failure Mechanisms of Braided Composite Tubes in Compression and Torsion", Acta Materialia 48 (2000) 1259-1271
10. Song H., Du X., "Off-axis Crushing of GFRP Tubes", Composite Science and Technology 62 (2002) 2065-2073
11. Gupta N., Abbas H., " Lateral Collapse of Composite Cylindrical Tubes Between Flat Platens", International Journal of Impact Engineering 24 (2000) 329-346

12. Perreux D., Choqueuse D., Davies P., " Anomalies in Moisture Absorption of Glass Fiber Reinforced Epoxy Tubes ", Composites: Part A 33 (2002) 147-154
13. Srivastava V., Kawada H., "Fatique Behaviour of Alumina-fibre-reinforced Epoxy Resin Composite Pipes Under Tensile and Compressive Loading Conditions", Composite Science and Technology 61 (2001) 2393-2403
14. Mirmiran A., Shao Y., Shahawy M., "Analysis and Field Tests on the Performance of Composite Tubes Under Pile Driving Impact", Composite Structures 55 (2002) 127-135
15. Richard F., Perreux D., " A Reliability Method for Optimization of $[+\vartheta,-\vartheta]_n$ Fiber Reinforced Composite Pipes", Reliability Engineering and System Safety 68 (2000) 53-59
16. Toutanji H., Saafi M., " Durability Studies on Concrete Columns Encased in PVC-FRP Composite Tubes ", Composite Structures 54 (2001) 27-35
17. Wingard C., "Characterization of Prepreg and Cured Epoxy/Fiberglass Composite Material for Use in Advanced Composite Piping Systems", Thermochimica Acta 357-358 (200) 293-301
18. Paul N., Hosani H., Masri A., " Use of GRP Material in Power and Desalination Plants" , Desalination 120 (1998) 83-88
19. Fukuda H., Watanabe T., Watanabe O., Itabashi M., and Wada A.," Compression Bending Test for CFRP Pipe"
20. Chiu C., Tsai K., " Crush-failure modes of 2D triaxially Braided Hybrid Composite Tubes", Composite Science and Technology 59 (1999) 1713-1723
21. Wild P., Vickers G.," Analysis of Filament-wound Cylindrical Shells Under Combined Centrifugal, Pressure and Axial Loading", S1359-835X(96)00093-0
22. Khalid A., Sahari B., Khalid Y.," Performance of Composite Cones Under Axial Compression Loading" , Composite Science and Technology 62 (2002) 17-27
23. Toutanji H., Dempsey S., " Stress Modeling of Pipelines Strengthened with Advanced Composite Materials", Thin-Walled Structures 39 (2001) 153-165
24. Jacquemin F., Vautrin A., " The Effect of Cyclic Hygrothermal Conditions on the Stresses Near the Surface of a Thick Composite Pipe", Composite Science and Technology 62 (2002) 567-570
25. Tarakçıoğlu N., Akdemir A., Avci A., "Strength of Filament Wound GRP Pipes with Surface Crack", Composites: Part B 32 (2001) 131-138

26. Rousseau J., Perreux D., Verdiere N.," The Influence of Winding Patterns on the Damage Behaviour of Filament-wound Pipes", Composite Science and Technology 62 (1999) 1439-1449
27. Zou Z., Reid S. R., Soden P. D., Li S., "Measurement of the Critical Energy Release Rate G_{IIC} for Filament Wound GRP Pipes", Composites: Part A 32 (2001) 271-280
28. Bouchet J., Jacquelin E., Hamelin P., "Dynamic Axial Crushing of Combined Composite Aluminum Tube: The Role of Both Reinforcement and Surface Treatments", Composite Structure 56 (2002) 87-96
29. www.geothermal.marin.org
30. Gallup D. L., "Geochemistry of Geothermal Fluids and Well Scales, and Potential for Mineral Recovery", Ore Geology Reviews 12 (1998) 225-236
31. K.L. Brown, "Scaling and Geothermal Development", May 1996
32. Serpen U., "Jeotermal Kaynak İşletmesinde Akışkan Taşıma ve Boru Hatları", Jeotermal Enerji Semineri 401-412
33. Batis G., Kouloumbi N., Kotsakou K., "Corrosion and Protection of Carbon Steel in Low Enthalpy Geothermal Fluids. The Case of Sousaki in Greece", Geothermics Vol.26 No.1 (1997) 65-82
34. Povarov O. A., Tomarov G. V., Semenov V. N., "Physical and Chemical Processes of Geothermal Fluid Impact on Metal of Geothermal Power Plant Equipment", Proceedings World Geothermal Congress 2000
35. Sanada N., Kurata Y., Nanjo H., Kim H., Ikeuchi J., Lichti K., "IEA Deep Geothermal Resources Subtask C: Materials, Progress With a Database for Materials Performance in Deep and Acidic Geothermal Wells", Proceedings World Geothermal Congress 2000
36. White S., Lichti K., Bacon L., "Application of Chemical and Wellbore Modeling to the Corrosion and Scaling Properties of Ohaaki Deep Wells", Proceedings World Geothermal Congress 2000
37. Mertoğlu O., "Geothermal District Heating Experience in Turkey", ORME Jeotermal, Ankara, Turkey
38. Rafferty K., "Well Pumps and Piping", Geo-Heat Center
39. www.eren.doe.gov/geothermal
40. Aksoy N., "Balçova-Narlıdere Jeothermal Sisteminin İzleyiciler İle İncelenmesi", June 2001, İzmir, Ph. D. Thesis

41. Haliloğlu N., “Korozyona Dayanıklı Malzeme Seçimi”, Sınai Eğitim ve Geliştirme Merkezi
42. Hayashi Y., “Fundamentals of Corrosion”, Textbook for the Fourth International Group Training Course on Geothermal Energy”, Held at Kyushu University
43. Boulton L. H., Wright G. A., “Fundamentals of Metallic Corrosion and Its Prevention”, Australasian Corrosion Association
44. Vendrell P.F., Atiles J. H., “Corrosive Or Scaling Water”, Your Household Water Quality Series, Circular 9
45. Bor Z Jang., “Advanced Polymer Composites”, published by ASM,1994
46. Hull D., Clyne T., ”An Introduction To Composite Materials”, Cambridge University Press, 1996
47. Aguiar J., “ Durability of Polymeric Pipes in Contact With Domestic Products”, Construction and Building Materials 13 (1999) 155-157
48. J. Brandrup, E.H. Immergut, and E.A. Grulke, eds, “Advanced Polymers Handbook”, published by John Wiley and Sons, 1999
49. Saunders R., Kent M., “Adhesive Systems Based on Funtionalized Block Copolymers”
50. Buckley C., Harding J., Hou J., Ruiz C., Trojanowski A.,” Deformation of Thermosetting Resins at Impact Rates of Strain. Part I: Experimental Study”, Journal of the Mechanics and Physics of Solids 49 (2001) 1517-1538
51. Chen W., Lu F., Cheng M.,“ Tension and Compression Tests of Two Polymers Under Quasistatic and Dynamic Loading”, Polymer Testing 21 (2002) 113-121
52. Khan M., Simpson G., Townsend C., “A Comparison of the Mechanical Properties in Compression of Two Resin Systems”, Material Letters 52 (2002) 173-179
53. Baschek G., Hartwig G., Zahradnik F., “ Effect of Water Absorption in Polymers at Low and High Temperatures”, Polymer 40 (1999) 3433-3441
54. www.globalcomposites.com
55. www.gfmco.com/centrifugal.htm
56. “Centifugal Casting Process Sends The Competition Reeling”, Composite Technology, March/April 2001
57. Loos A., Tzeng J., “Filament Winding”, Flow and Rheology in Polymer Composite Manufacturing, 571-575, 1994
58. www.eng.hawaii.edu/~asme/vehicle/design3.html

59. Schutte C., McAuliffe M., " Durability of Glass Fiber/Polymer Composites", Polymer Division
60. Cardon A. H., Quin Y., Van Vossole C., " Durability Analysis of Polymer Matrix Composites for Structural Applications ", Computers and Structures 76 (2000) 35-41
61. Scida D., Aboura Z., Benzeggagh M., " The Effect of Ageing on the Damage Events in Woven-fiber Composite Materials Under Different Loading conditions", Composites Science and Technology 62 (2002) 551-557
62. Buehler F., Seferis J., " Effect of Reinforcement and Solvent Content on Moisture Absorption in Epoxy Composite Materials", Composites: Part A 31 (2000) 741-748
63. Komai K., Minoshima K., Tanaka K., Tokura T., "Effects of Stress Waveform and Water Absorption on the Fatigue Strength of Angle-ply Aramid Fiber/epoxy Composites", International Journal of Fatigue 24 (2002) 339-348
64. Merdas I., Thominette F., Tcharkhtchi A., Verdu J., " Factors Governing Water Absorption by Composite Matrices", Composites Science and Technology 62 (2002) 487-492
65. Fiedler B., Hojo M., Ochiai S., Schulte K., Ando M., " Failure Behavior of an Epoxy Matrix Under Different Kinds of Static Loading", Composites Science and Technology 61 (2001) 1615-1624
66. Wan Y., Wang Y., Luo H., Dong X., Cheng G., " Moisture Absorption Behavior of C_{3D}/ EP Composite and Effect of External Stress", Materials Science and Engineering A326 (2002) 324-329
67. Schieffer A., Maire J., Leveque D., "A Coupled Analyses of Mechanical Behaviour and Ageing for Polymer-Matrix Composites", Composite Science and Technology 62 (2002) 543-549
68. Russell A., Street K., "Moisture and Temperature Effects on the Mixed-Mode Delamination Fracture of Unidirectional Graphite/Epoxy", American Society for Testing And Materials 1985 pp 349-370
69. Glavchev I., Petrova Kr., Ivanova M.," Determination of the Coefficient of Thermal Expansion of Epoxy Composites", Polymer Testing 21 (2002) 177-179
70. Santos C., Clarke R., Braden M., Guitian F., Davy K., "Water Absorption Characteristics Of Dental Composites Incorporation Hydroxyapatite Filler", Biomaterials 23 (2002) 1897-1904

71. Shen C., Springer G.,“ Moisture Absorption and Desorption of Composite Materials“, Department of Mechanical Engineering, The University of Michigan
72. Gautier L., Mortaigne B., Bellenger V.,“ Interface Damage Study of Hydrothermally Aged Glass-fibre-reinforced Polyester Composites”, Composite Science and Technology 59 (1999) 2329-2337
73. Gaur U., Chou C., Miller B., “ Effect of Hydrothermal Ageing on Bond Strength “, TRI/Princeton, USA
74. Glavchev I., Petrova Kr., Ivanova M., “ Determination of the Coefficient of Thermal Expansion of Epoxy Composites”, Polymer Testing 21 (2002) 177-179
75. Patel S. R., Case S.W., “Durability of Hygrothermally Aged Graphite/Epoxy Woven Composite Under Combined Hygrothermal Conditions”, International Journal of Fatigue 24 (2002) 1295-1301
76. Patel S. R., Case S.W., “Durability of a Graphite/Epoxy Woven Composite Under Combined Hygrothermal Conditions”, International Journal of Fatigue 22 (2000) 809-820
77. Çengel Yunus, *Heat Transfer*, International Edition, McGraw Hill
78. Çanakci Cihan., 2003, Personel communication
79. MMO, “Kalorifer Tesisatı Proje Hazırlama Esasları”, Yayın no: 84
80. Giese, L. B., 2003, Personal communication
81. Crank J., *The Mathematics of Diffusion*, Clarendon Press, Oxford

APPENDIX

Table A.1 The specifications of composite pipe specimens produced by filament winding

Sample Name	**Height (mm)**	**Inner Dia. (mm)**	**Outer Dia. (mm)**	**Dry Weight (gr)**
P-1	39,19	85	92,87	71,241
P-2	39,41	85	92,37	69,388
P-3	38,82	85	92,30	67,689
P-4	41,25	85	92,85	72,998
P-5	40,85	85	93,15	80,198
P-6	41,20	85	92,50	70,762
P-7	41,10	85	93,80	86,197
P-8	39,60	85	93,20	75,989
P-9	40,52	85	93,10	79,201
P-10	41,54	85	93,32	82,988
P-11	42,50	85	93,80	83,243
P-12	39,42	85	95,45	94,708
E-1	43,25	85	92,85	75,748
E-2	42,10	85	92,40	74,141
E-3	40,40	85	92,38	72,670
E-4	40,30	85	93,55	77,099
E-5	40,42	85	93,80	80,357
E-6	39,40	85	93,45	74,432
E-7	40,10	85	92,40	70,108
E-8	42,20	85	93,90	84,451
E-9	41,64	85	94,70	91,488
E-10	38,20	85	91,80	60,550
E-11	41,47	85	92,52	72,658
E-12	40,20	85	93,45	76,418
EC-1	39,90	85	93,56	77,038
EC-2	40,30	85	94,25	81,621
EC-3	42,25	85	94,07	83,889
EC-4	39,95	85	93,32	68,418
EC-5	41,85	85	94,75	90,101
EC-6	38,67	85	95,10	84,989
EC-7	39,10	85	94,20	79,498
EC-8	39,32	85	95,40	89,589
EC-9	42,75	85	96,12	105,589
EC-10	41,27	85	94,85	90,697
EC-11	40,73	85	94,14	81,607
EC-12	42,16	85	94,63	91,331

P = Polyester matrix composite pipe

E = Epoxy matrix composite pipe

EC = Graphite particles added epoxy matrix composite pipe

Table A.2 The specifications of composite pipe specimens produced by tube rolling

Sample Name	Height (mm)	Inner Dia. (mm)	Outer Dia. (mm)	Dry Weight (gr)
P-1	41,21	85	92,23	69,224
P-2	42,15	85	92,40	70,189
P-3	39,42	85	92,11	65,265
P-4	41,34	85	92,08	69,541
P-5	42,35	85	92,47	70,441
P-6	39,24	85	92,29	64,898
P-7	39,12	85	92,41	65,345
P-8	40,14	85	92,37	67,289
P-9	40,34	85	92,50	67,677
P-10	41,40	85	92,52	69,351
P-11	39,08	85	92,75	64,655
P-12	40,02	85	92,63	66,410
E-1	40,48	85	93,58	66,889
E-2	42,11	85	93,10	70,321
E-3	39,44	85	93,41	64,945
E-4	42,24	85	93,76	70,464
E-5	40,08	85	93,24	66,456
E-6	41,25	85	93,84	68,478
E-7	39,84	85	93,35	68,666
E-8	39,21	85	93,36	67,593
E-9	41,64	85	92,85	74,008
E-10	39,87	85	93,37	70,915
E-11	40,84	85	93,34	71,198
E-12	41,37	85	92,15	71,298
EC-1	39,21	85	93,95	70,256
EC-2	40,85	85	93,89	71,188
EC-3	39,26	85	94,21	70,214
EC-4	40,41	85	94,14	71,123
EC-5	40,64	85	94,24	71,225
EC-6	40,68	85	94,31	71,541
EC-7	39,89	85	93,97	75,913
EC-8	41,58	85	94,22	79,254
EC-9	38,70	85	94,01	74,655
EC-10	39,26	85	94,07	74,520
EC-11	41,18	85	94,28	75,954
EC-12	39,93	85	93,42	73,246

P = Polyester matrix composite pipe

E = Epoxy matrix composite pipe

EC = Graphite particles added epoxy matrix composite pipe

Table A.3 The specifications of neat polymers

Sample Name	Height (mm)	Length a (mm)	Length b (mm)	Dry Weight (gr)
P-1	14,63	7,90	8,00	1,059
P-2	13,70	7,62	7,99	0,966
P-3	14,45	7,36	8,16	1,010
P-4	14,71	6,77	8,11	0,948
P-5	14,44	7,70	8,16	1,036
P-6	14,70	7,65	8,07	1,040
P-7	14,11	8,05	8,04	1,052
P-8	15,23	7,82	7,76	1,046
P-9	14,28	8,40	8,14	1,123
P-10	14,45	8,16	7,91	1,071
P-11	13,86	8,09	8,01	1,029
P-12	13,78	6,59	7,97	0,833
P-13	1455	7,95	8,14	1,070
P-14	14,37	6,94	8,04	0,927
P-15	14,01	7,78	8,29	1,021
E-1	15,41	8,03	8,39	1,167
E-2	15,64	7,53	8,36	1,060
E-3	14,66	8,69	8,61	1,214
E-4	15,45	7,60	8,70	1,147
E-5	15,71	7,54	7,87	1,037
E-6	15,43	8,61	8,28	1,200
E-7	15,43	6,64	7,69	0,874
E-8	14,67	8,56	7,78	1,067
E-9	15,38	8,34	8,50	1,220
E-10	15,63	7,55	8,46	1,121
E-11	15,48	8,55	8,41	1,226
E-12	15,24	7,99	8,58	1,155
E-13	15,12	8,29	8,22	1,154
E-14	14,88	8,28	8,62	1,191
E-15	15,22	8,65	8,50	1,218
EC-1	14,96	8,50	7,05	1,002
EC-2	13,54	7,00	7,81	0,840
EC-3	14,53	8,38	8,53	1,144
EC-4	14,57	7,54	7,33	0,917
EC-5	14,59	8,02	8,23	1,037
EC-6	13,79	8,28	7,94	1,021
EC-7	13,70	7,23	7,75	0,862
EC-8	13,28	7,81	7,54	0,870
EC-9	13,65	6,92	7,69	0,827
EC-10	13,66	7,34	7,71	0,871
EC-11	13,67	6,95	8,21	0,886
EC-12	13,70	7,62	7,15	0,841
EC-13	13,52	7,06	7,03	0,762
EC-14	13,77	7,98	7,03	0,874
EC-15	14,18	7,50	7,78	0,916

P = Neat polyester

E = Neat epoxy

EC = Neat graphite particles added epoxy

Table A.4 Sample ident of IYTE composite precipitation of Balçova geothermal fluid at 25°C

SAMPLE IDENT - IYTE Composite Precipitation Balcova Water (TEMPERATURE = 25.00)

	PHASE	LOG (AP)	LOG (KT)	LOG (AP/KT)	DELG		PHASE	LOG (AP)	LOG (KT)	LOG (AP/KT)	DELG
2	AKERMANI	26.029	45.460	-19.431	-26.508	73	MERWINIT	36.549	68.170	-31.621	-43.138
11	ANHYDRIT	-6.447	-4.310	-2.137	-2.915	76	MIRABILT	-6.723	-1.090	-5.633	-7.684
17	ARAGONIT	-8.703	-8.340	-0.363	-0.495	77	MONTICEL	18.136	30.150	-12.014	-16.390
22	BRUCITE	-17.738	-11.470	-6.268	-8.551	81	NACHOLIT	-3.769	-0.430	-3.339	-4.555
24	CALCITE	-8.703	-8.480	-0.223	-0.304	82	NATRTHRM	-8.975	-0.010	-8.965	-12.231
26	CHALCEDO	-2.627	-3.730	1.103	1.505	83	NATRON	-8.978	-0.880	-8.098	-11.048
30	CRYSOTIL	25.473	32.030	-6.557	-8.945	85	NESQUHON	-8.981	-5.350	-3.631	-4.954
31	C-ENSTAT	7.616	11.290	-3.674	-5.013	95	PERICLAS	10.243	21.510	-11.267	-15.371
37	CRISTOBA	-2.627	-3.540	0.913	1.245	99	PORTLAN	-17.460	-5.420	-12.040	-16.426
38	CRISTOBB	-2.627	-2.940	0.313	0.427	100	POTASSI	7.716	84.120	-76.404	-104.233
40	DIOPSIDE	15.509	19.630	-4.121	-5.622	103	QUARTZ	-2.627	-3.930	1.303	1.778
41	DOLOMITE	-17.683	-18.060	0.377	0.515	110	SEPIOLIT	25.206	31.520	-6.314	-8.614
42	DSORD	-17.683	-16.520	-1.163	-1.586	111	SILICAAM	-2.627	-2.700	0.073	0.099
43	ENSTATIT	7.616	11.470	-3.854	-5.258	112	SILICGEL	-2.627	-2.710	0.083	0.113
45	FAYALITE	13.615	19.430	-5.815	-7.933	118	Na2O	10.248	67.430	-57.182	-78.010
46	FLUORITE	-10.630	-10.960	0.330	0.451	123	SYLVITE	-5.405	0.910	-6.315	-8.615
47	FORSTERI	17.858	29.070	-11.212	-15.295	124	TALC	20.219	21.130	-0.911	-1.242
50	GREENALI	19.108	22.580	-3.472	-4.736	125	THENARDI	-6.719	-0.290	-6.429	-8.771
51	GYPSUM	-6.447	-4.600	-1.847	-2.520	126	TREMOLIT	51.237	60.890	-9.653	-13.169
52	HALITE	-4.139	1.590	-5.729	-7.815	127	TRONA	-12.745	-0.630	-12.115	-16.527
55	HUNTITE	-35.643	-30.620	-5.023	-6.852	131	WOLLASTO	7.893	12.600	-4.707	-6.421
56	HYDRMAGN	-48.296	-38.530	-9.766	-13.323	144	FeCl2	-10.404	7.900	-18.304	-24.971
57	HYPHILIT	-8.005	11.800	-19.805	-27.019	145	FeCl3	-27.436	12.340	-39.776	-54.263
60	KENYAITE	-23.776	-25.000	1.224	1.670	146	FeCO3	-11.102	-10.540	-0.562	-0.766
64	LARNITE	18.413	38.880	-20.467	-27.921	147	FeO	8.121	13.500	-5.379	-7.338
67	LIME	-17.200	32.660	-49.860	-68.020	148	Fe2O3HEM	0.704	0.040	0.664	0.906
68	MAGADITE	-13.267	-14.340	1.073	1.464	149	Fe2O3MGH	0.704	6.400	-5.696	-7.770
69	MgFe2O4	10.947	21.100	-10.153	-13.851	150	Fe3O4	8.825	10.750	-1.925	-2.626
70	MAGNESIT	-8.980	-8.050	-0.930	-1.269	151	Fe(OH)3	-41.618	-37.200	-4.418	-6.028
71	MgCl2	-8.283	22.150	-30.433	-41.517	152	GOETHITE	0.352	0.480	-0.128	-0.175

Table A.5 Sample ident of IYTE composite precipitation Balçova geothermal fluid at 84°C

SAMPLE IDENT - IYTE Composite Precipitation Balcova Water (TEMPERATURE = 84.00)

	PHASE	LOG (AP)	LOG (KT)	LOG (AP/KT)	DELG		PHASE	LOG (AP)	LOG (KT)	LOG (AP/KT)	DELG
2	AKERMANI	25.549	36.802	-11.253	-18.389	73	MERWINIT	35.918	55.529	-19.611	-32.048
11	ANHYDRIT	-6.637	-5.080	-1.557	-2.544	76	MIRABILT	-6.845	1.232	-8.077	-13.200
17	ARAGONIT	-8.647	-8.930	0.284	0.464	77	MONTICEL	17.836	24.246	-6.410	-10.475
22	BRUCITE	-14.936	-11.719	-3.217	-5.257	81	NACHOLIT	-3.801	0.191	-3.992	-6.524
24	CALCITE	-8.647	-9.044	0.397	0.649	82	NATRTHRM	-8.852	-0.588	-8.264	-13.505
26	CHALCEDO	-2.656	-3.015	0.360	0.588	83	NATRON	-8.855	1.024	-9.879	-16.144
30	CRYSOTIL	25.056	25.374	-0.318	-0.520	85	NESQUHON	-8.894	-5.154	-3.739	-6.111
31	C-ENSTAT	7.467	8.748	-1.281	-2.094	95	PERICLAS	10.123	17.182	-7.059	-11.536
37	CRISTOBA	-2.656	-2.930	0.275	0.449	99	PORTLAN	-14.690	-6.161	-8.529	-13.938
38	CRISTOBB	-2.656	-2.572	-0.083	-0.136	100	POTASSI	7.644	71.786	-64.142	-104.821
40	DIOPSIDE	15.180	15.669	-0.489	-0.799	103	QUARTZ	-2.656	-3.256	0.601	0.982
41	DOLOMITE	-17.539	-19.818	2.279	3.724	110	SEPIOLIT	24.555	25.982	-1.427	-2.333
42	DSORD	-17.539	-18.627	1.088	1.777	111	SILICAAM	-2.656	-2.318	-0.337	-0.551
43	ENSTATIT	7.467	8.894	-1.427	-2.332	112	SILICGEL	-2.656	-2.301	-0.354	-0.579
45	FAYALITE	13.367	14.824	-1.457	-2.380	118	Na2O	10.164	57.345	-47.181	-77.103
46	FLUORITE	-10.785	-10.560	-0.225	-0.367	123	SYLVITE	-5.420	1.299	-6.718	-10.979
47	FORSTERI	17.590	22.819	-5.229	-8.546	124	TALC	19.745	16.189	3.556	5.812
50	GREENALI	18.722	17.499	1.223	1.998	125	THENARDI	-6.841	-0.584	-6.258	-10.227
51	GYPSUM	-6.637	-4.895	-1.742	-2.847	126	TREMOLIT	50.106	47.916	2.190	3.578
52	HALITE	-4.160	1.605	-5.765	-9.421	127	TRONA	-12.653	-2.404	-10.249	-16.749
55	HUNTITE	-35.325	-34.392	-0.933	-1.525	131	WOLLASTO	7.713	11.242	-3.528	-5.766
56	HYDRMAGN	-45.296	-42.543	-2.754	-4.500	144	FeCl2	-10.473	5.333	-15.806	-25.830
57	HYPHILIT	-8.115	9.189	-17.304	-28.278	145	FeCl3	-25.992	7.641	-33.633	-54.963
60	KENYAITE	-24.130	-25.000	0.870	1.421	146	FeCO3	-11.004	-11.338	0.334	0.546
64	LARNITE	18.082	32.111	-14.029	-22.926	147	FeO	8.011	9.957	-1.946	-3.181
67	LIME	-17.239	27.086	-44.325	-72.435	148	Fe2O3HEM	3.467	-3.589	7.056	11.531
68	MAGADITE	-13.508	-14.340	0.832	1.359	149	Fe2O3MGH	3.467	6.400	-2.933	-4.794
69	MgFe2O4	13.590	13.089	0.500	0.817	150	Fe3O4	11.478	4.572	6.907	11.287
70	MAGNESIT	-8.893	-9.023	0.130	0.213	151	Fe(OH)3	-35.855	-35.071	-0.784	-1.281
71	MgCl2	-8.361	17.441	-25.803	-42.167	152	GOETHITE	1.733	-1.226	2.960	4.837